Angewandte Chemie
Eine Zeitschrift der Gesellschaft Deutscher Chemiker

Supporting Information

The Influence of Strain on the Rotation of an Artificial Molecular Motor

M. Kathan, S. Crespi, A. Troncossi, C. N. Stindt, R. Toyoda, B. L. Feringa**

General

Chemicals were purchased from commercial sources and used without purification. If not stated otherwise, all reactions were carried out in dried glassware under a nitrogen atmosphere using standard Schlenk techniques. For NMR experiments, solvents were added using glass syringes and stainless steel needles (stored at 80 °C). Analytical thin layer chromatography (TLC) was performed on silica gel 60 G/UV254 aluminium sheets from Merck (0.25 mm). Flash column chromatography was performed on silica gel Davisil LC60A (Merck type 9385, 230–400 mesh) or Reveleris X2 Flash Chromatography system (MPLC) using the indicated solvents. NMR spectra were recorded on a Varian Mercury Plus (^{1}H: 400 MHz, ^{13}C: 101 MHz) or a Varian Unity Plus (^{1}H: 500 MHz). Chemical shifts (δ) are given in parts per million (ppm) relative to TMS. For the calibration of the chemical shift, the residual solvent resonance was used as the internal standard. Data are reported as follows: chemical shift (δ in ppm), multiplicity (s = singlet, d = doublet, t = triplet, p = pentet, m = multiplet), coupling constants (*J* in Hz). High resolution mass spectra (HRMS) were recorded on an LTQ Orbitrap XL. UV/vis absorption spectra were recorded on an Agilent Cary 8454 spectrometer in 1 cm quartz cuvettes. Single crystals were measured on a Bruker-AXS D8 Venture diffractometer. Illuminations were carried out using a UV lamp from Vilber Lourmat (6 W, λ_{irr} = 313 or 365 nm) or a LED from THORLABS (LED M300F2, λ_{irr} = 300 nm).

Synthesis

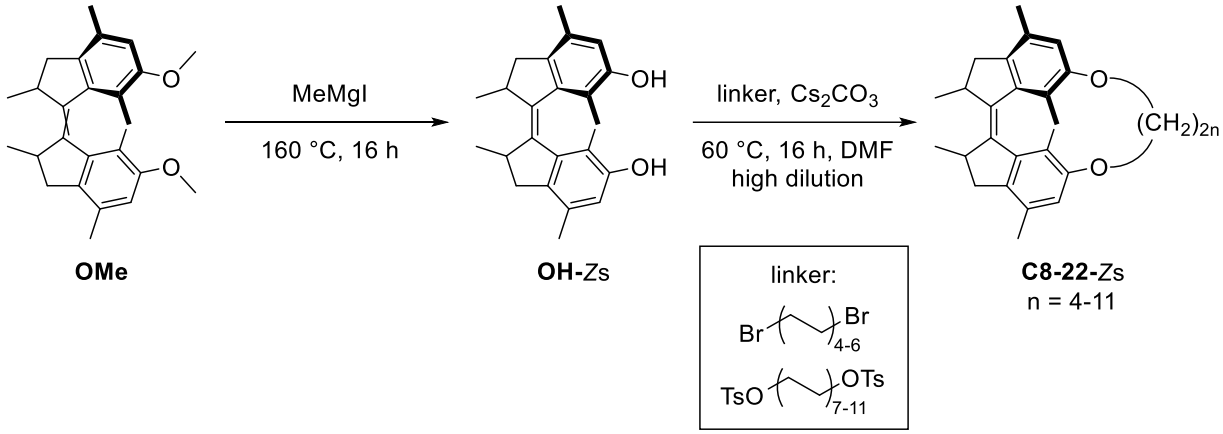

Ditosylates[1] (1,14-ditosyltetradecane, 1,16-ditosylhexadecane, 1,18-ditosyloctadecane, 1,20-ditosylicosane and 1,22-ditosyldocosane) and dihydroxy motor **OH-*Z*s**[2] were prepared according to literature procedures.

General procedure for the synthesis of macrocycles C8–22-*Z*s: Under a nitrogen atmosphere, a Schlenk flask was charged with Cs_2CO_3 (3.7 eq.), dihydroxy motor **OH**-*Z*s (1.0 eq.) and dry DMF (10 mM) and the reaction mixture was heated to 60 °C.[3,4] Then, a solution of dibromide/ditosylate (1.0 eq.) in dry DMF/THF (23 mM) was added to the suspension over the course of 5 h. After stirring the reaction mixture for additional 16 h at 60 °C, the solvent was removed in vacuum, the residue was redissolved in DCM, extensively washed with water and dried over $MgSO_4$. Macrocycles **C8–C22**-*Z*s were purified by flash column or preparative thin-layer chromatography.

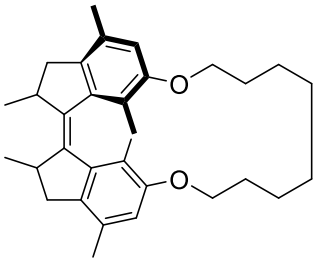

C8-*Zs*: According to the general procedure, a Schlenk flask was charged with Cs_2CO_3 (273 mg, 0.838 mmol), dihydroxy motor **OH**-*Zs* (80 mg, 0.230 mmol) and dry DMF (23 mL). 1,8-Dibromooctane (63 mg, 0.230 mmol) was dissolved in dry DMF (9.8 mL). Purification by preparative thin-layer chromatography (pentane/DCM 80:20) afforded **C8**-*Zs* as a colorless solid (34.8 mg, 33%). **^{1}H NMR** (400 MHz, $CDCl_3$) δ = 6.54 (s, 2H), 4.21–4.17 (m, 2H), 3.86–3.81 (m, 2H), 3.33 (*pseudo*-p, *J* = 6.7 Hz, 2H), 3.04 (dd, *J* = 14.6, 6.3 Hz, 2H), 2.38 (d, *J* = 14.6 Hz, 2H), 2.24 (s, 6H), 1.91–1.80 (m, 2H), 1.66–1.56 (m, 4H), 1.52–1.43 (m, 2H), 1.42–1.24 (m, 12H), 1.09 (d, *J* = 6.8 Hz, 6H) ppm. **^{13}C NMR** (101 MHz, $CDCl_3$) δ = 156.5, 142.1, 141.0, 136.0, 130.6, 122.7, 112.6, 68.2, 41.7, 38.3, 28.8, 28.4, 25.9, 20.6, 18.9, 14.6 ppm. **HRMS-ESI** (ESI+): *m/z* calculated for $C_{32}H_{42}O_2^{\cdot+}$ ($[M]^{\cdot+}$): 458.3179, found 458.3170.

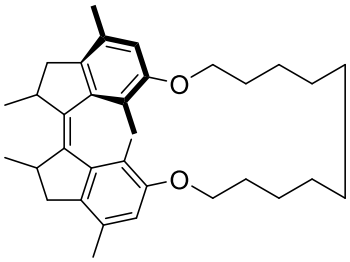

C10-*Zs*: According to the general procedure, a Schlenk flask was charged with Cs_2CO_3 (273 mg, 0.838 mmol), dihydroxy motor **OH**-*Zs* (80 mg, 0.230 mmol) and dry DMF (23 mL). 1,10-Dibromodecane (69 mg, 0.230 mmol) was dissolved in dry DMF (9.8 mL). Purification by preparative thin-layer chromatography (pentane/DCM 80:20) afforded **C10**-*Zs* as a colorless solid (40.2 mg, 36%). **^{1}H NMR** (400 MHz, $CDCl_3$) δ = 6.57 (s, 2H), 4.02–3.94 (m, 4H), 3.34 (*pseudo*-p, *J* = 6.7 Hz, 2H), 3.04 (dd, *J* = 14.5, 6.3 Hz, 2H), 2.39 (d, *J* = 14.5 Hz, 2H), 2.26 (s, 6H), 1.84–1.65 (m, 4H), 1.63–1.32 (m, 20H), 1.09 (d, *J* = 6.7 Hz, 6H) ppm. **^{13}C NMR** (101 MHz, $CDCl_3$) δ = 156.0, 142.1, 141.0, 136.1, 130.5, 122.8, 112.1, 68.4, 42.0, 38.1, 28.9, 28.1, 27.8, 25.9, 20.7, 19.0, 14.6 ppm. **HRMS-ESI** (ESI+): *m/z* calculated for $C_{34}H_{46}O_2^{\cdot+}$ ($[M]^{\cdot+}$): 486.3492, found 486.3482.

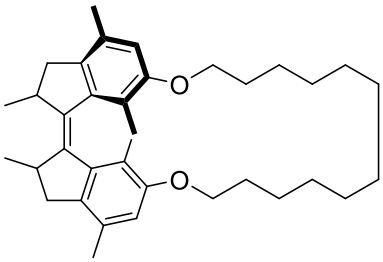

C12-*Zs*: According to the general procedure, a Schlenk flask was charged with Cs_2CO_3 (273 mg, 0.838 mmol), dihydroxy motor **OH**-*Zs* (80 mg, 0.230 mmol) and dry DMF (23 mL). 1,12-Dibromododecane (75 mg, 0.230 mmol) was dissolved in dry DMF (9.8 mL). Purification by preparative thin-layer chromatography (pentane/DCM 80:20) afforded **C12**-*Zs* as a colorless solid (45.1 mg, 38%). **^{1}H NMR** (400 MHz, $CDCl_3$) δ = 6.57 (s, 2H), 4.01–3.96 (m, 2H), 3.93–3.88 (m, 2H), 3.34 (*pseudo*-p, *J* = 6.7 Hz, 2H), 3.05 (dd, *J* = 14.5, 6.3 Hz, 2H), 2.38 (d, *J* = 14.5 Hz, 2H), 2.26 (s, 6H), 1.82–1.66 (m, 4H), 1.54–1.25 (m, 22H), 1.09 (d, *J* = 6.7 Hz, 6H) ppm. **^{13}C NMR** (101 MHz, $CDCl_3$) δ = 156.1, 142.1, 141.1, 136.2, 130.5, 122.9, 112.2, 68.7, 42.1, 38.1, 29.5, 28.1, 27.9, 27.4, 25.6, 20.7, 19.0, 14.4 ppm. **HRMS-ESI** (ESI+): *m/z* calculated for $C_{36}H_{50}O_2^{\cdot+}$ ($[M]^{\cdot+}$): 514.3805, found 514.3792.

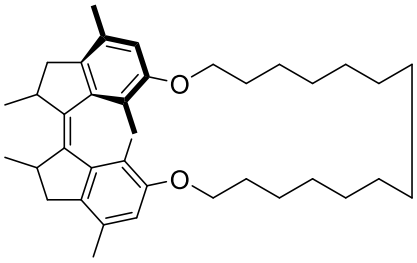

C14-*Zs*: According to the general procedure, a Schlenk flask was charged with Cs_2CO_3 (273 mg, 0.838 mmol), dihydroxy motor **OH**-*Zs* (80 mg, 0.230 mmol) and dry DMF (23 mL). 1,14-Ditosyltetradecane (124 mg, 0.230 mmol) was dissolved in dry DMF (9.8 mL). Purification by preparative thin-layer chromatography (pentane/DCM 80:20) afforded **C14**-*Zs* as a colorless solid (46.3 mg, 37%). **^{1}H NMR** (400 MHz, $CDCl_3$) δ = 6.55 (s, 2H), 4.05–3.93 (m, 2H), 3.90–3.82 (m, 2H), 3.32 (pseudo-p, *J* = 6.7 Hz, 2H), 3.03 (dd, *J* = 14.5, 6.3 Hz, 2H), 2.37 (d, *J* = 14.5 Hz, 2H), 2.24 (s, 6H), 1.83–1.63 (m, 4H), 1.55 (s, 6H), 1.51–1.28 (m, 26H), 1.07 (d, *J* = 6.7 Hz, 6H) ppm. **^{13}C NMR** (101 MHz, $CDCl_3$) δ = 156.2, 142.2, 141.1, 136.2, 130.5, 122.9, 112.3, 69.0, 42.0, 38.1, 29.8, 28.6, 28.3, 27.6, 27.4, 25.7, 20.7, 19.0, 14.5 ppm. **HRMS-ESI** (ESI+): *m/z* calculated for $C_{38}H_{55}O_2^{+}$ ($[M+H]^{+}$): 543.4224, found 543.4225.

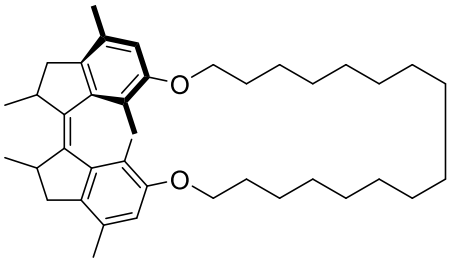

C16-*Zs*: According to the general procedure, a Schlenk flask was charged with Cs_2CO_3 (273 mg, 0.838 mmol), dihydroxy motor **OH**-*Zs* (80 mg, 0.230 mmol) and dry DMF (23 mL). 1,16-Ditosylhexadecane (130 mg, 0.230 mmol) was dissolved in dry DMF (9.8 mL). Purification by preparative thin-layer chromatography (pentane/DCM 80:20) afforded **C16**-*Zs* as a colorless solid (45.0 mg, 34%). **^{1}H NMR** (400 MHz, $CDCl_3$) δ = 6.56 (s, 2H), 3.99–3.94 (m, 2H), 3.88–3.83 (m, 2H), 3.33 (*pseudo*-p, *J* = 6.7 Hz, 2H), 3.04 (dd, *J* = 14.5, 6.3 Hz, 2H), 2.38 (d, *J* = 14.5 Hz, 2H), 2.25 (s, 6H), 1.82–1.67 (m, 4H), 1.52–1.28 (m, 30H), 1.08 (d, *J* = 6.7 Hz, 6H) ppm. **^{13}C NMR** (101 MHz, $CDCl_3$) δ = 156.2, 142.2, 141.1, 136.2, 130.5, 122.9, 112.4, 69.2, 42.0, 38.2, 29.8, 29.1, 28.5, 28.2, 28.1, 27.5, 25.9, 20.7, 18.9, 14.5 ppm. **HRMS-ESI** (ESI+): *m/z* calculated for $C_{40}H_{58}O_2^{\cdot+}$ ($[M]^{\cdot+}$): 570.4431, found 570.4418.

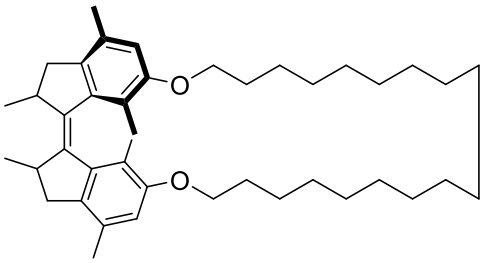

C18-*Zs*: According to the general procedure, a Schlenk flask was charged with Cs_2CO_3 (137 mg, 0.419 mmol), dihydroxy motor **OH**-*Zs* (40 mg, 0.115 mmol) and dry DMF (12 mL). 1,18-Ditosyloctadecane (68 mg, 0.115 mmol) was dissolved in dry DMF (5 mL). Purification by flash column chromatography (pentane/EtOAc 99:1) and subsequent precipitation and filtration of oligomeric side products from a solution in chloroform by slow addition of methanol afforded **C18**-*Zs* as a colorless solid (40.0 mg, 58%). **^{1}H NMR** (400 MHz, $CDCl_3$) δ = 6.55 (s, 2H), 3.98–3.92 (m, 2H), 3.88–3.78 (m, 2H), 3.32 (*pseudo*-p, *J* = 6.5 Hz, 2H), 3.03 (dd, *J* = 14.5, 6.2 Hz, 2H), 2.37 (d, *J* = 14.5 Hz, 2H), 2.24 (s, 6H), 1.81–1.68 (m, 4H), 1.50–1.27 (m, 34H), 1.06 (d, *J* = 6.8 Hz, 6H) ppm. **^{13}C NMR** (101 MHz, $CDCl_3$) δ = 156.1, 142.2, 141.1, 136.2, 130.5, 122.8, 112.4, 69.3, 42.0, 38.2, 29.8, 29.4, 28.8, 28.8, 28.6, 28.1, 27.9, 26.0, 20.7, 19.0, 14.4 ppm. **HRMS-ESI** (ESI+): *m/z* calculated for $C_{42}H_{62}O_2^{\cdot+}$ ($[M]^{\cdot+}$): 598.4744, found 598.4728.

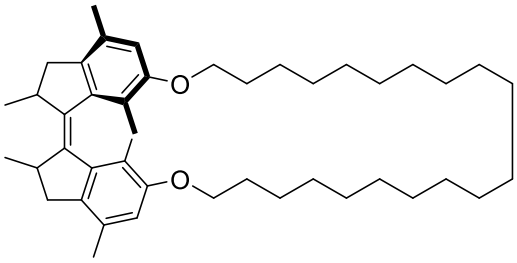

C20-*Zs*: According to the general procedure, a Schlenk flask was charged with Cs_2CO_3 (137 mg, 0.419 mmol), dihydroxy motor **OH**-*Zs* (40 mg, 0.115 mmol) and dry DMF (12 mL). 1,20-Ditosylicosane (72 mg, 0.115 mmol) was dissolved in dry DMF/THF (5 mL, 4:1). Purification by flash column chromatography (pentane/EtOAc 99:1) and subsequent precipitation and filtration of oligomeric side products from a solution in chloroform by slow addition of methanol afforded **C20**-*Zs* as a colorless solid (31.3 mg, 44%). **^{1}H NMR** (400 MHz, $CDCl_3$) δ = 6.54 (s, 2H), 4.01–3.90 (m, 2H), 3.88–3.78 (m, 2H), 3.32 (*pseudo*-p, *J* = 6.7 Hz, 2H), 3.03 (dd, *J* = 14.4, 6.2 Hz, 2H), 2.36 (d, *J* = 14.5 Hz, 2H), 2.24 (s, 6H), 1.88–1.69 (m, 4H), 1.44–1.29 (m, 38H), 1.06 (d, *J* = 6.7 Hz, 6H) ppm. **^{13}C NMR** (101 MHz, $CDCl_3$) δ = 156.1, 142.2, 141.1, 136.2, 130.5, 122.8, 112.3, 69.3, 42.0, 38.2, 29.8, 29.4, 29.2, 29.1, 28.8, 28.5, 28.4, 28.1, 26.1, 20.7, 19.0, 14.4 ppm. **HRMS-ESI** (ESI+): *m/z* calculated for $C_{44}H_{66}O_2^{\cdot+}$ ($[M]^{\cdot+}$): 626.5057, found 626.5045.

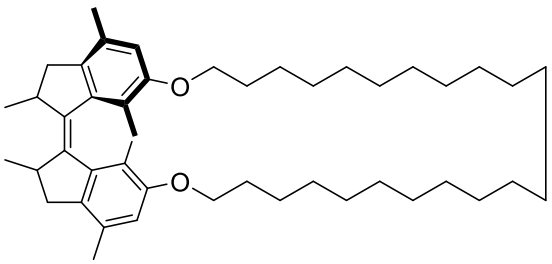

C22-*Zs*: According to the general procedure, a Schlenk flask was charged with Cs_2CO_3 (137 mg, 0.419 mmol), dihydroxy motor **OH**-*Zs* (40 mg, 0.115 mmol) and dry DMF (12 mL). 1,22-Ditosyldocosane (75 mg, 0.115 mmol) was dissolved in dry DMF/THF (5 mL, 3:1). Purification by flash column chromatography (pentane/EtOAc 99:1) and subsequent precipitation and filtration of oligomeric side products from a solution in chloroform by slow addition of methanol afforded **C22**-*Zs* as a colorless solid (33.7 mg, 45%). **^{1}H NMR** (400 MHz, $CDCl_3$) δ = 6.54 (s, 2H), 3.98–3.93

(m, *J* = 6.8 Hz, 2H), 3.90–3.77 (m, 2H), 3.32 (*pseudo*-p, *J* = 6.5 Hz, 2H), 3.03 (dd, *J* = 14.5, 6.2 Hz, 2H), 2.37 (d, *J* = 14.5 Hz, 2H), 2.24 (s, 6H), 1.79–1.69 (m, 4H), 1.45–21.25(m, 42H), 1.06 (d, *J* = 6.8 Hz, 6H) ppm. **^{13}C NMR** (101 MHz, $CDCl_3$) δ = 156.1, 142.2, 141.1, 136.2, 130.5, 122.8, 112.3, 69.2, 42.0, 38.2, 29.8, 29.49, 29.4, 29.3, 29.0, 28.8, 28.8, 28.4, 28.3, 26.2, 20.7, 19.0, 14.4 ppm. **HRMS-ESI** (ESI+): *m/z* calculated for $C_{46}H_{70}O_2^{\cdot+}$ ($[M]^{\cdot+}$): 654.5370, found 654.5355.

NMR Spectroscopy

Degassed NMR samples in toluene-d_8 (~1 mM) were recorded and irradiated (λ_{irr} = 313 nm or 365 nm, Vilber Lourmat, 6 W) at −20 °C (−40 °C and −46 °C in case of **C8** and **OMe**, respectively). Irradiations were carried out in a cryostat. For the determination of photostationary states (PSS, Tab S1) and to prevent significant thermal relaxation, samples were cooled to −20 °C (−46 °C in case of **OMe**) in an ethanol bath before the respective measurement. Equilibrium constants between stable and metastable states were determined from fully relaxed samples. The respective energy differences (ΔG) were calculated with the Gibbs equation (Tab. S2). Under the conservative assumption that the absolute measurement error for NMR spectroscopy is ±3%, energy differences of ≥ |2.0| kcal/mol cannot be reliably determined.

Table S1 | Photostationary states (PSS) for macrocycles C8–22 and reference compound OMe. PSS were determined by ^{1}H NMR spectroscopy in toluene-d_8.

Compound	**PSS** (*Z*s ⟶ *E*m)	**PSS** (*E*s ⟶ *Z*m)
C8	50±2%	---
C10	74±2%	---
C12	81±2%	---
C14	81±2%	---
C16	83±2%	67±4%
C18	80±2%	65±4%
C20	81±2%	63±4%
C22	80±2%	65±4%
OMe	78±2%	70±4%

Table S2 Energy differences between stable and metastable states of macrocycles C8–22 and reference compound OMe. Energies were determined by ^{1}H NMR spectroscopy in toluene-d_8 and are reported for 20 °C.

Compound	**ΔG** (*E*m ⟶ *Z*s)	**ΔG** (*E*m ⟶ *E*s)	**ΔG** (*Z*m ⟶ *Z*s)
C8	≤ −2.0 kcal/mol	---	---
C10	≤ −2.0 kcal/mol	---	---
C12	≤ −2.0 kcal/mol	---	---
C14	≤ −2.0 kcal/mol	---	---
C16	---	+0.9±1 kcal/mol	≤ −2.0 kcal/mol
C18	---	−0.5±1 kcal/mol	≤ −2.0 kcal/mol
C20	---	−1.0±1 kcal/mol	≤ −2.0 kcal/mol
C22	---	−1.4±1 kcal/mol	≤ −2.0 kcal/mol
OMe	---	≤ −2.0 kcal/mol	≤ −2.0 kcal/mol

Switching behavior of C8

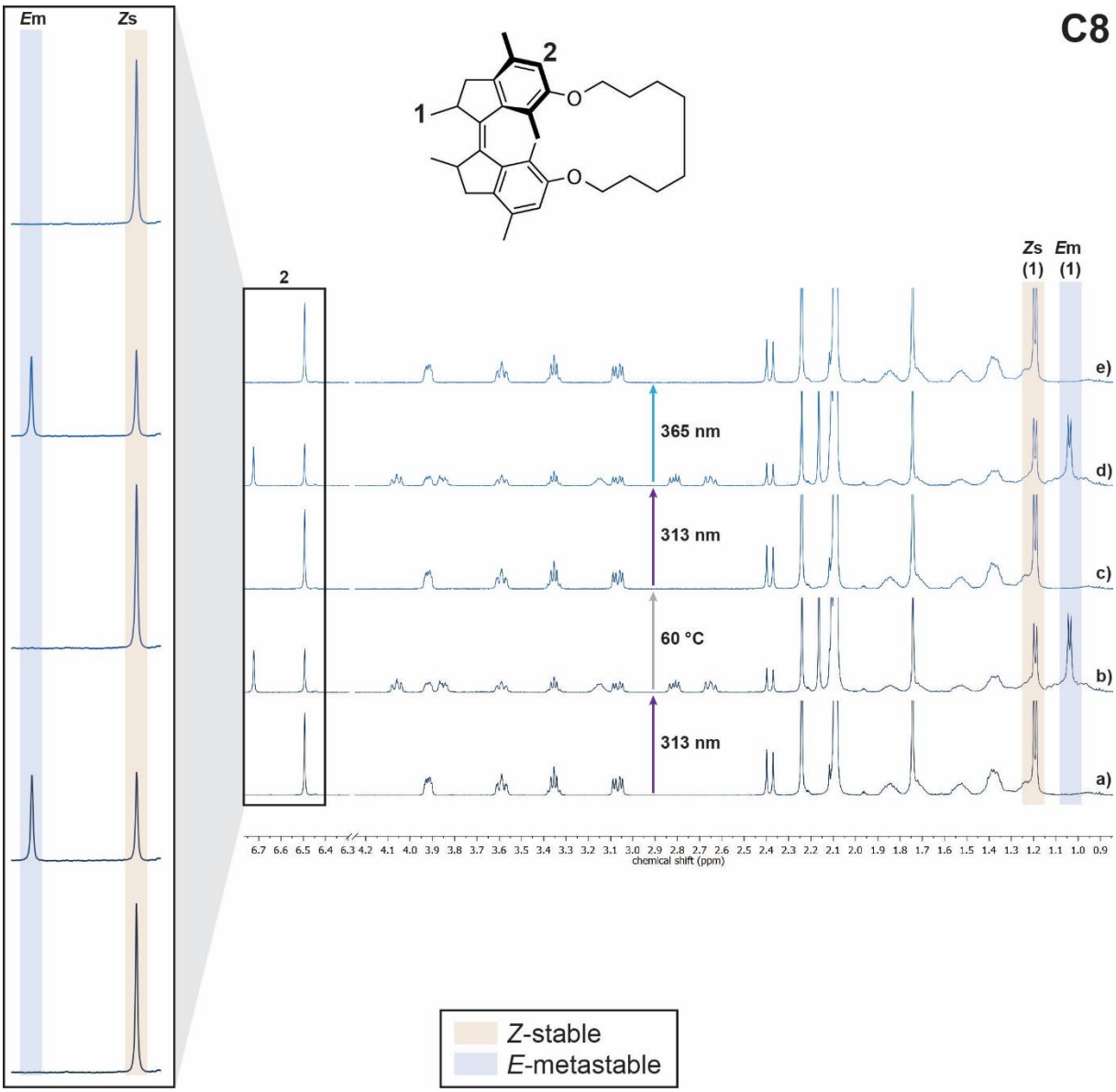

Fig. S1 | Switching behavior of C8 followed by ^{1}H NMR spectroscopy (500 MHz, −20 °C, toluene-d_8). a) Non irradiated **C8**-*Z* stable sample, b) PSS mixture after irradiation with 313 nm at −40 °C, c) composition after full relaxation at 60 °C, d) PSS mixture after irradiation with 313 nm at −40 °C, e) PSS mixture after irradiation with 365 nm at −40 °C.

Switching behavior of C10

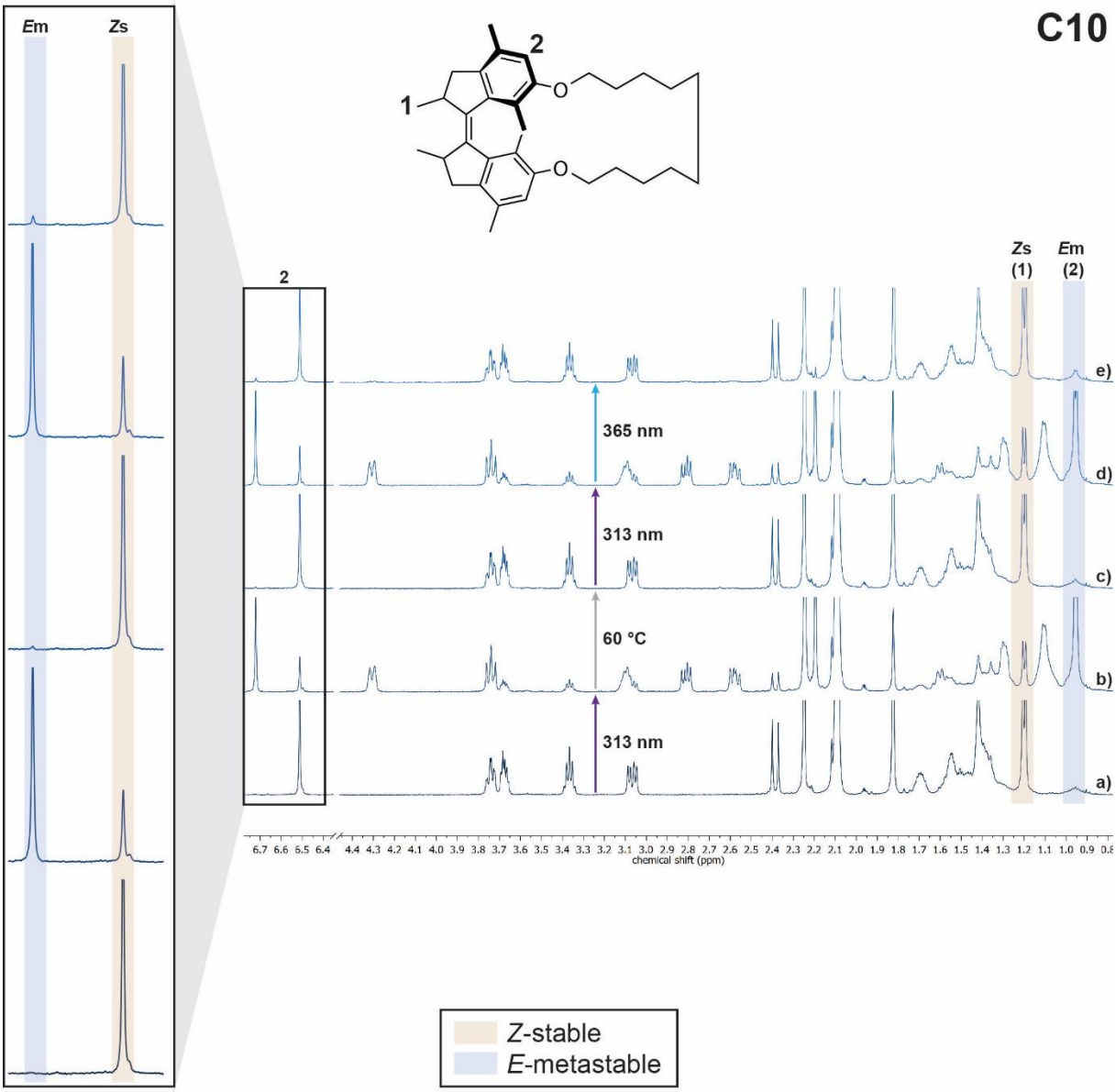

Fig. S2 | Switching behavior of C10 followed by ^{1}H NMR spectroscopy (500 MHz, −20 °C, toluene-d_8). a) Non irradiated **C10**-*Z* stable sample, b) PSS mixture after irradiation with 313 nm at −20 °C, c) composition after full relaxation at 60 °C, d) PSS mixture after irradiation with 313 nm at −20 °C, e) PSS mixture after irradiation with 365 nm at −20 °C.

Switching behavior of C12

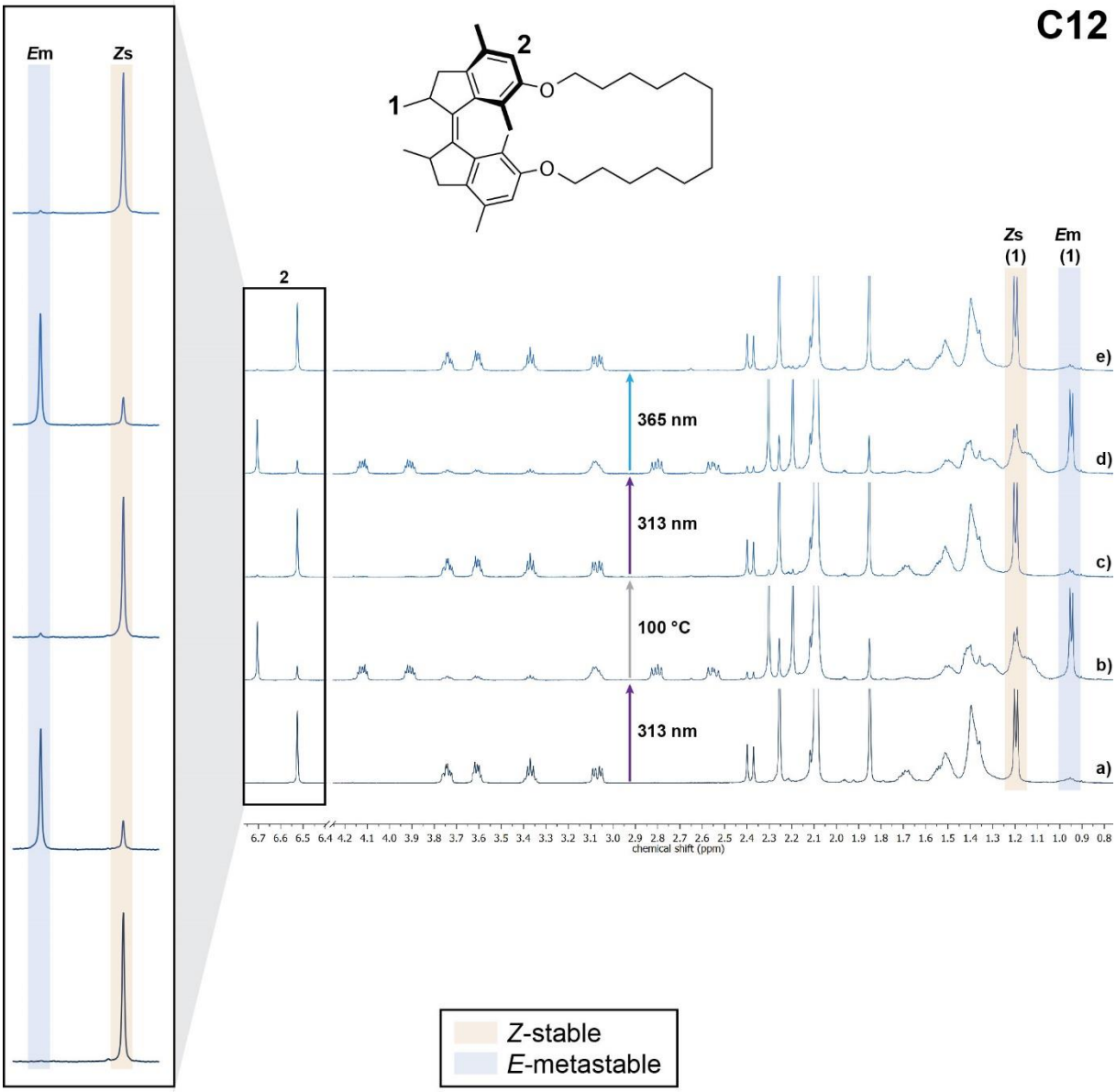

Fig. S3 | Switching behavior of C12 followed by ^{1}H NMR spectroscopy (500 MHz, −20 °C, toluene-d_8). a) Non irradiated **C12**-*Z* stable sample, b) PSS mixture after irradiation with 313 nm at −20 °C, c) composition after full relaxation at 100 °C, d) PSS mixture after irradiation with 313 nm at −20 °C, e) PSS mixture after irradiation with 365 nm at −20 °C.

Switching behavior of C14

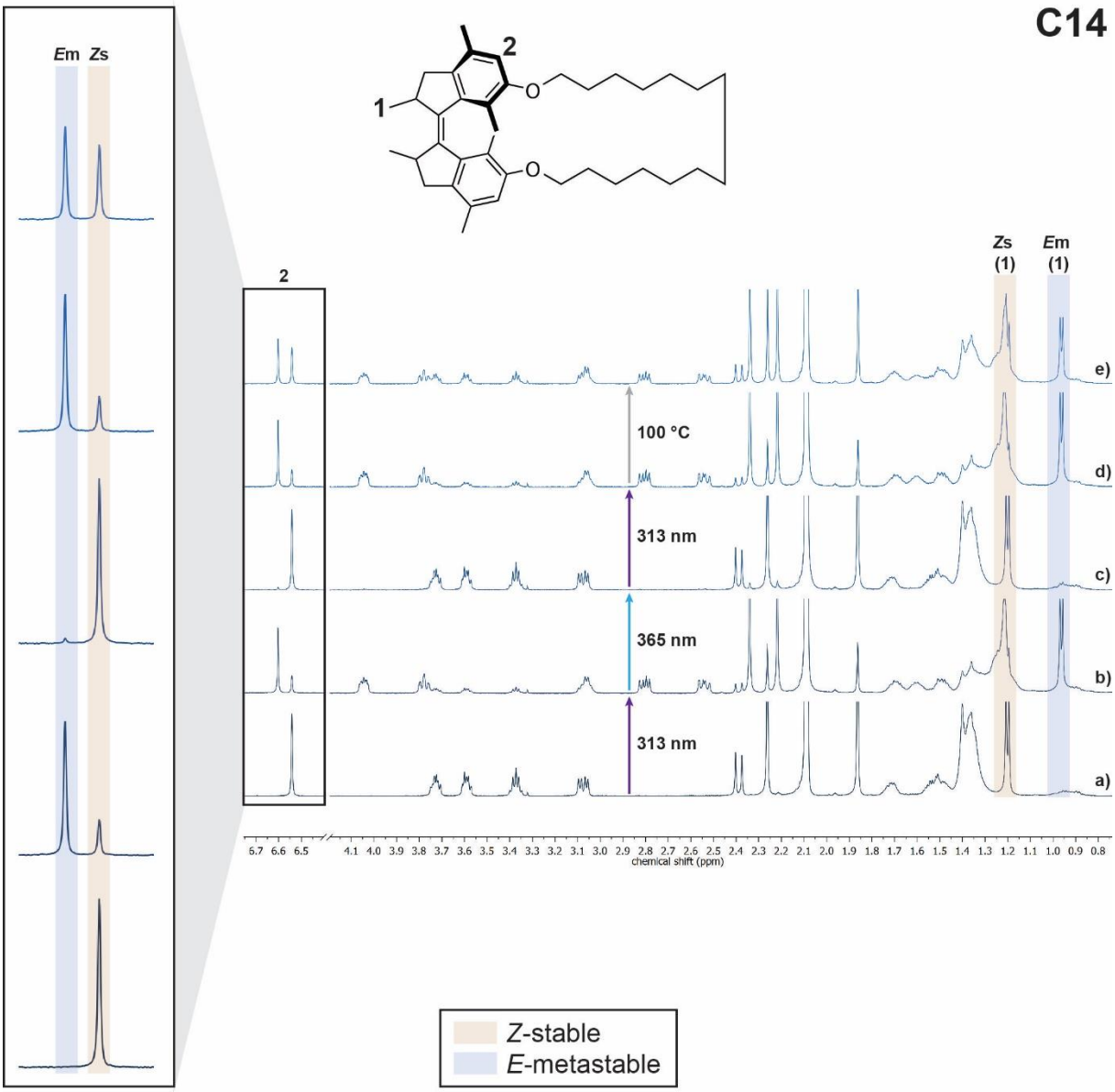

Fig. S4 | Switching behavior of C14 followed by ^{1}H NMR spectroscopy (500 MHz, −20 °C, toluene-d_8). a) Non irradiated **C14**-*Z* stable sample, b) PSS mixture after irradiation with 313 nm at −20 °C, c) PSS mixture after irradiation with 365 nm at −20 °C, d) PSS mixture after irradiation with 313 nm at −20 °C, e) composition after partial relaxation at 100 °C for 3 d.

Full rotational cycle of C16

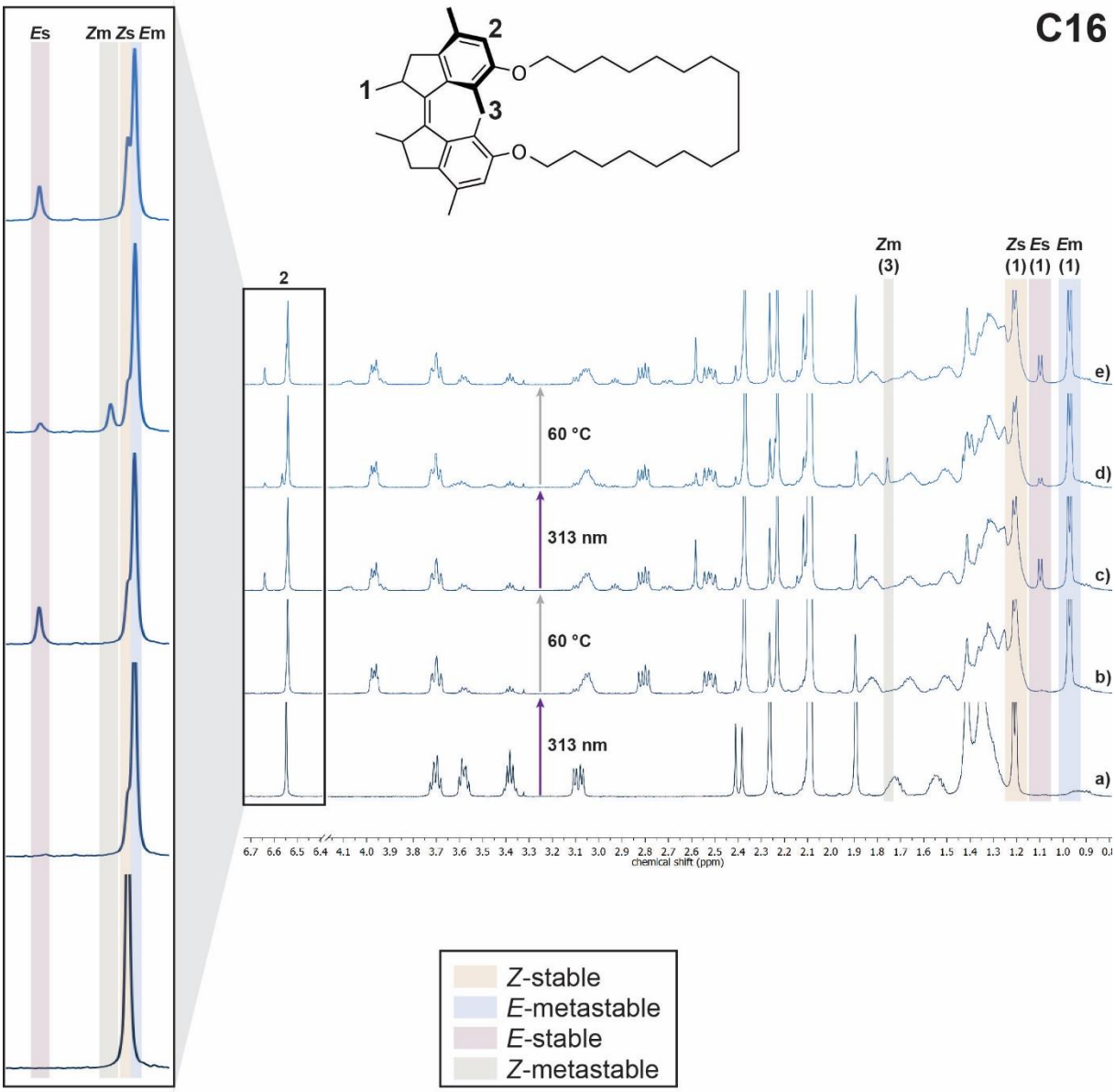

Fig. S5 | Full rotational cycle of C16 followed by ^{1}H NMR spectroscopy (500 MHz, −20 °C, toluene-d_8). a) Non irradiated **C16**-*Z* stable sample, b) PSS mixture after irradiation with 313 nm at −20 °C, c) composition after full relaxation at 60 °C, d) PSS mixture after irradiation with 313 nm at −20 °C, e) composition after full relaxation at 60 °C.

Full rotational cycle of C18

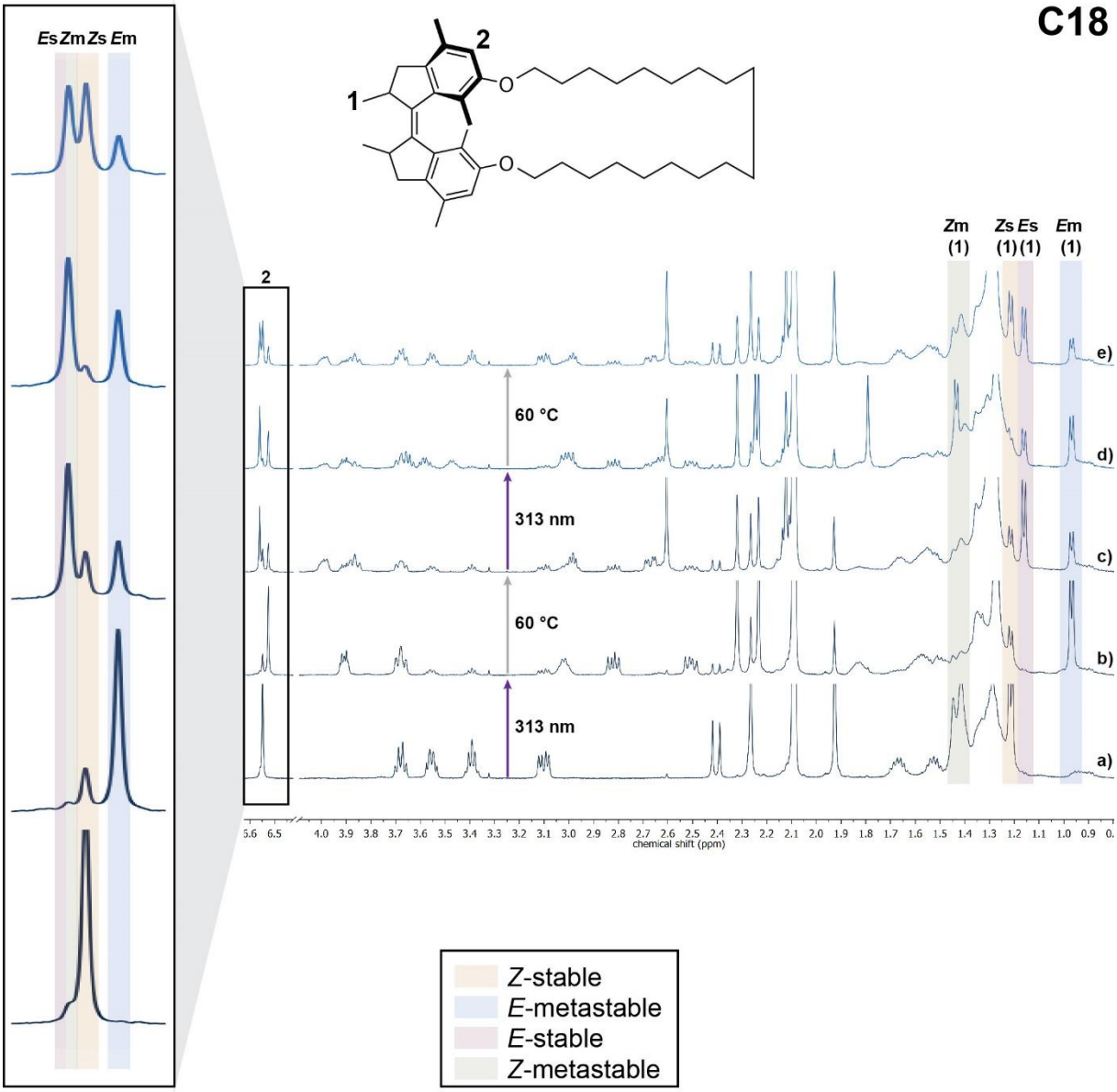

Fig. S6 | Full rotational cycle of C18 followed by ^{1}H NMR spectroscopy (500 MHz, −20 °C, toluene-d_8). a) Non irradiated **C18**-*Z* stable sample, b) PSS mixture after irradiation with 313 nm at −20 °C, c) composition after full relaxation at 60 °C, d) PSS mixture after irradiation with 313 nm at −20 °C, e) composition after full relaxation at 60 °C.

Full rotational cycle of C20

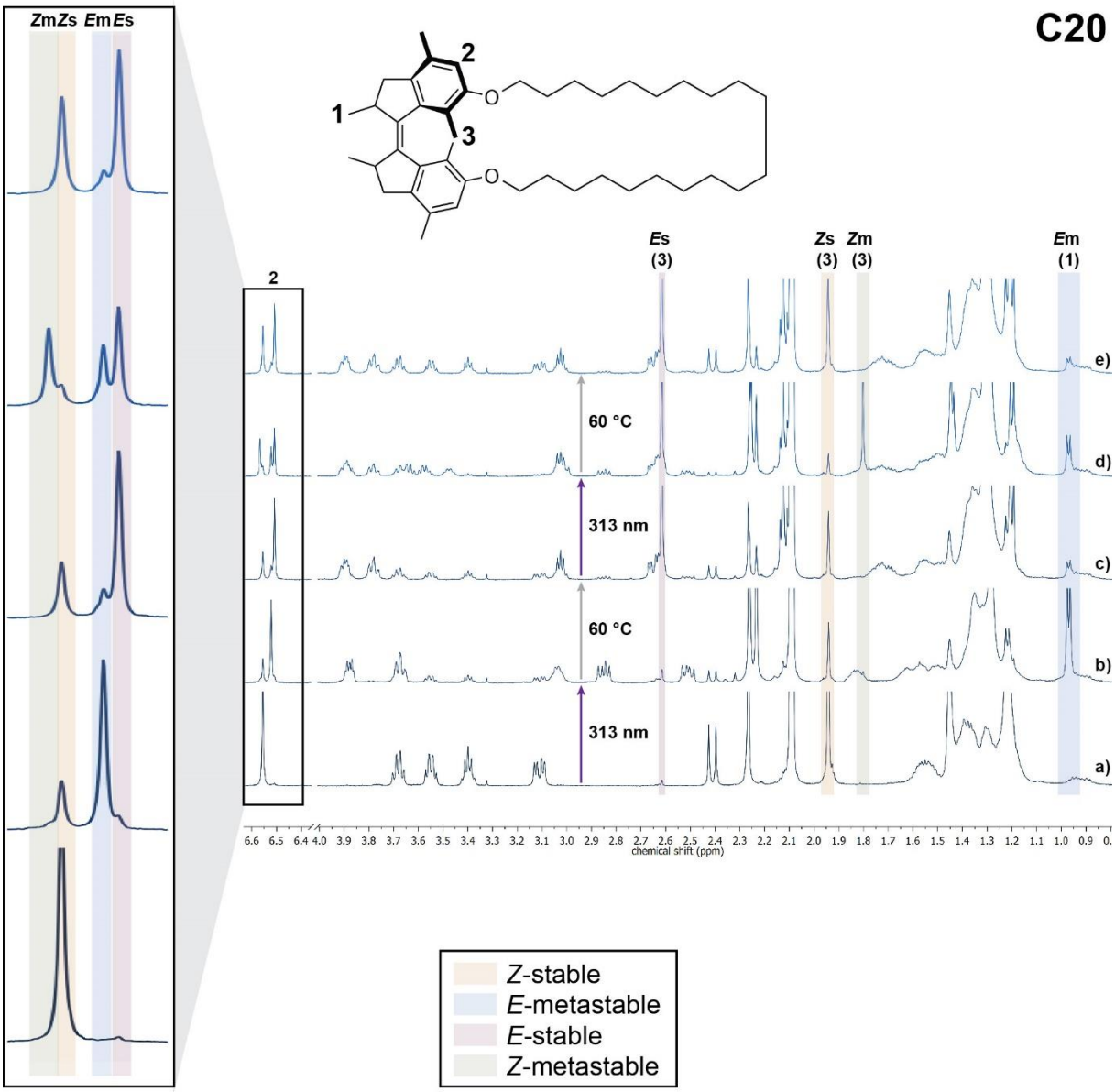

Fig. S7 | Full rotational cycle of C20 followed by ^{1}H NMR spectroscopy (500 MHz, −20 °C, toluene-d_8). a) Non irradiated **C20**-*Z* stable sample, b) PSS mixture after irradiation with 313 nm at −20 °C, c) composition after full relaxation at 60 °C, d) PSS mixture after irradiation with 313 nm at −20 °C, e) composition after full relaxation at 60 °C.

Full rotational cycle of C22

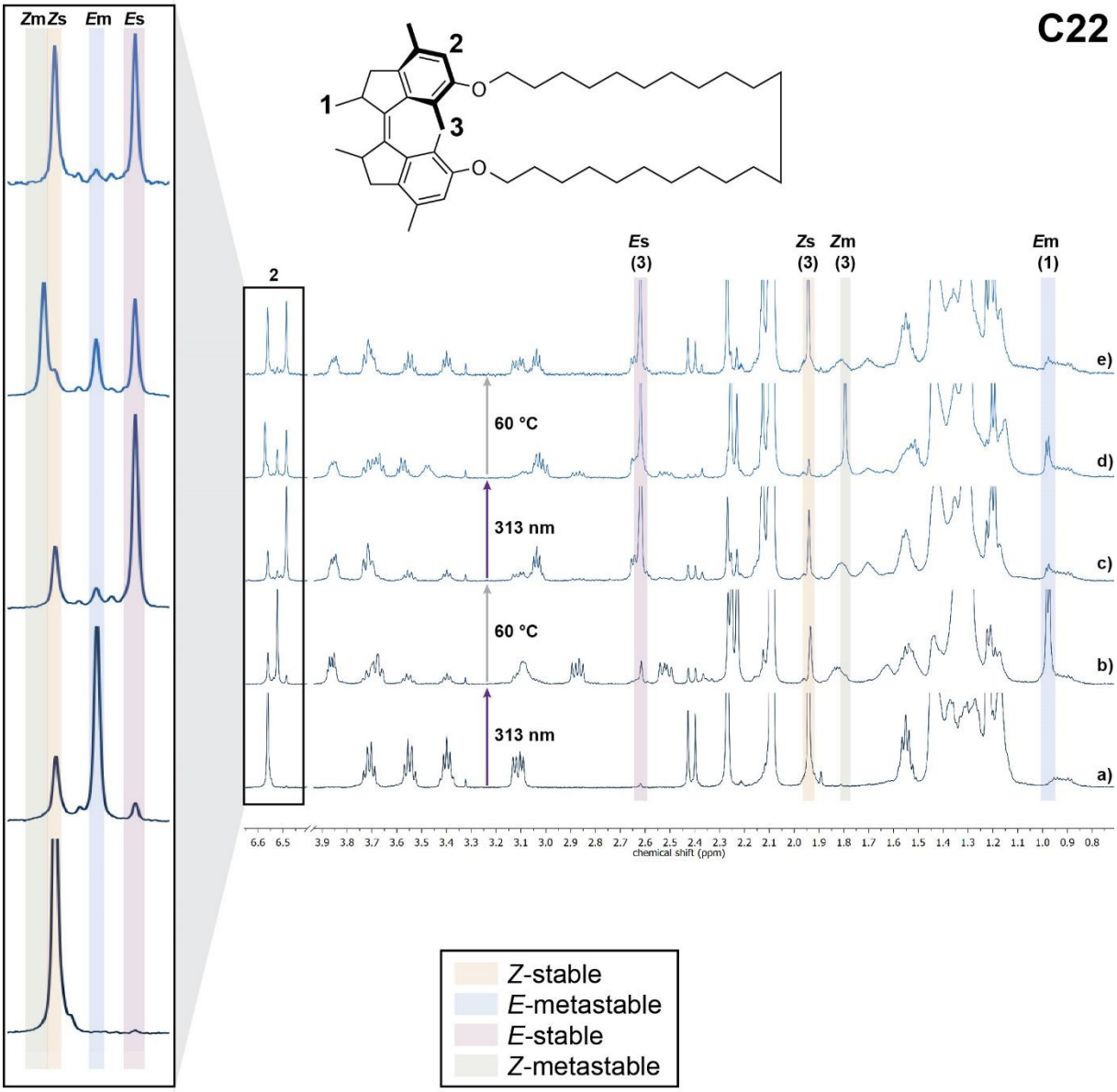

Fig. S8 | Full rotational cycle of C22 followed by ^{1}H NMR spectroscopy (500 MHz, −20 °C, toluene-d_8). a) Non irradiated **C22**-*Z* stable sample, b) PSS mixture after irradiation with 313 nm at −20 °C, c) composition after full relaxation at 60 °C, d) PSS mixture after irradiation with 313 nm at −20 °C, e) composition after full relaxation at 60 °C.

Full rotational cycle of OMe

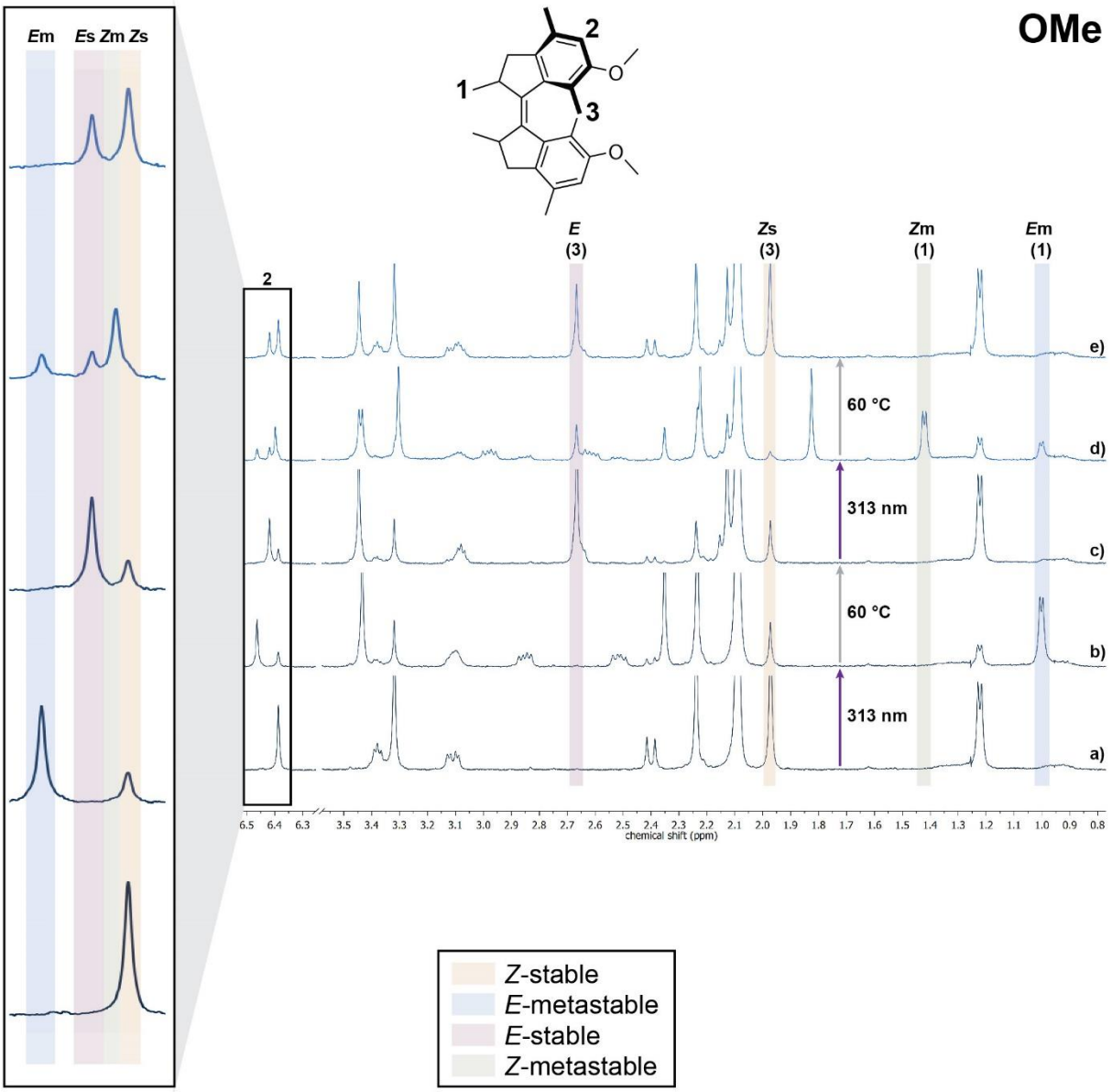

Fig. S9 | Full rotational cycle of OMe followed by ^{1}H NMR spectroscopy (500 MHz, −46 °C, toluene-d_8). a) Non irradiated **OMe**-*Z* stable sample, b) PSS mixture after irradiation with 313 nm at −50 °C, c) composition after full relaxation at 60 °C, d) PSS mixture after irradiation with 313 nm at −50 °C, e) composition after full relaxation at 60 °C.

Eyring Analysis

Degassed UV/vis samples in octane (~20 μM) were measured and irradiated (λ_{irr} = 300 nm THORLABS, LED M300F2) to PSS at −15 °C (−20 °C in case of **OMe**). After switching off the LED, the samples were heated to the desired temperature and the THI was followed by plotting the decay of the absorbance at 355 nm against time to extract the respective rate constants. In order to determine the activation energy $\Delta G^{\ddagger}$, a least square analysis was performed on the Eyring equation (Tab. S3).

Since the activation energies for both THIs of **C16** are similar in energy, ^{1}H NMR spectroscopy was used to determine the rate constants for the THI from *Z* metastable → *Z* stable. A degassed NMR sample in toluene-d_8 (~1 mM) was irradiated (λ_{irr} = 313 nm, Vilber Lourmat, 6W) to PSS at −20 °C. After switching off the light source, the sample was heated to the desired temperature and the THI was followed by plotting the decay of the integrals at 1.64 ppm against time to extract the respective rate constants.

Table S3 | Activation energies for thermal helix inversions and double bond isomerizations of macrocycles C8–22 and reference compound OMe. If not otherwise stated, energies were determined by UV/vis spectroscopy in octane and are reported for 20 °C. $\Delta G^{\ddagger}$ and $\Delta H^{\ddagger}$ are given in kcal/mol; $\Delta S^{\ddagger}$ is given in cal/(K · mol).

Compound	**ΔG‡** (*E*m ⟶ *Z*s) [ΔH‡, ΔS‡, $t_{1/2}$]	**ΔG‡** (*E*m ⟶ *E*s) [ΔH‡, ΔS‡, $t_{1/2}$]	**ΔG‡** (*Z*m ⟶ *Z*s) [ΔH‡, ΔS‡, $t_{1/2}$]
C8	18.8±0.2 [18.2, −2.16, 12 s]	---	---
C10	25.3±0.1 [26.3, 3.56, 9.4 d]	---	---
C12	29.0±0.1[a] [29.8, 2.22, 49 min]	---	---
C14	≥ 32[a,b] [38 h]	---	---
C16	---	22.1±0.1 [14.1, −27.5, 58 min]	23.6±0.2[c] [19.9, −12.5, 13 h]
C18	---	20.4±0.1 [18.1, −7.70, 3.0 min]	23.7±0.1 [19.9, −12.8, 14 h]
C20	---	20.3±0.1 [17.3, −9.95, 2.4 min]	23.7±0.1 [19.3, −15.0, 14 h]
C22	---	20.1±0.1 [18.6, −4.99, 1.7 min]	23.7±0.1 [19.5, −14.4, 15 h]
OMe	---	18.6±0.3 [15.7, −9.99, 11 s]	23.4±0.2 [19.5, −13.3, 9.0 h]

(a) energy given at 110 °C; (b) energy estimated from a single relaxation at 110 °C; (c) energy determined by ^{1}H NMR spectroscopy in toluene-d_8

Thermal double bond isomerization from C8-*E* metastable to C8-*Z* stable

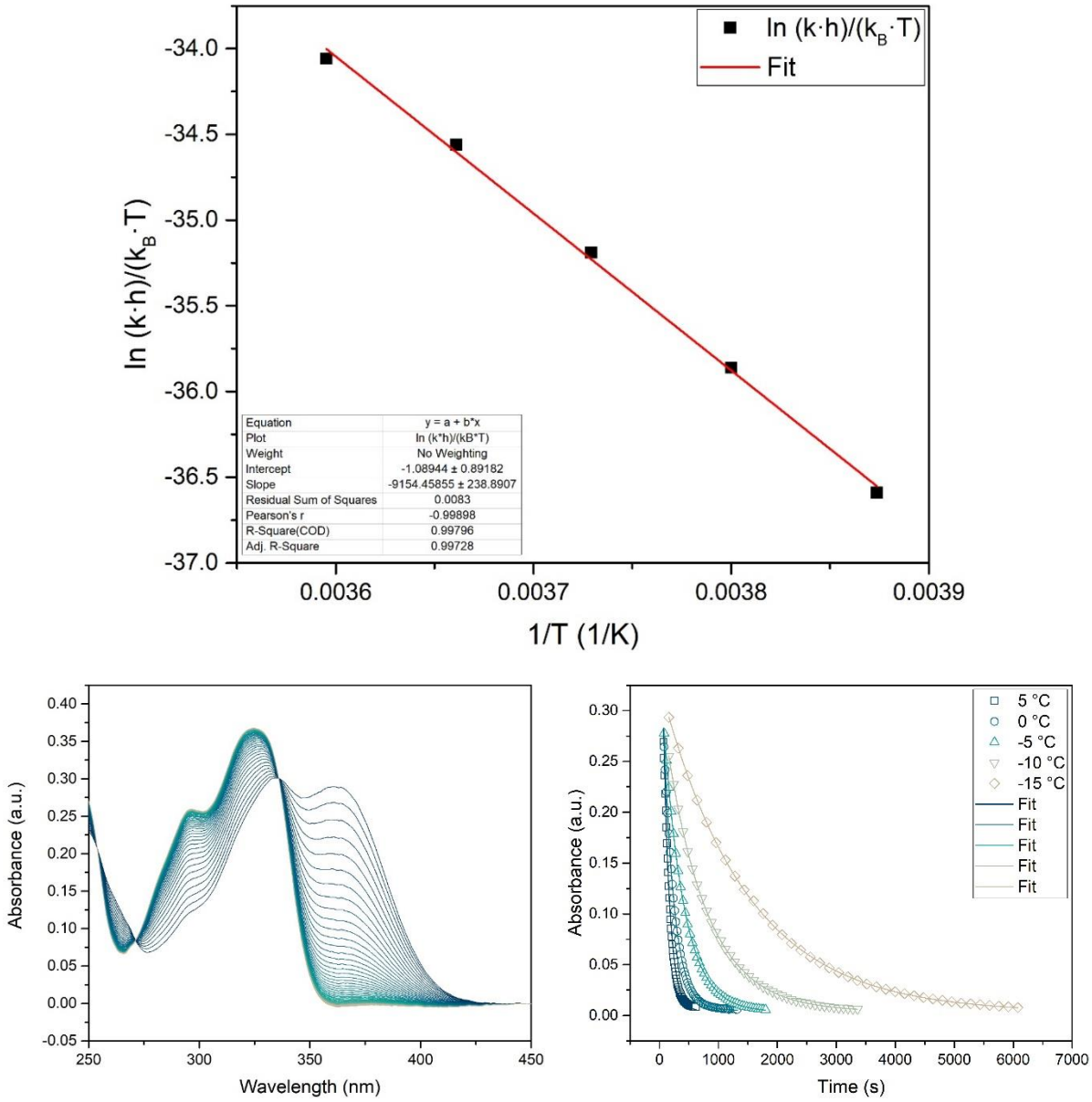

Fig. S10 | Eyring analysis of thermal double bond isomerization from C8-*E* metastable to C8-*Z* stable. Rate constants were determined by UV/vis spectroscopy in octane (~20 μM) at −15, −10, −5, 0 and 5 °C. Eyring plot (top), representative example for thermal isomerization followed by UV/vis spectroscopy at 0 °C (bottom left) and decay curves (bottom right). Start: blue spectrum, end: brown spectrum.

Thermal double bond isomerization from C10-*E* metastable to C10-*Z* stable

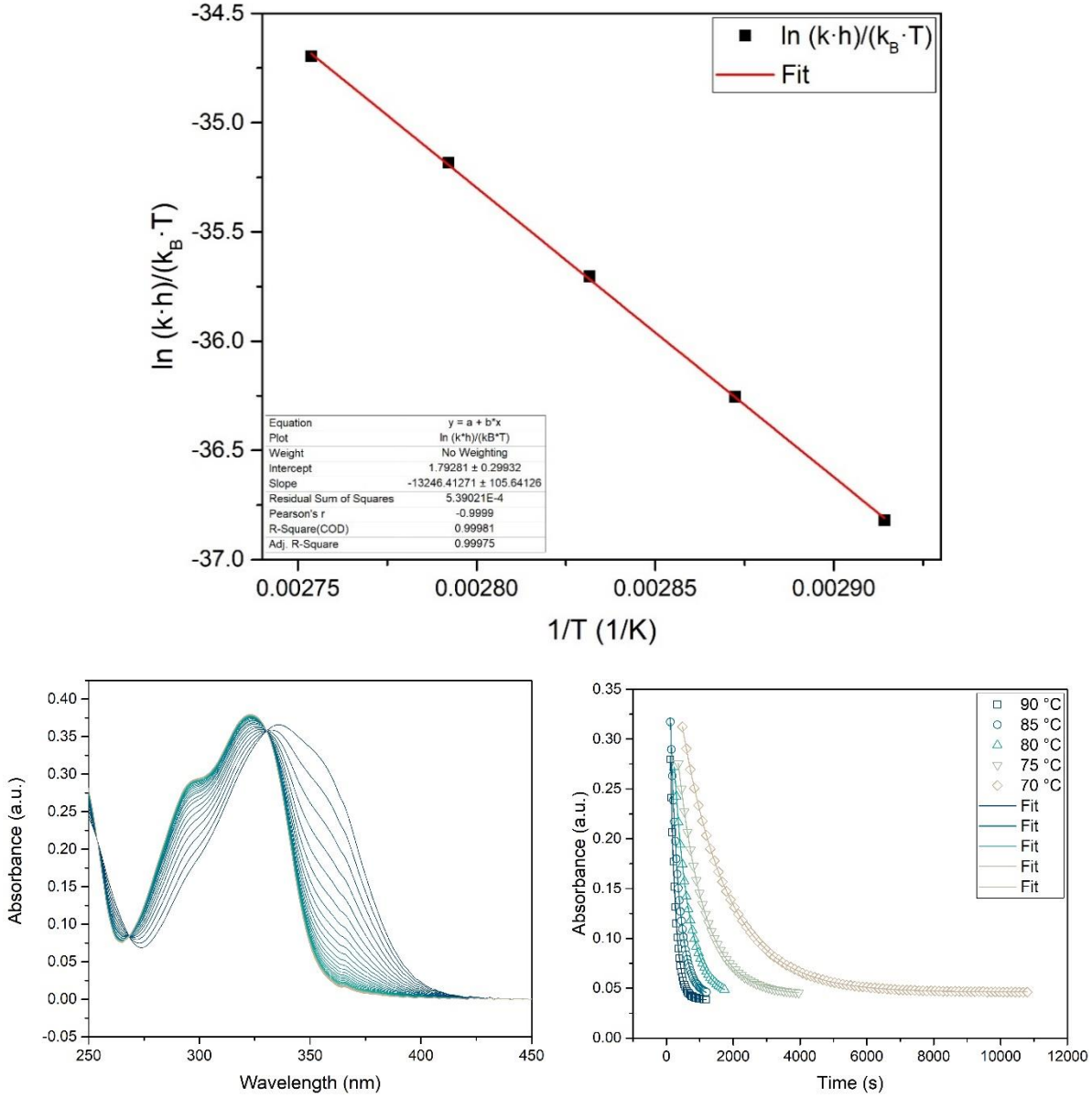

Fig. S11 | Eyring analysis of thermal double bond isomerization from C10-*E* metastable to C10-*Z* stable. Rate constants were determined by UV/vis spectroscopy in octane (~20 μM) at 70, 75, 80, 85 and 90 °C. Eyring plot (top), representative example for thermal isomerization followed by UV/vis spectroscopy at 90 °C (bottom left) and decay curves (bottom right). Start: blue spectrum, end: brown spectrum.

Thermal double bond isomerization from C12-*E* metastable to C12-*Z* stable

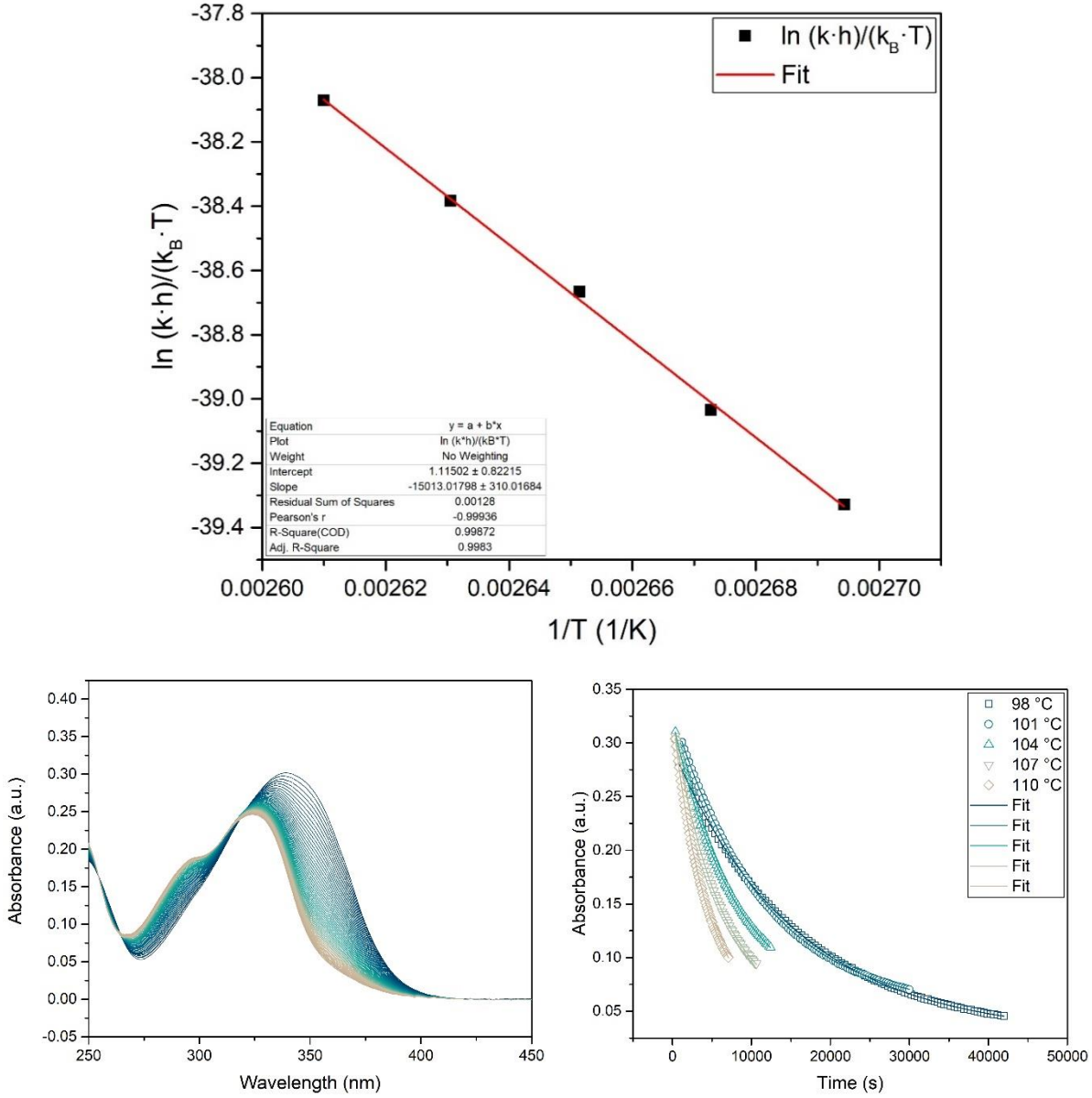

Fig. S12 | Eyring analysis of thermal double bond isomerization from C12-*E* metastable to C12-*Z* stable. Rate constants were determined by UV/vis spectroscopy in octane (~20 μM) at 98, 101, 104, 107 and 110 °C. Eyring plot (top), representative example for thermal isomerization followed by UV/vis spectroscopy at 101 °C (bottom left) and decay curves (bottom right). Start: blue spectrum, end: brown spectrum.

Thermal double bond isomerization from C14-*E* metastable to C14-*Z* stable

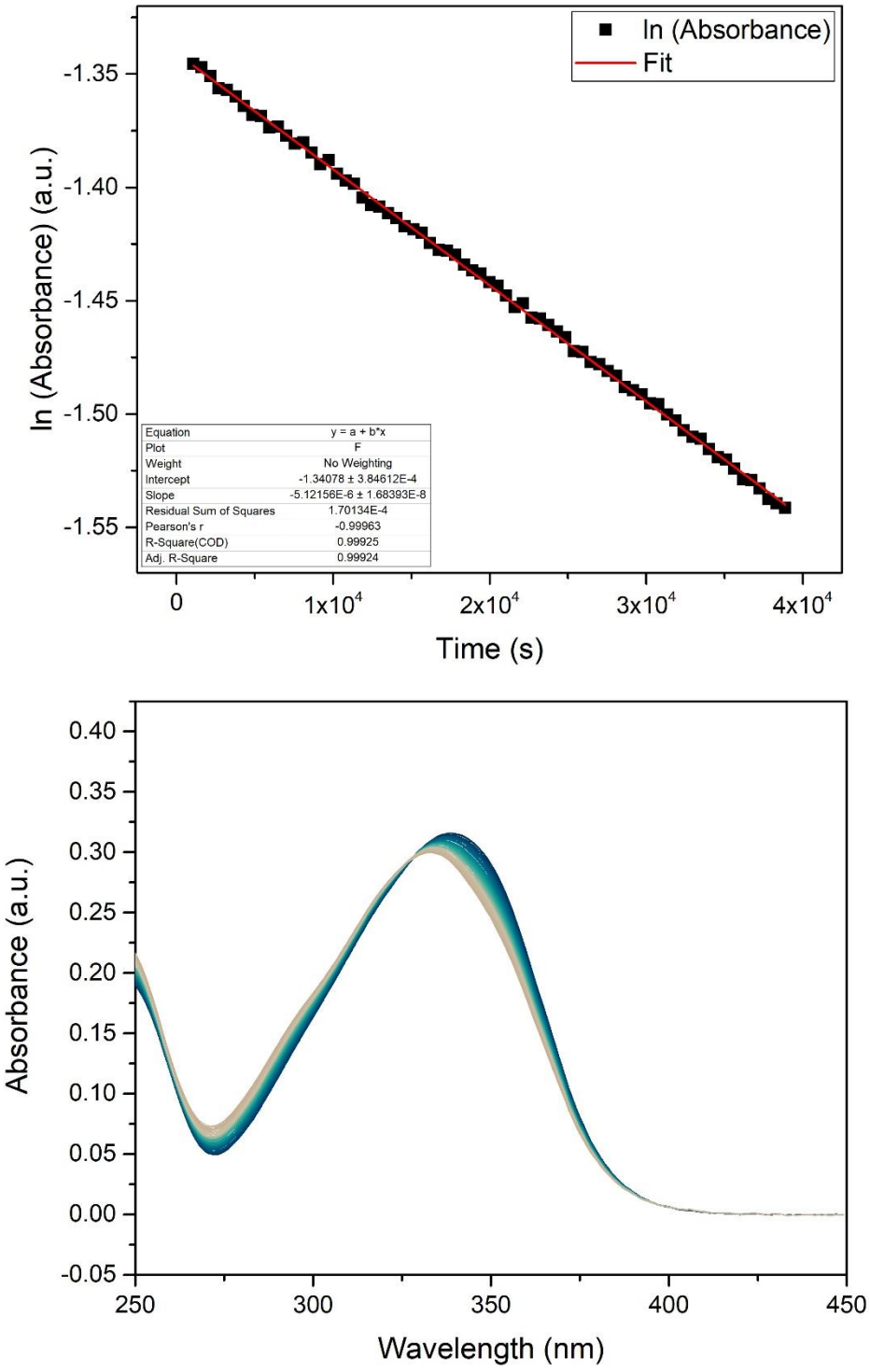

Fig. S13 | Half-life of thermal double bond isomerization from C14-*E* metastable to C14-*Z* stable. Rate constant was determined by UV/vis spectroscopy in octane (~20 μM) at 110 °C. Linear fit (top) and thermal isomerization followed by UV/vis spectroscopy at 110 °C (bottom). Start: blue spectrum, end: brown spectrum.

Thermal helix inversion from C16-*E* metastable to C16-*E* stable

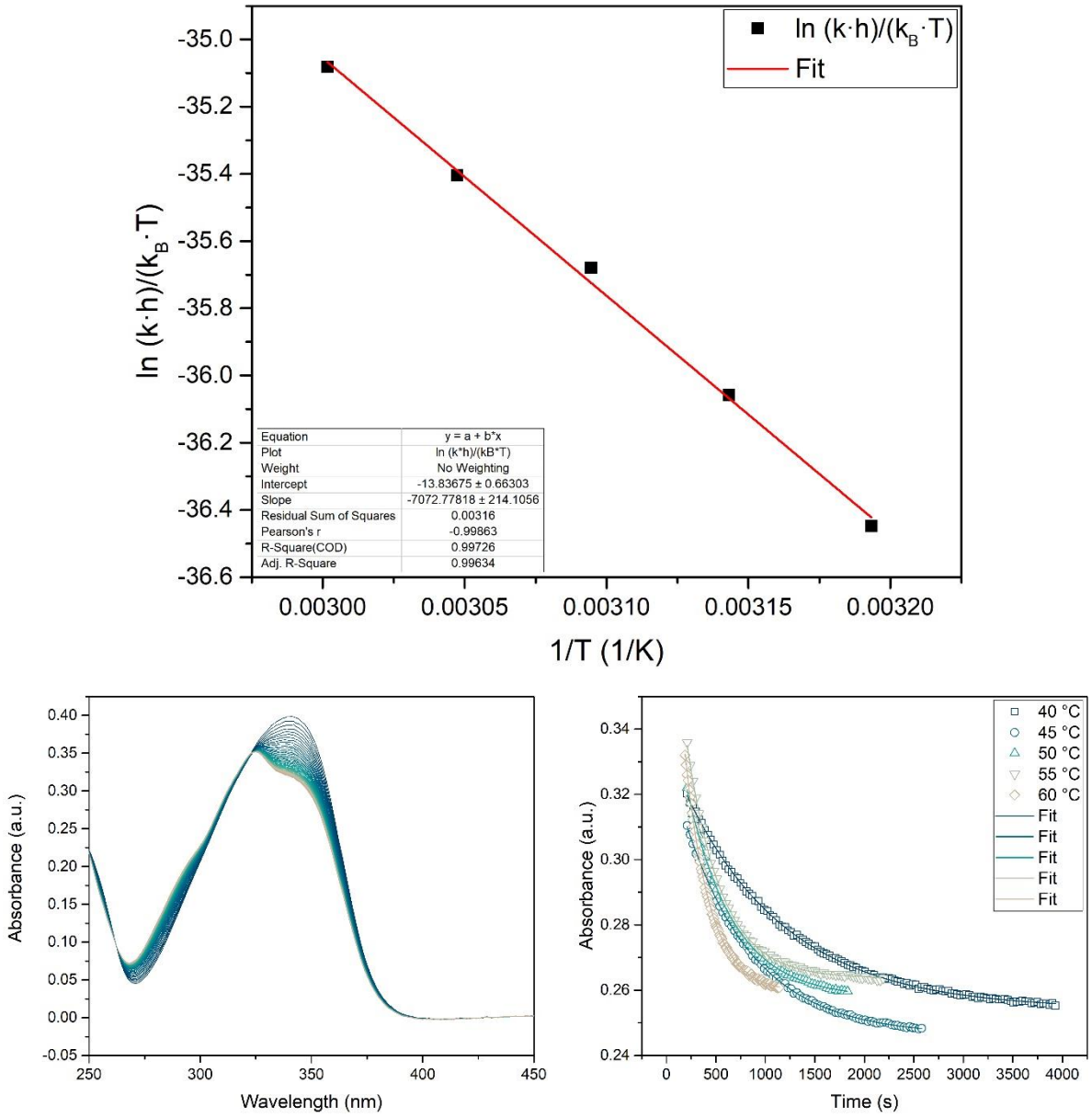

Fig. S14 | Eyring analysis of thermal helix inversion from C16-*E* metastable to C16-*E* stable. Rate constants were determined by UV/vis spectroscopy in octane (~20 μM) at 40, 45, 50, 55 and 60 °C. Eyring plot (top), representative example for thermal isomerization followed by UV/vis spectroscopy at 50 °C (bottom left) and decay curves (bottom right). Start: blue spectrum, end: brown spectrum.

Thermal helix inversion from C16-*Z* metastable to C16-*Z* stable

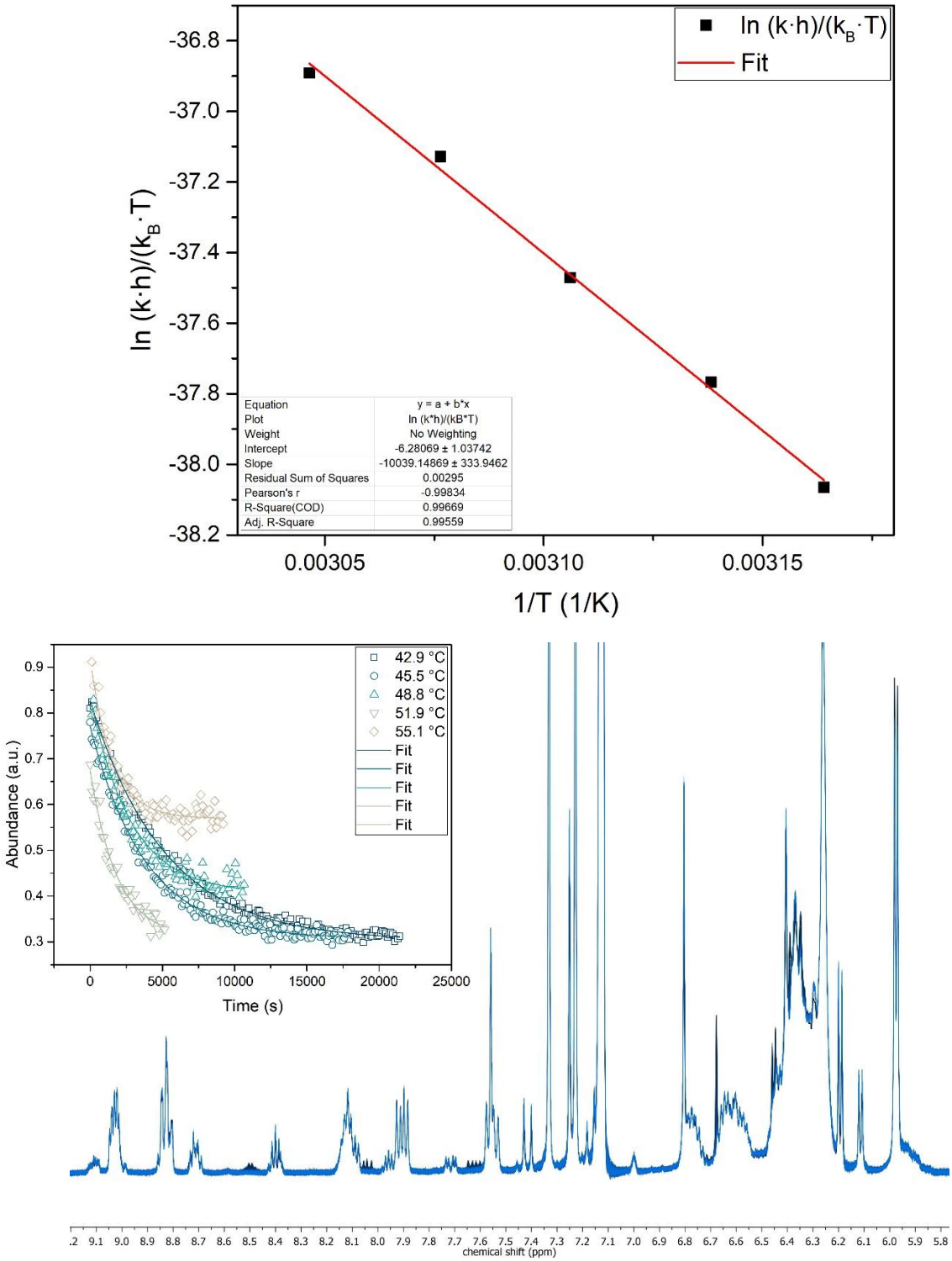

Fig. S15 | Eyring analysis of thermal helix inversion from C16-*Z* metastable to C16-*Z* stable. Rate constants were determined by ^{1}H NMR spectroscopy in toluene-d_8 (~1 mM) at 42.9, 45.5, 48.8, 51.9 and 55.1 °C. Eyring plot (top), representative example for thermal isomerization followed by ^{1}H NMR spectroscopy at 42.9 °C (bottom) and decay curves (inset). Start: black spectrum, end: blue spectrum.

Thermal helix inversion from C18-*E* metastable to C18-*E* stable

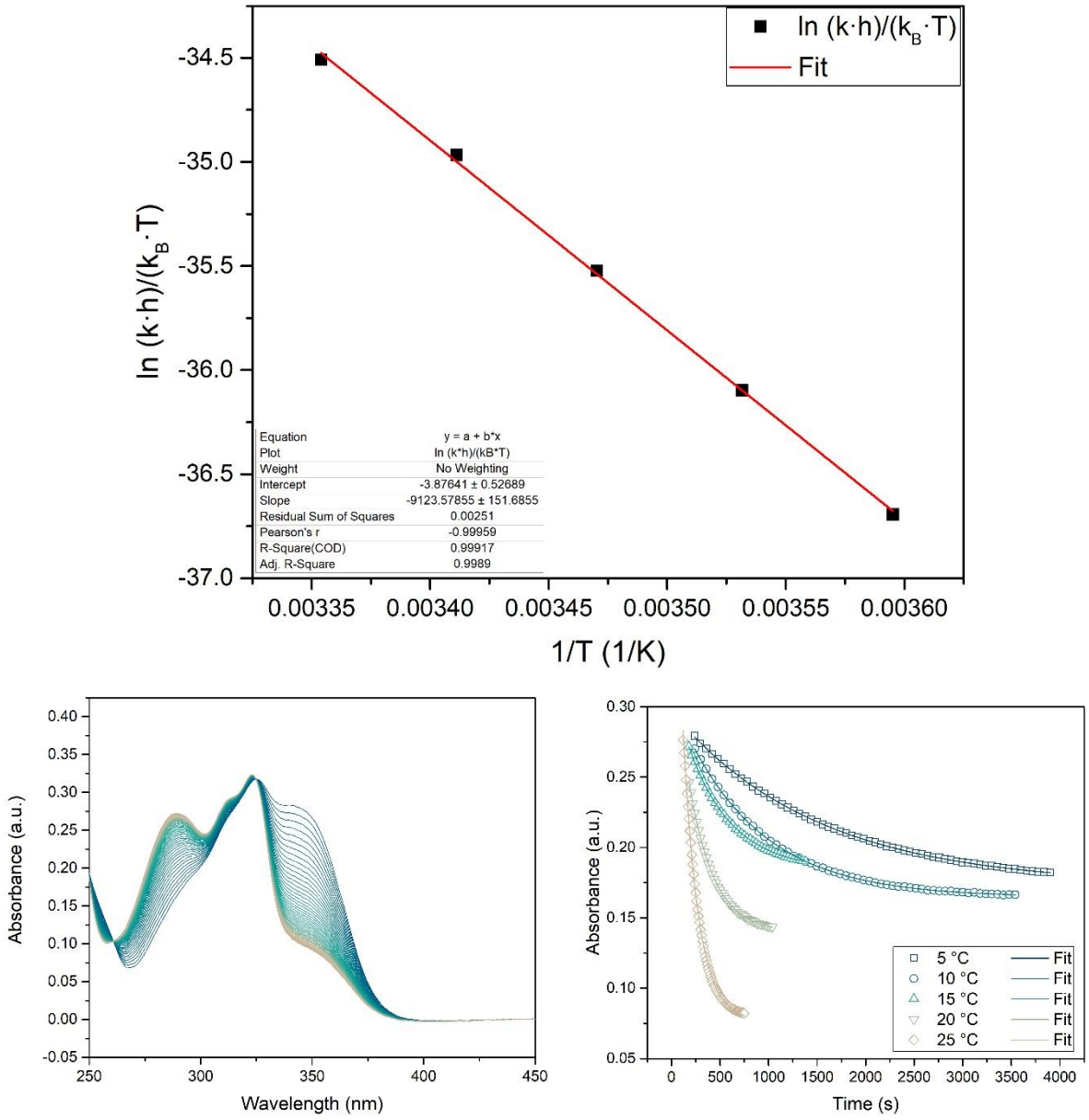

Fig. S16 | Eyring analysis of thermal helix inversion from C16-*E* metastable to C18-*E* stable. Rate constants were determined by UV/vis spectroscopy in octane (~20 μM) at 5, 10, 15, 20 and 25 °C. Eyring plot (top), representative example for thermal isomerization followed by UV/vis spectroscopy at 25 °C (bottom left) and decay curves (bottom right). Start: blue spectrum, end: brown spectrum.

Thermal helix inversion from C18-*Z* metastable to C18-*Z* stable

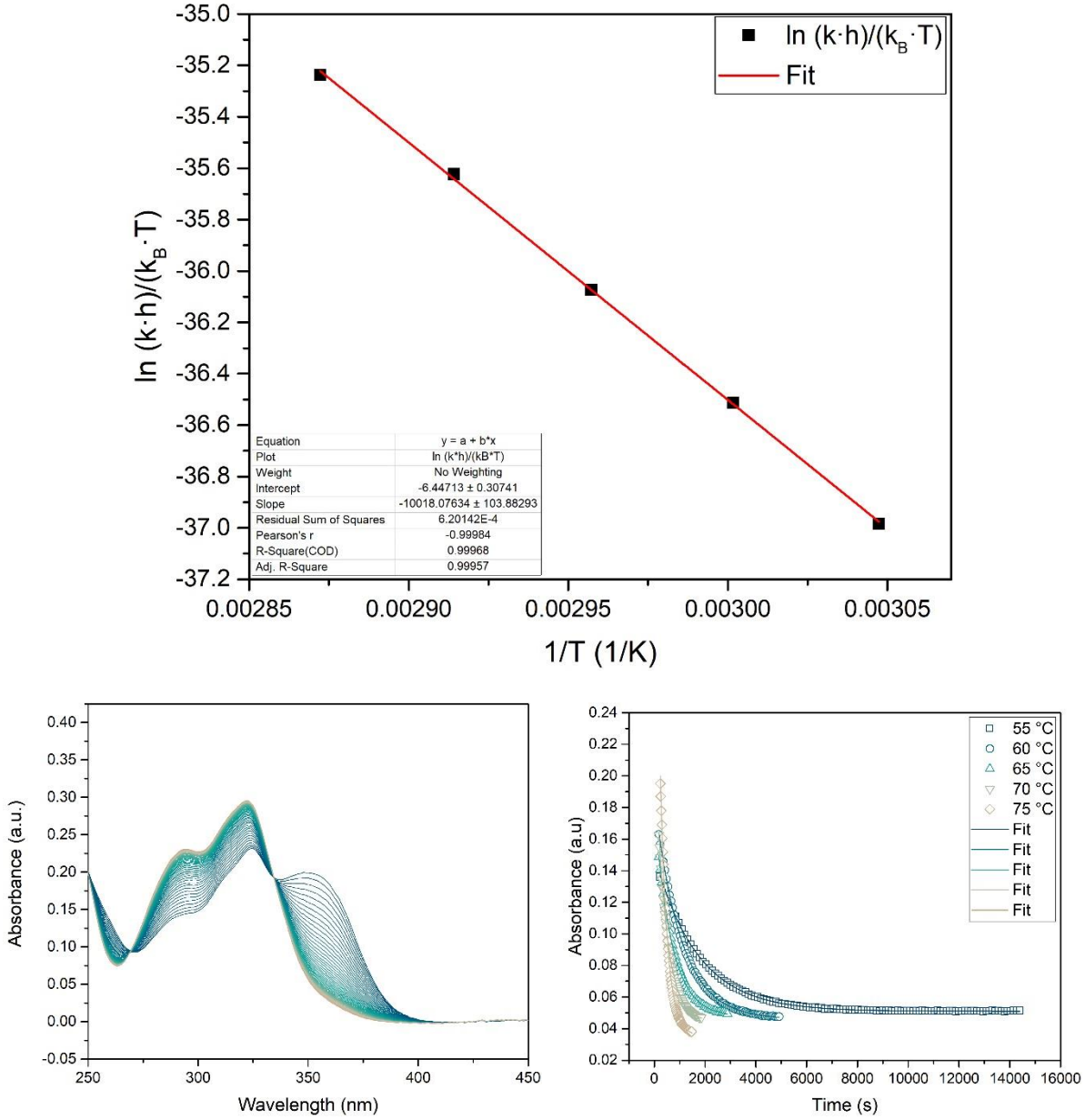

Fig. S17 | Eyring analysis of thermal helix inversion from C18-*Z* metastable to C18-*Z* stable. Rate constants were determined by UV/vis spectroscopy in octane (~20 μM) at 55, 60, 65, 70 and 75 °C. Eyring plot (top), representative example for thermal isomerization followed by UV/vis spectroscopy at 75 °C (bottom left) and decay curves (bottom right). Start: blue spectrum, end: brown spectrum.

Thermal helix inversion from C20-*E* metastable to C20-*E* stable

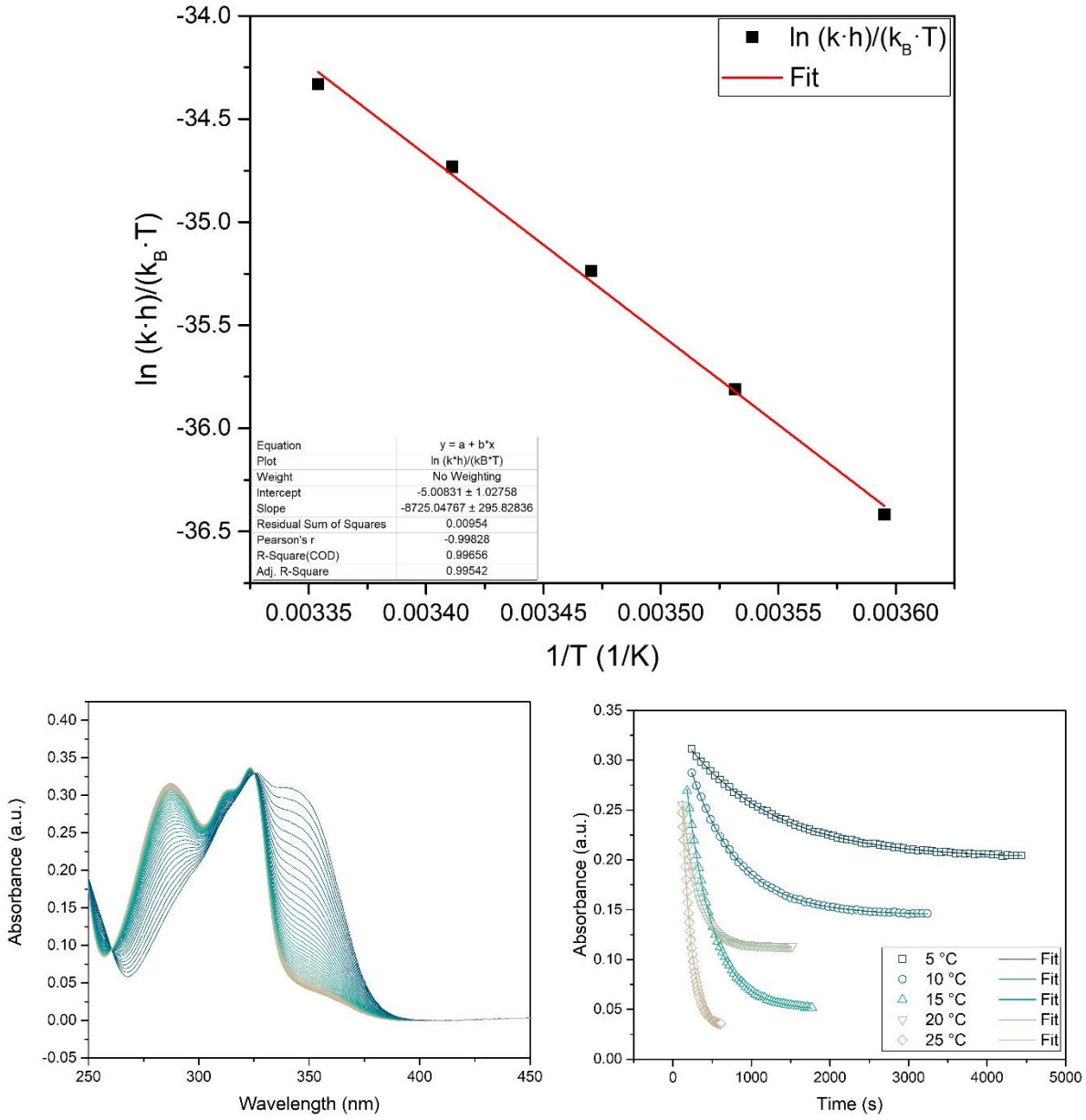

Fig. S18 | Eyring analysis of thermal helix inversion from C20-*E* metastable to C20-*E* stable. Rate constants were determined by UV/vis spectroscopy in octane (~20 μM) at 5, 10, 15, 20 and 25 °C. Eyring plot (top), representative example for thermal isomerization followed by UV/vis spectroscopy at 25 °C (bottom left) and decay curves (bottom right). Start: blue spectrum, end: brown spectrum.

Thermal helix inversion from C20-*Z* metastable to C20-*Z* stable

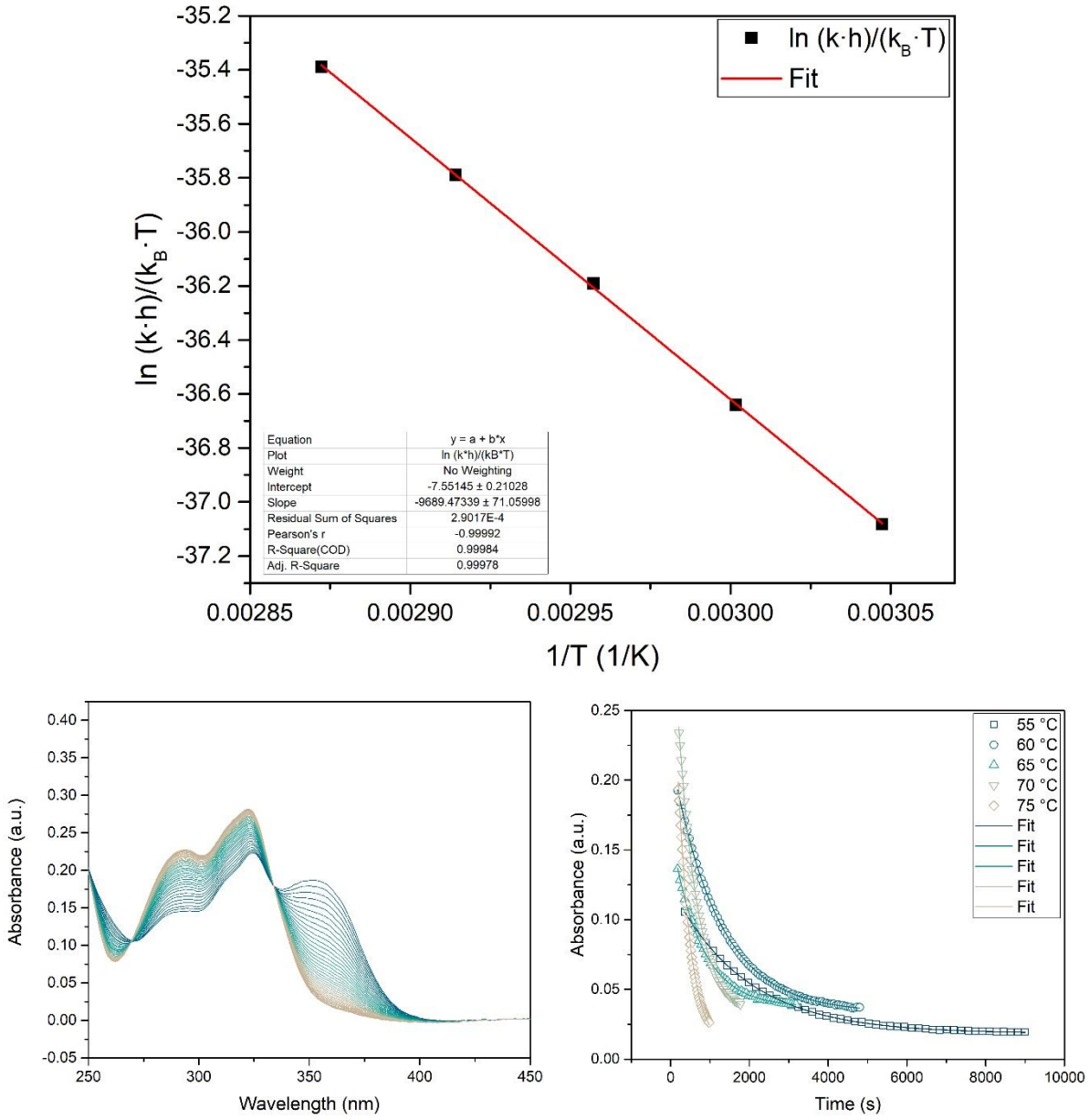

Fig. S19 | Eyring analysis of thermal helix inversion from C20-*Z* metastable to C20-*Z* stable. Rate constants were determined by UV/vis spectroscopy in octane (~20 μM) at 55, 60, 65, 70 and 75 °C. Eyring plot (top), representative example for thermal isomerization followed by UV/vis spectroscopy at 75 °C (bottom left) and decay curves (bottom right). Start: blue spectrum, end: brown spectrum.

Thermal helix inversion from C22-*E* metastable to C22-*E* stable

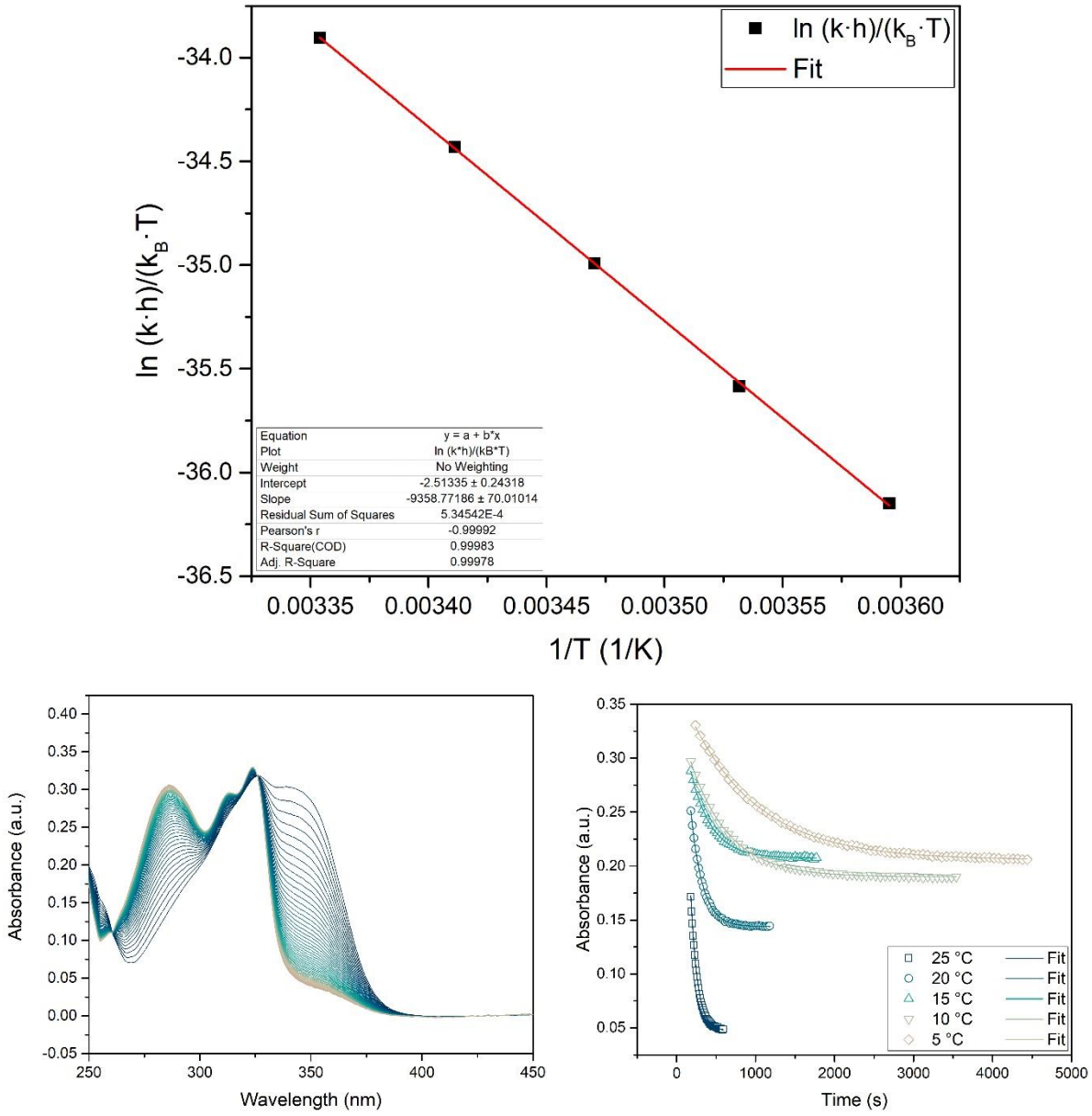

Fig. S20 | Eyring analysis of thermal helix inversion from C22-*E* metastable to C22-*E* stable. Rate constants were determined by UV/vis spectroscopy in octane (~20 μM) at 5, 10, 15, 20 and 25 °C. Eyring plot (top), representative example for thermal isomerization followed by UV/vis spectroscopy at 5 °C (bottom left) and decay curves (bottom right). Start: blue spectrum, end: brown spectrum.

Thermal helix inversion from C22-*Z* metastable to C22-*Z* stable

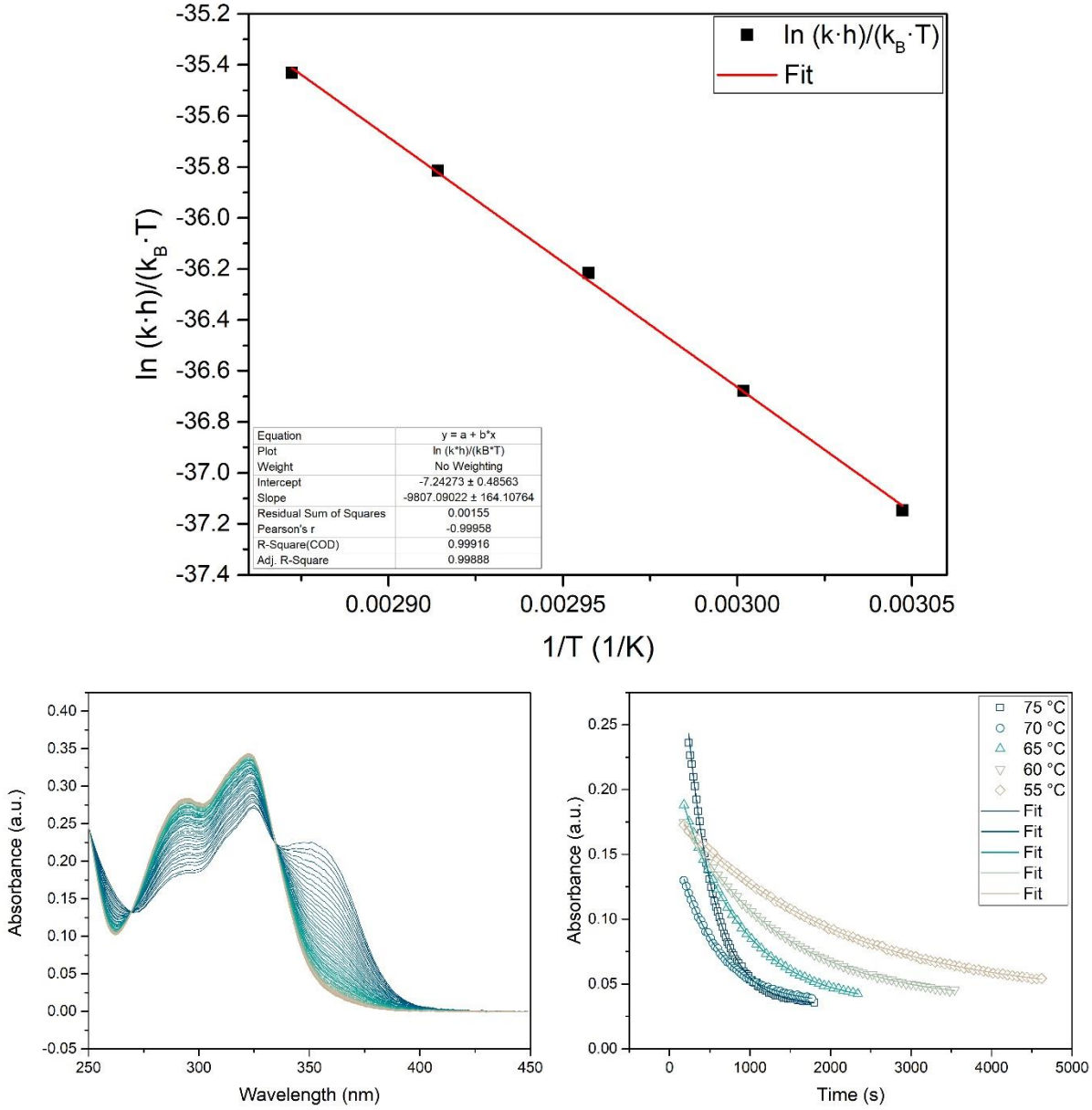

Fig. S21 | Eyring analysis of thermal helix inversion from C22-*Z* metastable to C22-*Z* stable. Rate constants were determined by UV/vis spectroscopy in octane (~20 μM) at 50, 55, 60, 65 and 70 °C. Eyring plot (top), representative example for thermal isomerization followed by UV/vis spectroscopy at 50 °C (bottom left) and decay curves (bottom right). Start: blue spectrum, end: brown spectrum.

Thermal helix inversion from OMe-*E* metastable to OMe-*E* stable

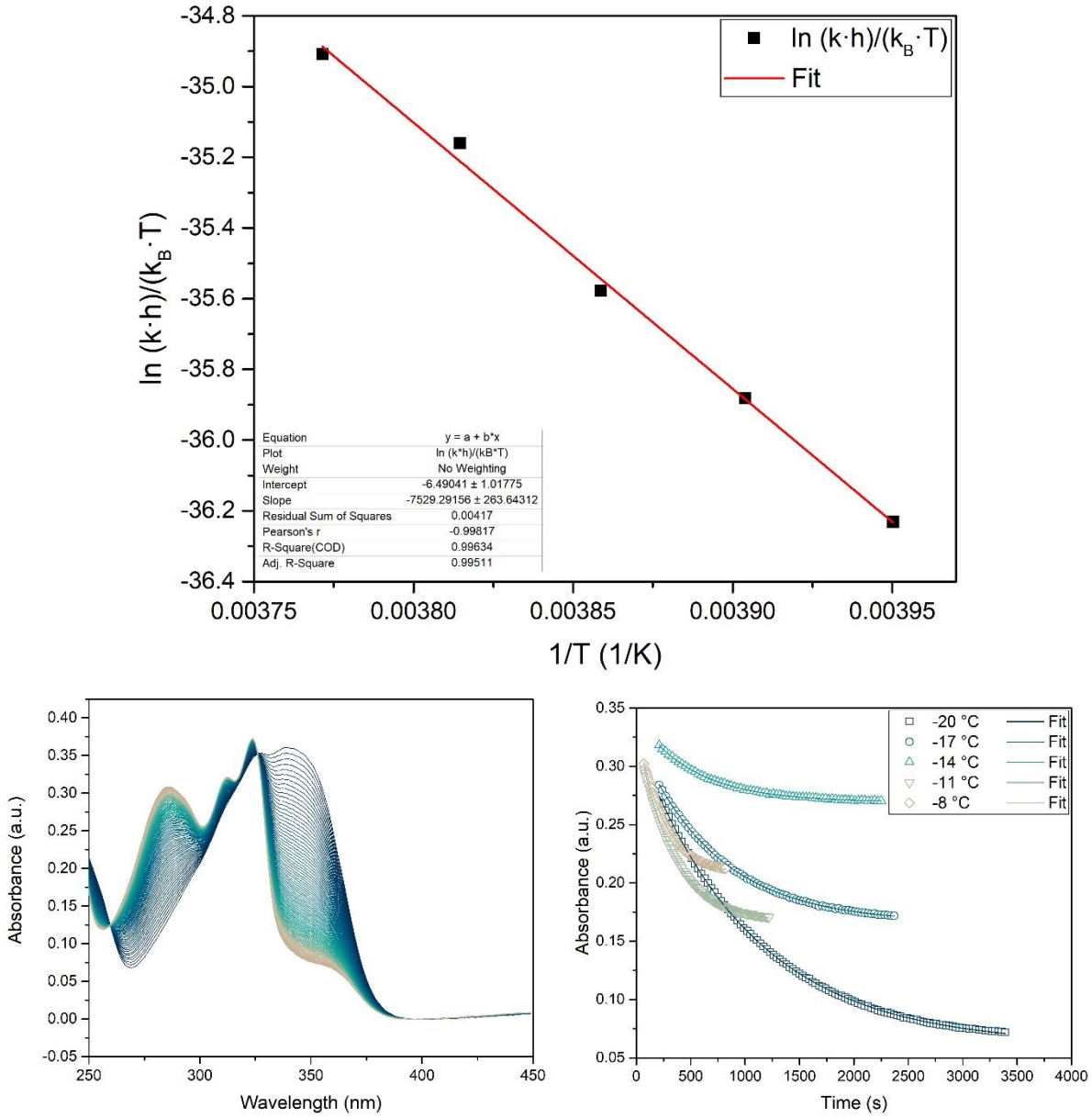

Fig. S22 | Eyring analysis of thermal helix inversion from OMe-*E* metastable to OMe-*E* stable. Rate constants were determined by UV/vis spectroscopy in octane (~20 μM) at −20, −17, −14, −11 and −8 °C. Eyring plot (top), representative example for thermal isomerization followed by UV/vis spectroscopy at −20 °C (bottom left) and decay curves (bottom right). Start: blue spectrum, end: brown spectrum.

Thermal helix inversion from OMe-*Z* metastable to OMe-*Z* stable

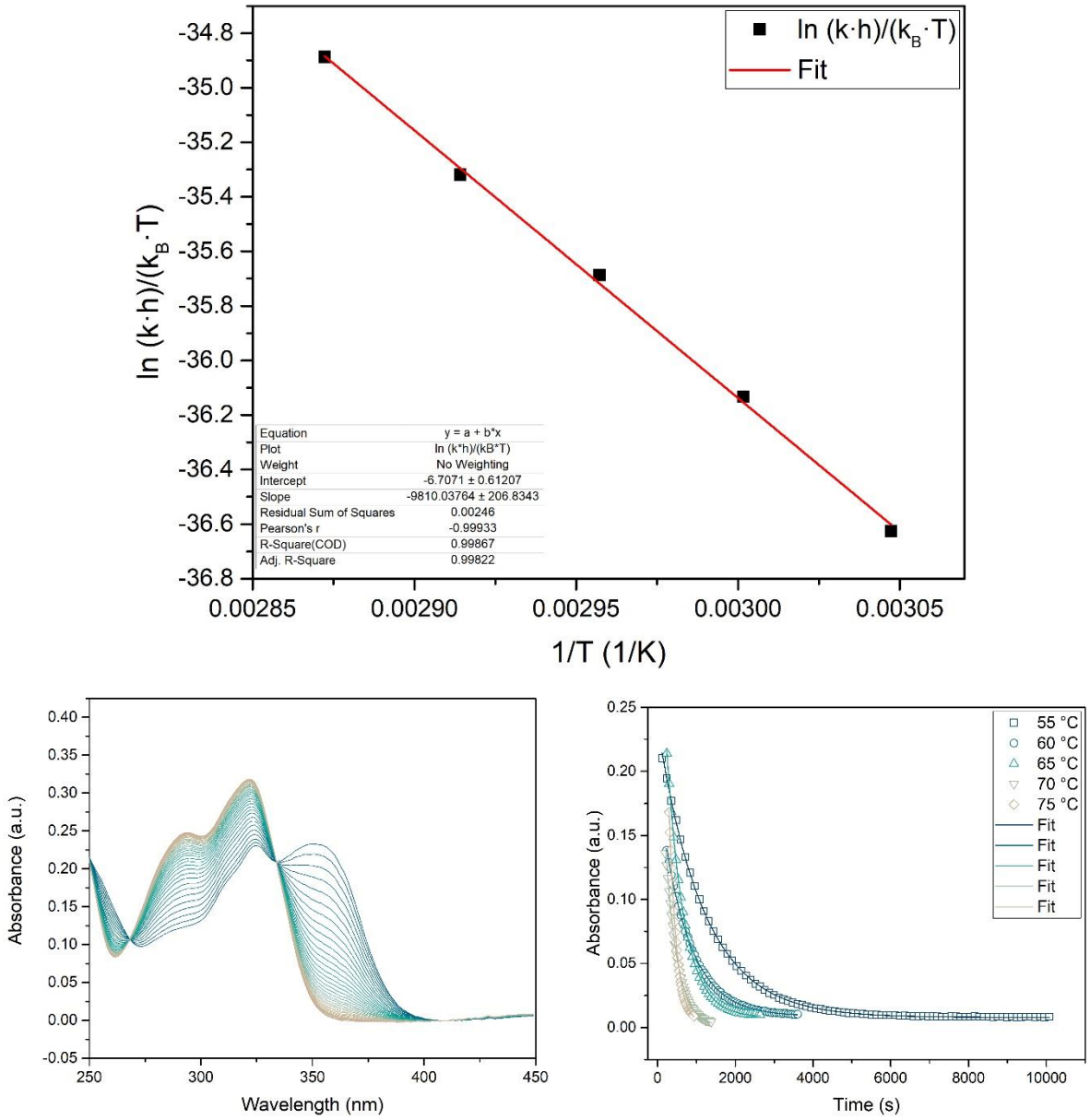

Fig. S23 | Eyring analysis of thermal helix inversion from OMe-*Z* metastable to OMe-*Z* stable. Rate constants were determined by UV/vis spectroscopy in octane (~20 μM) at 55, 60, 65, 70 and 75 °C. Eyring plot (top), representative example for thermal isomerization followed by UV/vis spectroscopy at 75 °C (bottom left) and decay curves (bottom right). Start: blue spectrum, end: brown spectrum.

UV/vis spectroscopy

Degassed UV/vis samples in octane (~20 μM) were irradiated with a 300 nm LED (THORLABS, M300F2) at −15 °C (−20 °C in case of **OMe**).

Switching behavior of C8

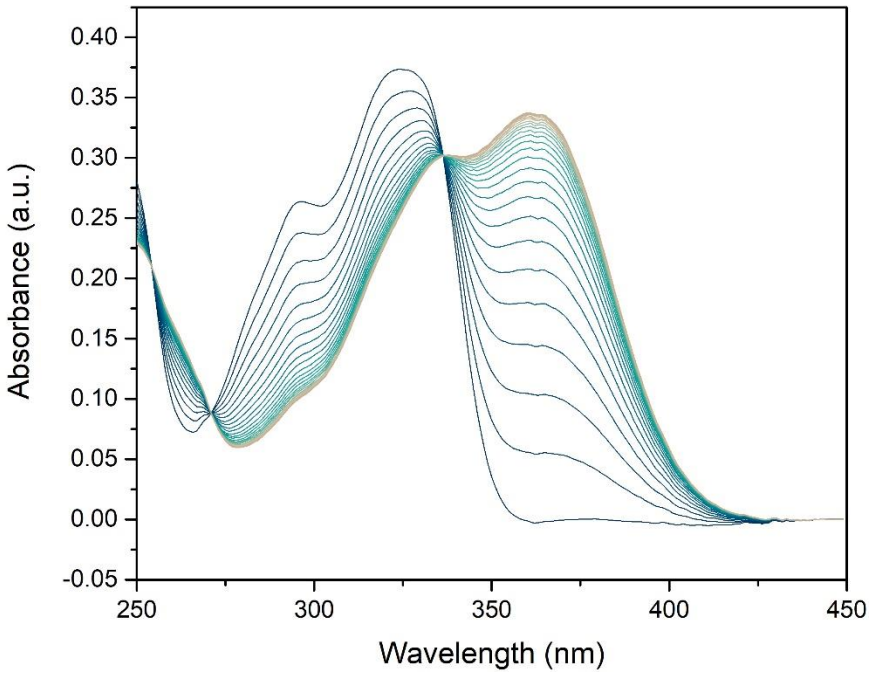

Fig. S24 | Irradiation of C8 followed by UV/vis spectroscopy (octane, ~20 μM, −15 °C). A solution of **C8**-*Z* stable was irradiated with 300 nm. Start: blue spectrum, end: brown spectrum.

Switching behavior of C10

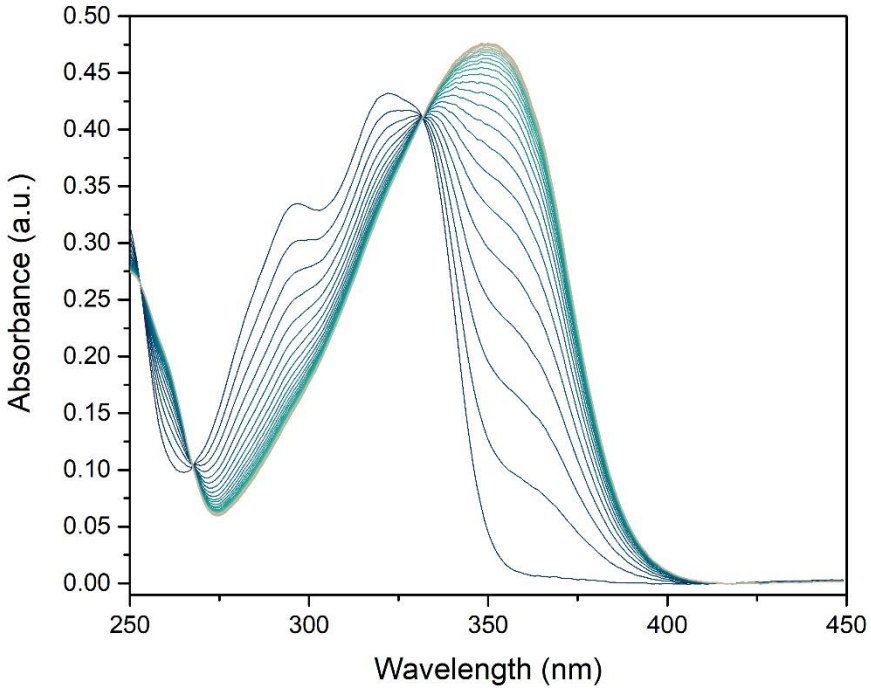

Fig. S25 | Irradiation of C10 followed by UV/vis spectroscopy (octane, ~20 μM, −15 °C). A solution of **C10**-*Z* stable was irradiated with 300 nm. Start: blue spectrum, end: brown spectrum.

Switching behavior of C12

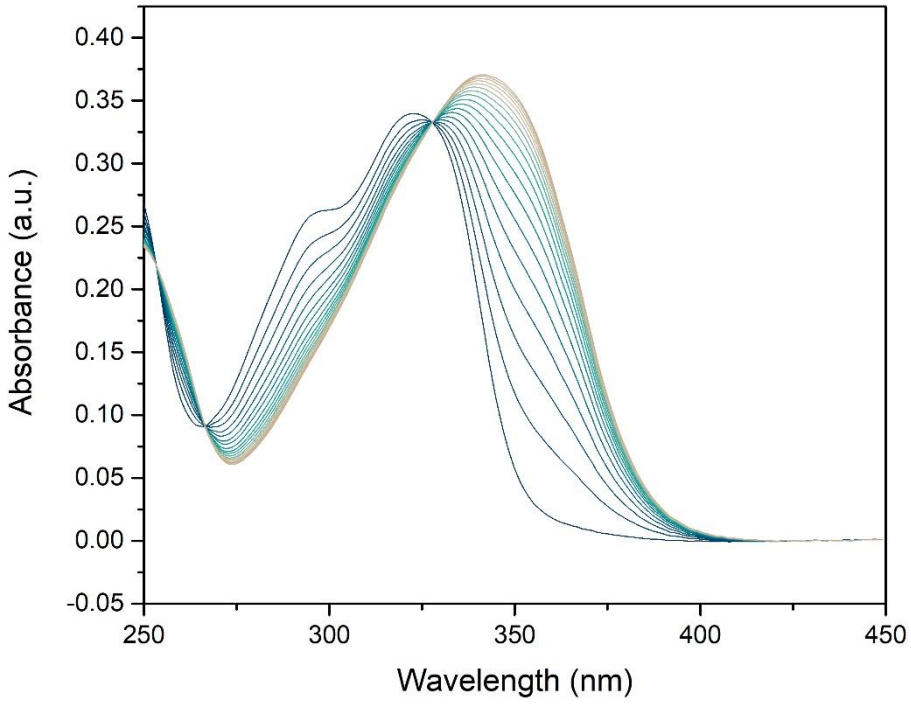

Fig. S26 | Irradiation of C12 followed by UV/vis spectroscopy (octane, ~20 μM, −15 °C). A solution of **C12**-*Z* stable was irradiated with 300 nm. Start: blue spectrum, end: brown spectrum.

Switching behavior of C14

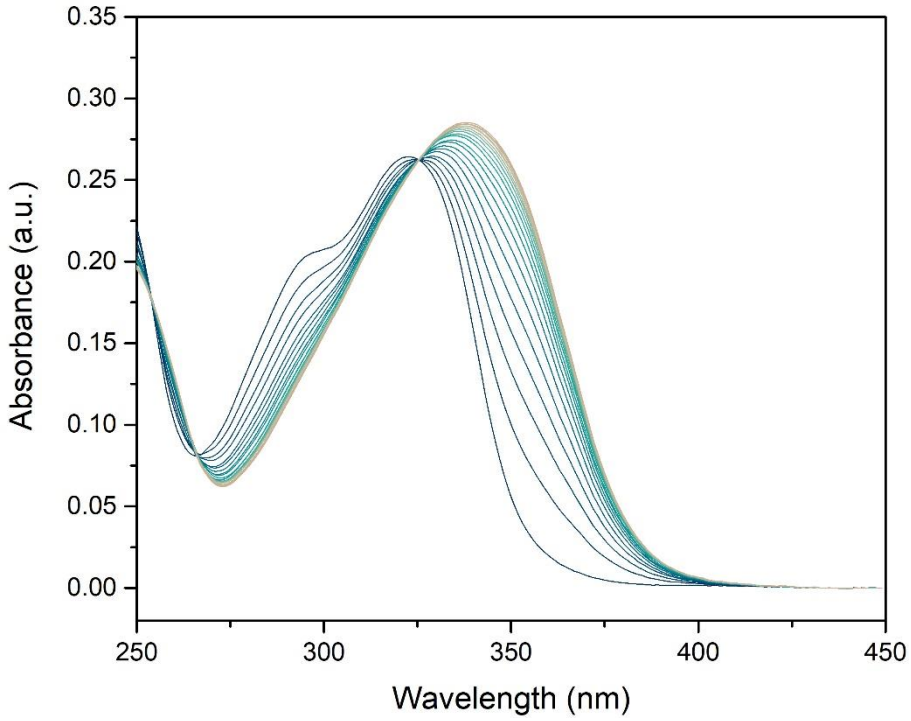

Fig. S27 | Irradiation of C14 followed by UV/vis spectroscopy (octane, ~20 μM, −15 °C). A solution of **C14**-*Z* stable was irradiated with 300 nm. Start: blue spectrum, end: brown spectrum.

Switching behavior of C16

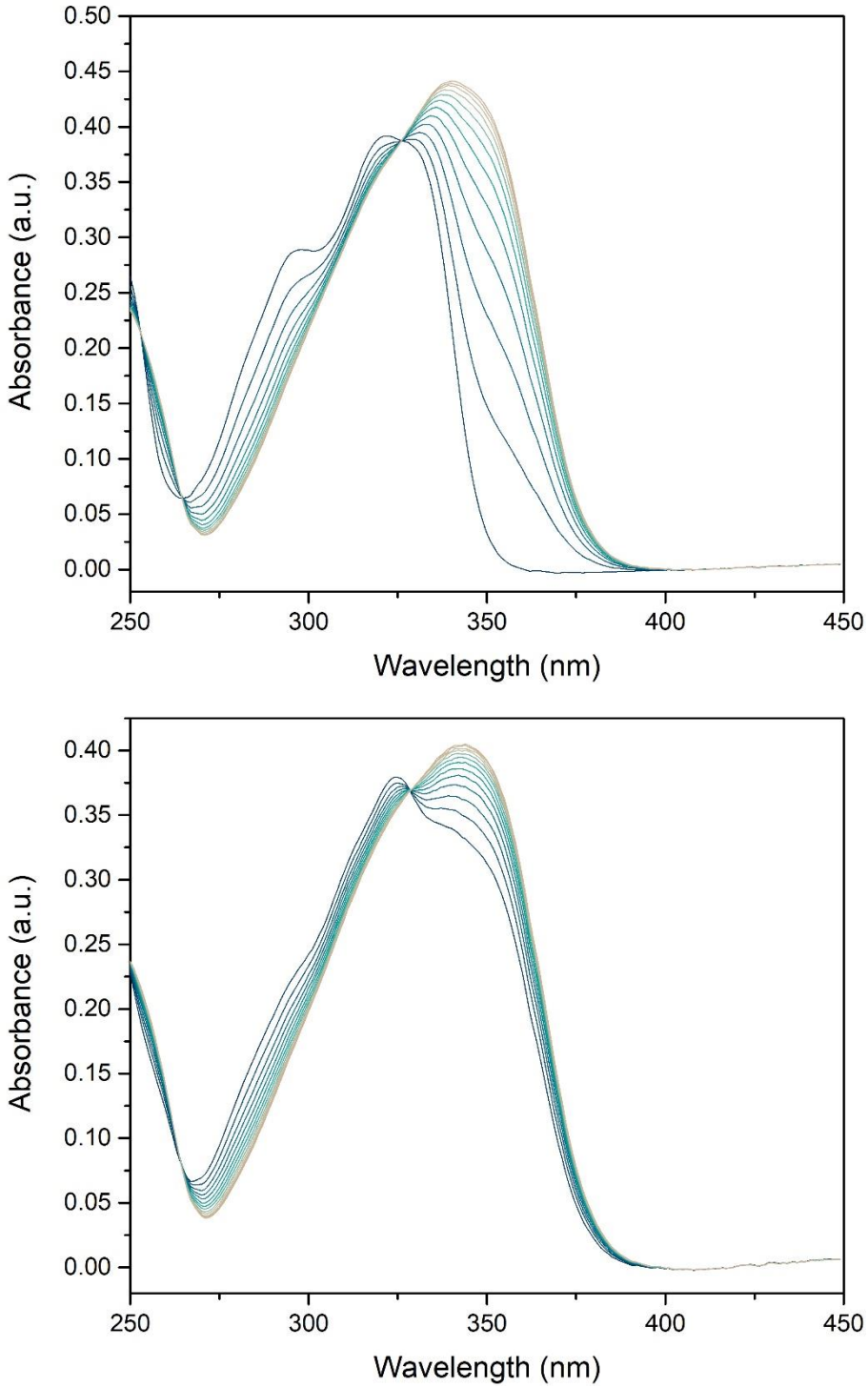

Fig. S28 | Irradiation of C16 followed by UV/vis spectroscopy (octane, ~20 μM, −15 °C). A solution of **C16**-*Z* stable was irradiated with 300 nm (top) to PSS. After full thermal relaxation, the same solution was irradiated again with 300 nm (bottom) to PSS. Start: blue spectrum, end: brown spectrum.

Switching behavior of C18

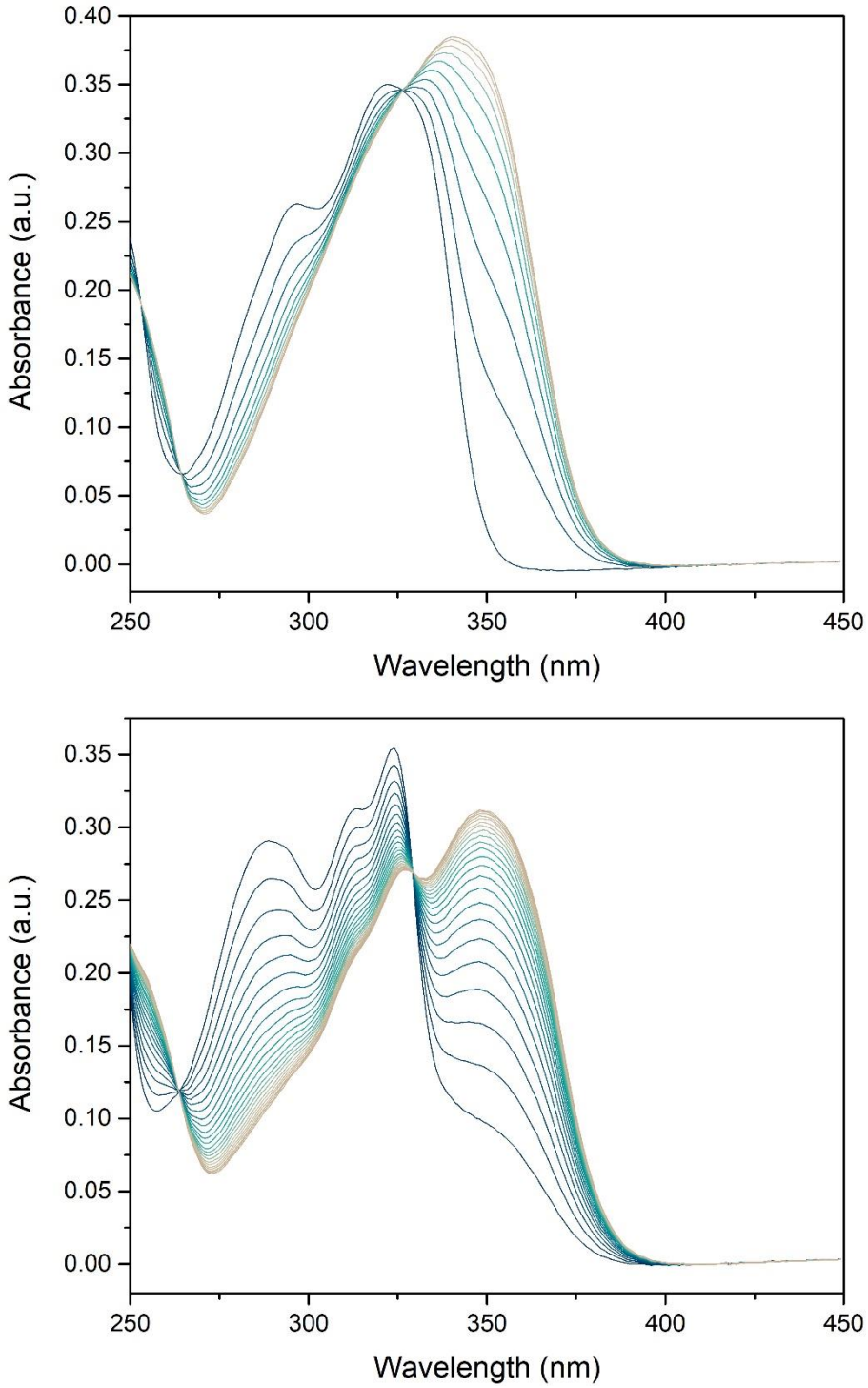

Fig. S29 | Irradiation of C18 followed by UV/vis spectroscopy (octane, ~20 μM, −15 °C). A solution of **C18**-*Z* stable was irradiated with 300 nm (top) to PSS. After full thermal relaxation, the same solution was irradiated again with 300 nm (bottom) to PSS. Start: blue spectrum, end: brown spectrum.

Switching behavior of C20

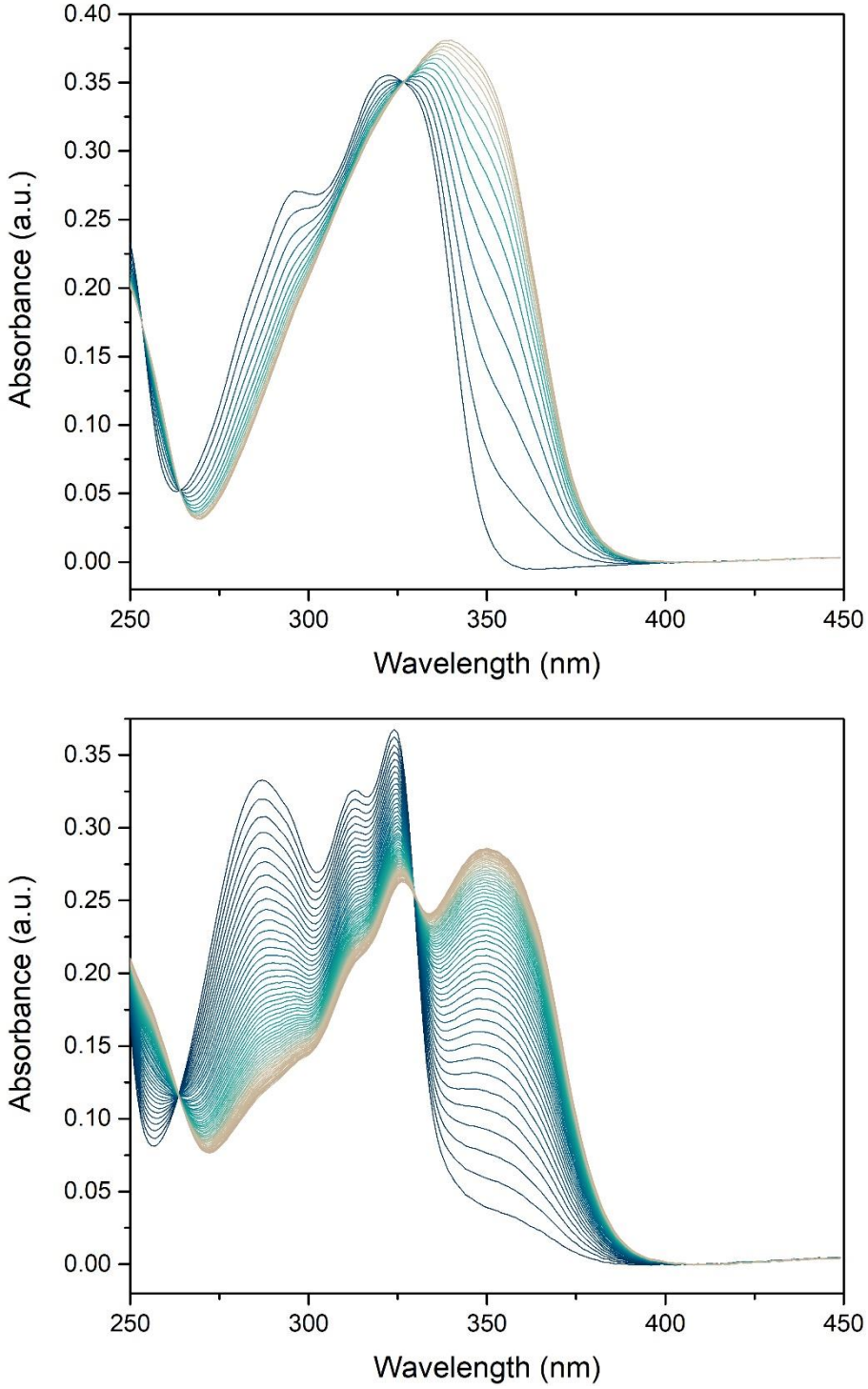

Fig. S30 | Irradiation of C20 followed by UV/vis spectroscopy (octane, ~20 μM, −15 °C). A solution of **C20**-*Z* stable was irradiated with 300 nm (top) to PSS. After full thermal relaxation, the same solution was irradiated again with 300 nm (bottom) to PSS. Start: blue spectrum, end: brown spectrum.

Switching behavior of C22

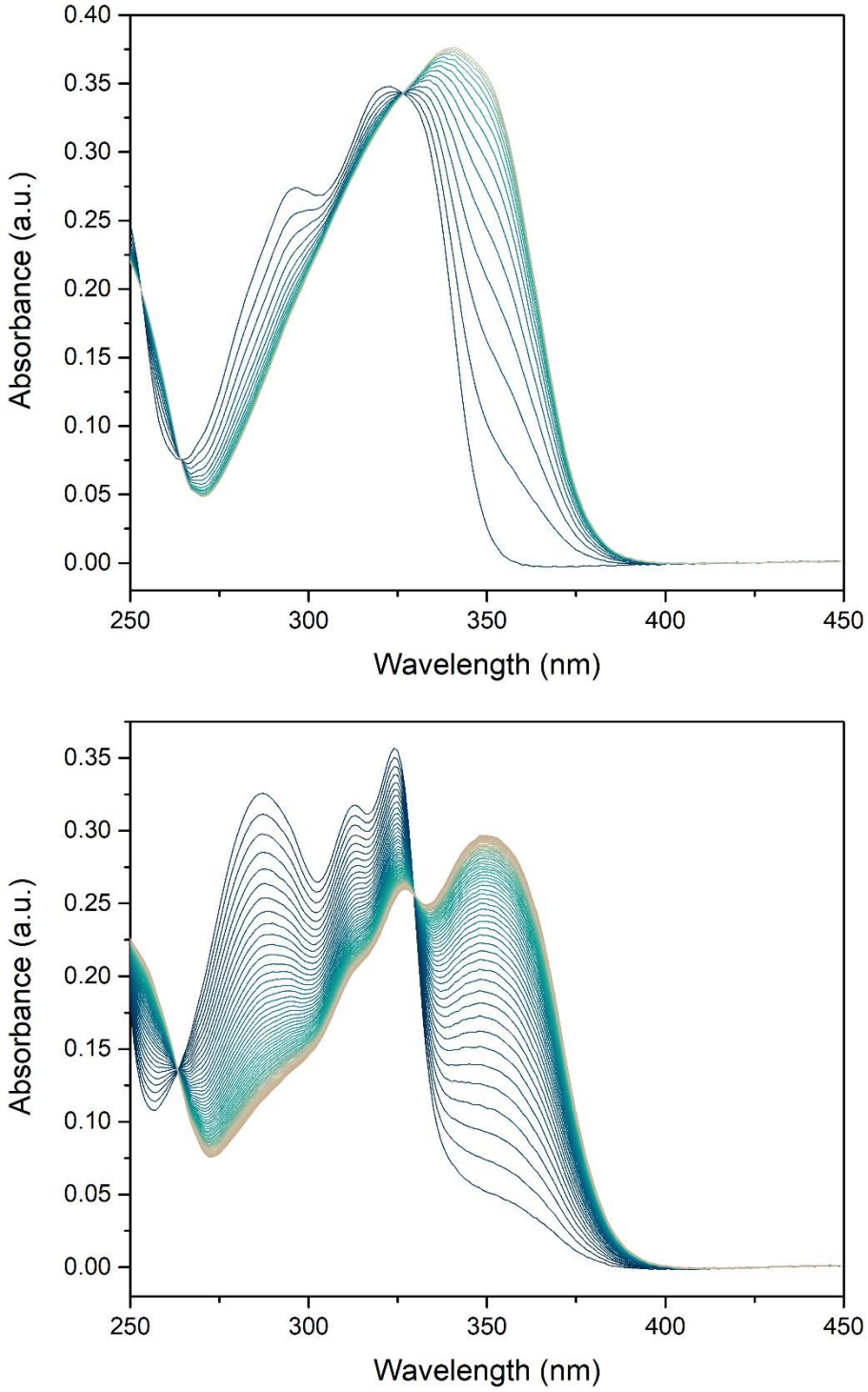

Fig. S31 | Irradiation of C22 followed by UV/vis spectroscopy (octane, ~20 μM, −15 °C). A solution of **C22**-*Z* stable was irradiated with 300 nm (top) to PSS. After full thermal relaxation, the same solution was irradiated again with 300 nm (bottom) to PSS. Start: blue spectrum, end: brown spectrum.

Switching behavior of OMe

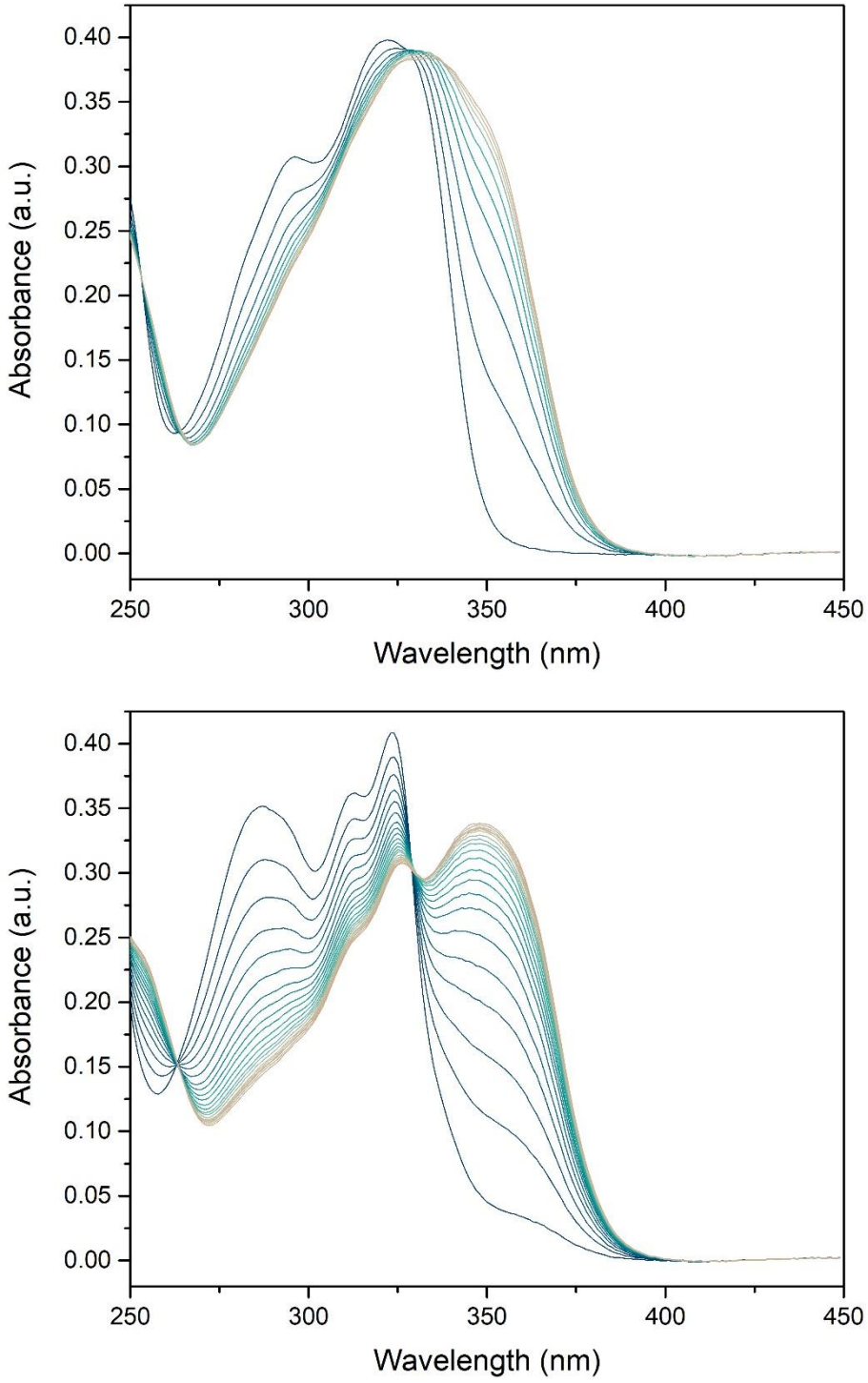

Fig. S32 | Irradiation of OMe followed by UV/vis spectroscopy (octane, ~20 μM, −20 °C). A solution of **OMe**-*Z* stable was irradiated with 300 nm (top) for 270 s. After full thermal relaxation, the same solution was irradiated again with 300 nm (bottom) for 630 s. Note that the halflife of **OMe**-*E* metastable is 12 min at −20 °C; therefore, no isosbestic points were observed. Start: blue spectrum, end: brown spectrum.

References

[1] C. Schink, S. Spielvogel, W. Imhof, *J. Label. Compd. Radiopharm.* **2021**, *64*, 14–29.
[2] T. van Leeuwen, J. Gan, J. C. M. Kistemaker, S. F. Pizzolato, M.-C. Chang, B. L. Feringa, *Chem. – A Eur. J.* **2016**, *22*, 7054–7058.
[3] B. K. Vriesema, J. Buter, R. M. Kellogg, *J. Org. Chem.* **2002**, *49*, 110–113.
[4] V. Martí-Centelles, M. D. Pandey, M. I. Burguete, S. V. Luis, *Chem. Rev.* **2015**, *115*, 8736–8834.

Appendix - X-ray analysis

OMe-*Z*s

Suitable single crystals for X-Ray analysis were obtained by slow diffusion of a methanol layer into a chloroform solution of **OMe**-*Z*s. Ellipsoids drawn at 50% probability; hydrogen atoms are omitted for clarity.

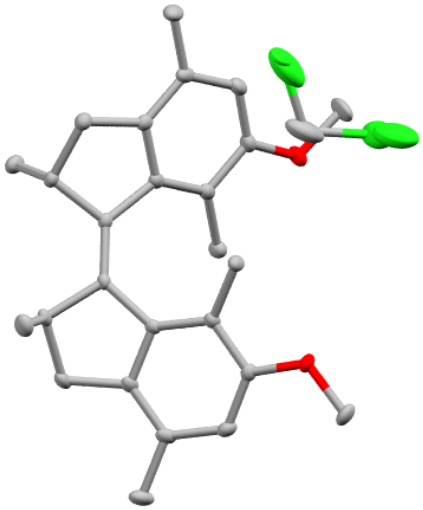

Crystal data and structure refinement for OMe-*Z*s.

Identification code	cu_MKomeZ3_0m_a
Empirical formula	$C_{27}H_{34}Cl_2O_2$
Formula weight	461.44
Temperature/K	100.0
Crystal system	orthorhombic
Space group	Pbca
a/Å	14.746(2)
b/Å	14.851(2)
c/Å	22.351(3)
α/°	90
β/°	90
γ/°	90
Volume/Å^3	4894.8(12)
Z	8
ρ_{calc}g/cm^3	1.252
μ/mm^{-1}	2.539
F(000)	1968.0
Crystal size/mm^3	0.718 × 0.66 × 0.526
Radiation	CuKα (λ = 1.54178)
2Θ range for data collection/°	7.91 to 142.216
Index ranges	-18 ≤ h ≤ 17, -18 ≤ k ≤ 18, -27 ≤ l ≤ 27
Reflections collected	102290
Independent reflections	4662 [R_{int} = 0.0891, R_{sigma} = 0.0387]
Data/restraints/parameters	4662/0/309
Goodness-of-fit on F^2	1.065
Final R indexes [I>=2σ (I)]	R_1 = 0.0443, wR_2 = 0.1141
Final R indexes [all data]	R_1 = 0.0478, wR_2 = 0.1205
Largest diff. peak/hole / e Å^{-3}	0.36/-0.29

OMe-*E* stable

Suitable single crystals for X-Ray analysis were obtained by slow solvent evaporation of a pentane solution of **OMe**-*Es*. Ellipsoids drawn at 50% probability; hydrogen atoms are omitted for clarity.

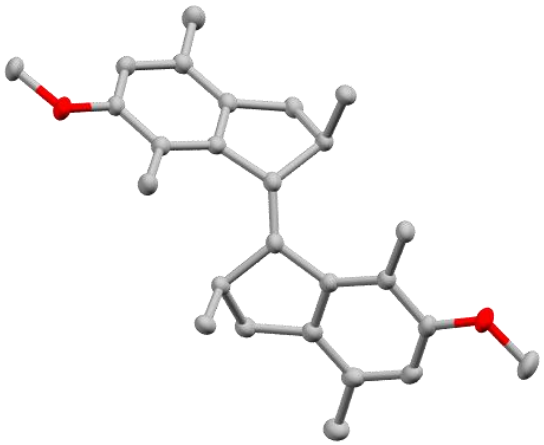

Crystal data and structure refinement for OMe-*E*s

Identification code	cu_MKomeE_0m
Empirical formula	$C_{26}H_{32}O_2$
Formula weight	376.51
Temperature/K	100.0
Crystal system	monoclinic
Space group	$P2_1/n$
a/Å	11.9655(4)
b/Å	12.9546(4)
c/Å	13.8621(5)
α/°	90
β/°	93.7040(10)
γ/°	90
Volume/Å^3	2144.25(12)
Z	4
ρ_{calc}g/cm^3	1.166
μ/mm^{-1}	0.553
F(000)	816.0
Crystal size/mm^3	0.356 × 0.267 × 0.135
Radiation	CuKα (λ = 1.54178)
2Θ range for data collection/°	9.352 to 149.284
Index ranges	-14 ≤ h ≤ 14, -16 ≤ k ≤ 16, -17 ≤ l ≤ 16
Reflections collected	44577
Independent reflections	4336 [R_{int} = 0.1050, R_{sigma} = 0.0691]
Data/restraints/parameters	4336/0/262
Goodness-of-fit on F^2	1.115
Final R indexes [I>=2σ (I)]	R_1 = 0.0552, wR_2 = 0.1549
Final R indexes [all data]	R_1 = 0.0742, wR_2 = 0.1599
Largest diff. peak/hole / e Å^{-3}	0.38/-0.29

C8-*Zs*

Suitable single crystals for X-Ray analysis were obtained by slow diffusion of a methanol layer into a chloroform solution of **C8**-*Zs*. Ellipsoids drawn at 50% probability; hydrogen atoms are omitted for clarity.

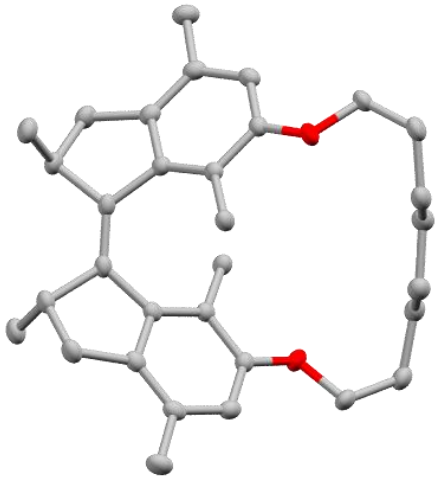

Crystal data and structure refinement for C8-*Zs*

Identification code	cu_MKcisC8_0m_a
Empirical formula	$C_{32}H_{42}O_2$
Formula weight	458.65
Temperature/K	100.0
Crystal system	monoclinic
Space group	C2/c
a/Å	20.7965(7)
b/Å	12.4119(4)
c/Å	11.1170(4)
α/°	90
β/°	114.9890(10)
γ/°	90
Volume/Å^3	2600.94(15)
Z	4
ρ_{calc}g/cm^3	1.171
μ/mm^{-1}	0.540
F(000)	1000.0
Crystal size/mm^3	0.246 × 0.235 × 0.102
Radiation	CuKα (λ = 1.54178)
2Θ range for data collection/°	8.53 to 136.572
Index ranges	-24 ≤ h ≤ 24, -14 ≤ k ≤ 14, -11 ≤ l ≤ 13
Reflections collected	20224
Independent reflections	2374 [R_{int} = 0.0541, R_{sigma} = 0.0331]
Data/restraints/parameters	2374/0/158
Goodness-of-fit on F^2	1.149
Final R indexes [I>=2σ (I)]	R_1 = 0.0433, wR_2 = 0.1100
Final R indexes [all data]	R_1 = 0.0495, wR_2 = 0.1260
Largest diff. peak/hole / e Å^{-3}	0.48/-0.34

C12-*Zs*

Suitable single crystals for X-Ray analysis were obtained by slow diffusion of a methanol layer into a chloroform solution of **C12**-*Zs*. Ellipsoids drawn at 50% probability; hydrogen atoms are omitted for clarity.

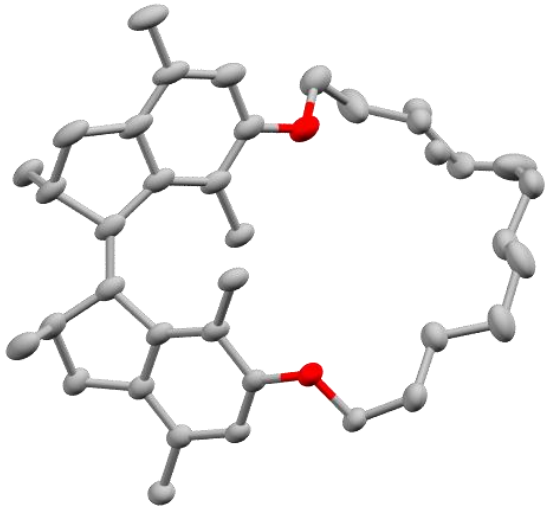

Crystal data and structure refinement for C12-*Zs*.

Identification code	cu_MKC12_0ma_a
Empirical formula	$C_{36}H_{50}O_2$
Formula weight	514.76
Temperature/K	100.0
Crystal system	monoclinic
Space group	$P2_1/c$
a/Å	13.6901(5)
b/Å	21.3691(6)
c/Å	10.5948(3)
α/°	90
β/°	103.2090(10)
γ/°	90
Volume/Å^3	3017.45(16)
Z	4
ρ_{calc}g/cm^3	1.133
μ/mm^{-1}	0.514
F(000)	1128.0
Crystal size/mm^3	0.27 × 0.23 × 0.03
Radiation	CuKα (λ = 1.54178)
2Θ range for data collection/°	7.818 to 136.66
Index ranges	-16 ≤ h ≤ 16, -25 ≤ k ≤ 25, -11 ≤ l ≤ 12
Reflections collected	47317
Independent reflections	5313 [R_{int} = 0.1084, R_{sigma} = 0.0572]
Data/restraints/parameters	5313/0/370
Goodness-of-fit on F^2	1.052
Final R indexes [I>=2σ (I)]	R_1 = 0.0782, wR_2 = 0.1745
Final R indexes [all data]	R_1 = 0.1075, wR_2 = 0.2029
Largest diff. peak/hole / e Å^{-3}	0.24/-0.26

C12-*E*m

C12-*E*m was prepared by irradiating 10 mg of **C12**-*Z*s in 100 mL of dry and degassed toluene with 313 nm (Vilber Lourmat, 6W) for 30 min. After evaporation of toluene, suitable single crystals for X-Ray analysis were obtained by slow solvent evaporation of a pentane solution of **C12**-*E*m. Ellipsoids drawn at 50% probability; hydrogen atoms are omitted for clarity.

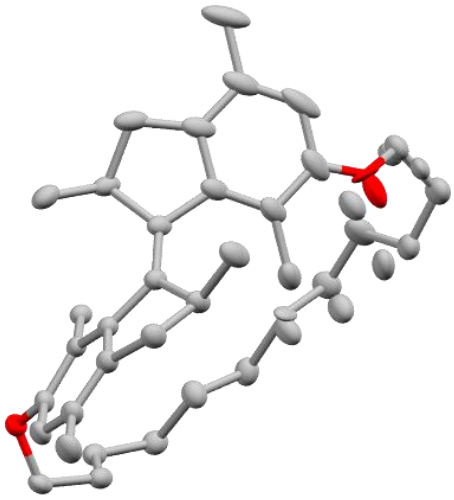

Crystal data and structure refinement for C12-*E*m.

Identification code	cu_MKtransC12_0m_a
Empirical formula	$C_{36}H_{50}O_2$
Formula weight	514.76
Temperature/K	100.0
Crystal system	monoclinic
Space group	$P2_1/n$
a/Å	14.5668(4)
b/Å	10.4353(3)
c/Å	19.9879(5)
α/°	90
β/°	93.1350(10)
γ/°	90
Volume/Å^3	3033.79(14)
Z	4
ρ_{calc}g/cm^3	1.127
μ/mm^{-1}	0.511
F(000)	1128.0
Crystal size/mm^3	0.219 × 0.129 × 0.086
Radiation	CuKα (λ = 1.54178)
2Θ range for data collection/°	7.322 to 144.334
Index ranges	-17 ≤ h ≤ 17, -12 ≤ k ≤ 12, -24 ≤ l ≤ 24
Reflections collected	69537
Independent reflections	5973 [R_{int} = 0.0491, R_{sigma} = 0.0179]
Data/restraints/parameters	5973/444/516
Goodness-of-fit on F^2	1.026
Final R indexes [I>=2σ (I)]	R_1 = 0.0352, wR_2 = 0.0866
Final R indexes [all data]	R_1 = 0.0432, wR_2 = 0.0935
Largest diff. peak/hole / e Å^{-3}	0.21/-0.18

Appendix – NMR spectra (400 MHz, 25 °C, $CDCl_3$)

C8-*Zs*

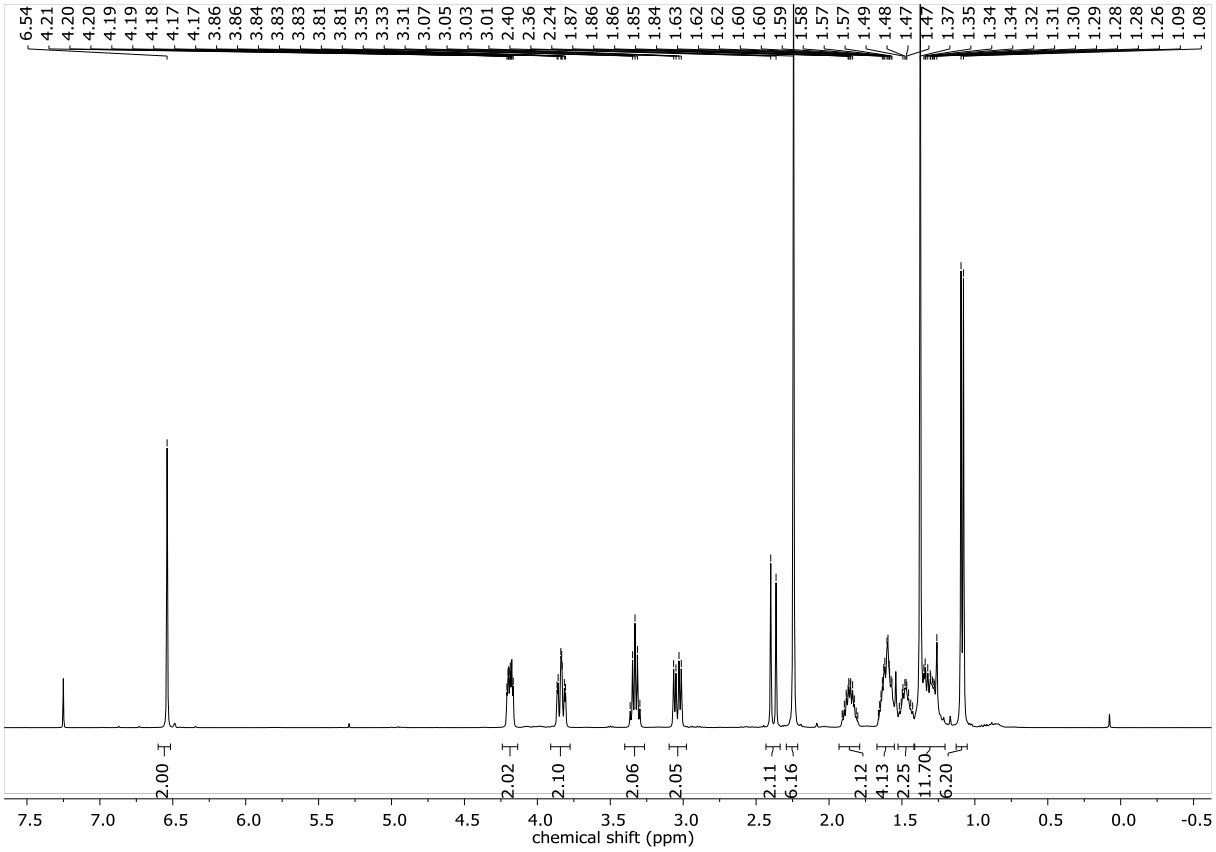

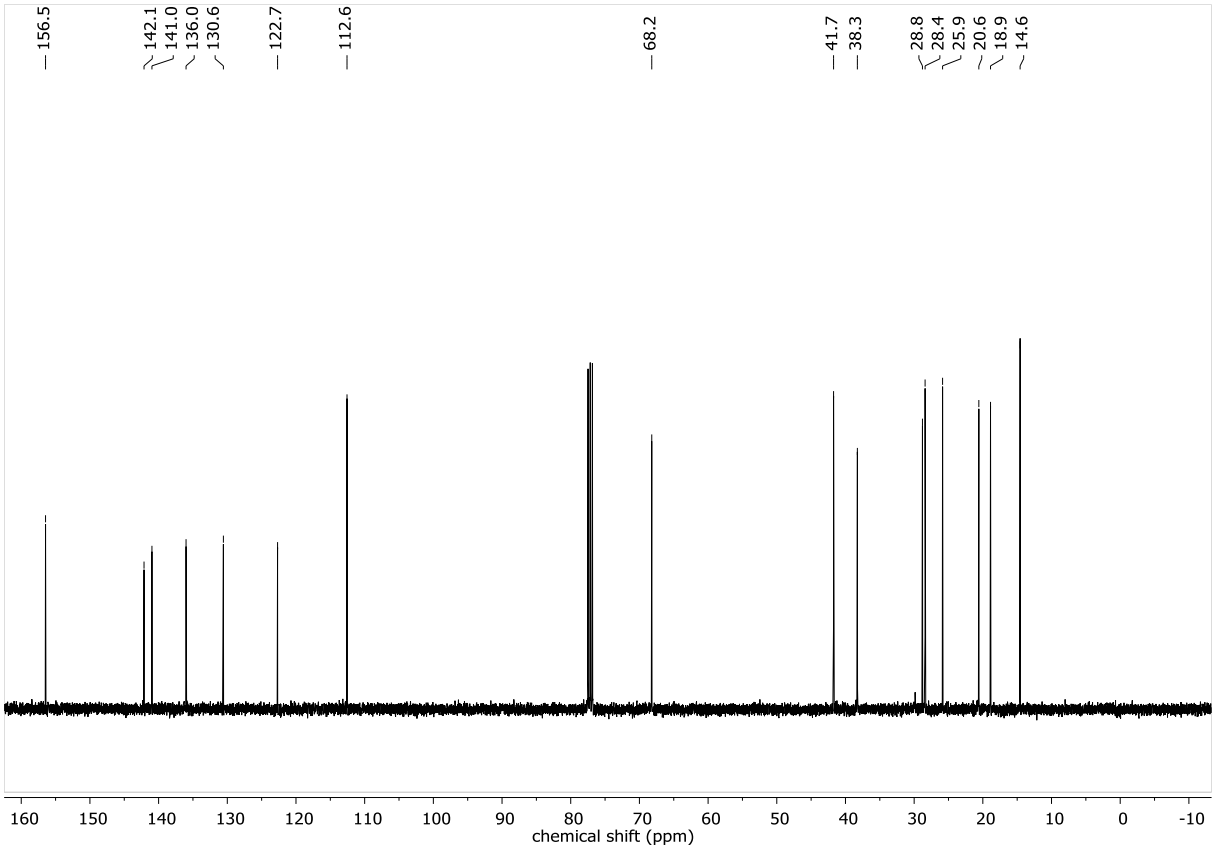

C10-*Zs*

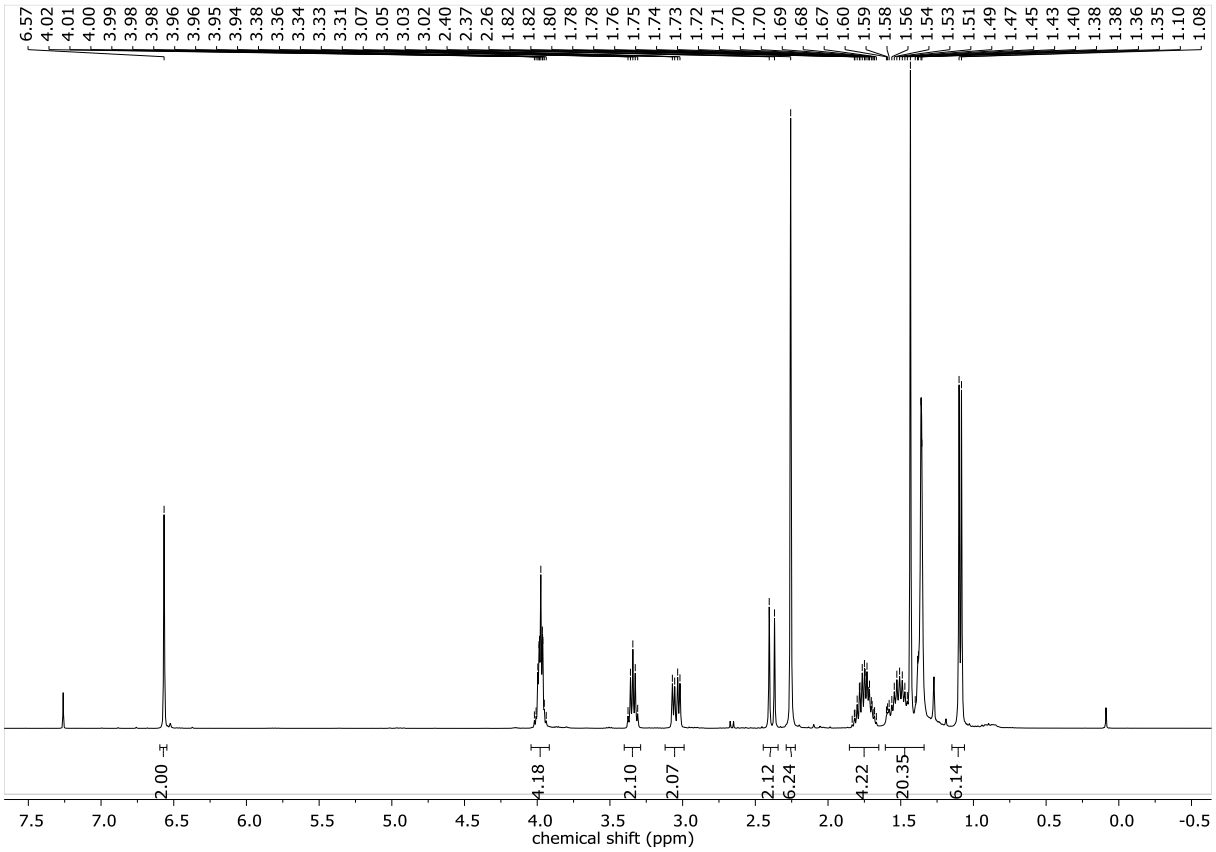
6.57 4.02 4.01 4.00 3.99 3.98 3.98 3.96 3.96 3.95 3.94 3.38 3.36 3.34 3.33 3.31 3.07 3.05 3.03 3.02 2.40 2.37 2.26 1.82 1.82 1.80 1.78 1.78 1.76 1.75 1.74 1.73 1.72 1.71 1.70 1.70 1.69 1.68 1.67 1.60 1.59 1.58 1.56 1.54 1.53 1.51 1.49 1.47 1.45 1.43 1.40 1.38 1.38 1.36 1.35 1.10 1.08
2.00 4.18 2.10 2.07 2.12 6.24 4.22 20.35 6.14
7.5 7.0 6.5 6.0 5.5 5.0 4.5 4.0 3.5 3.0 2.5 2.0 1.5 1.0 0.5 0.0 -0.5
chemical shift (ppm)

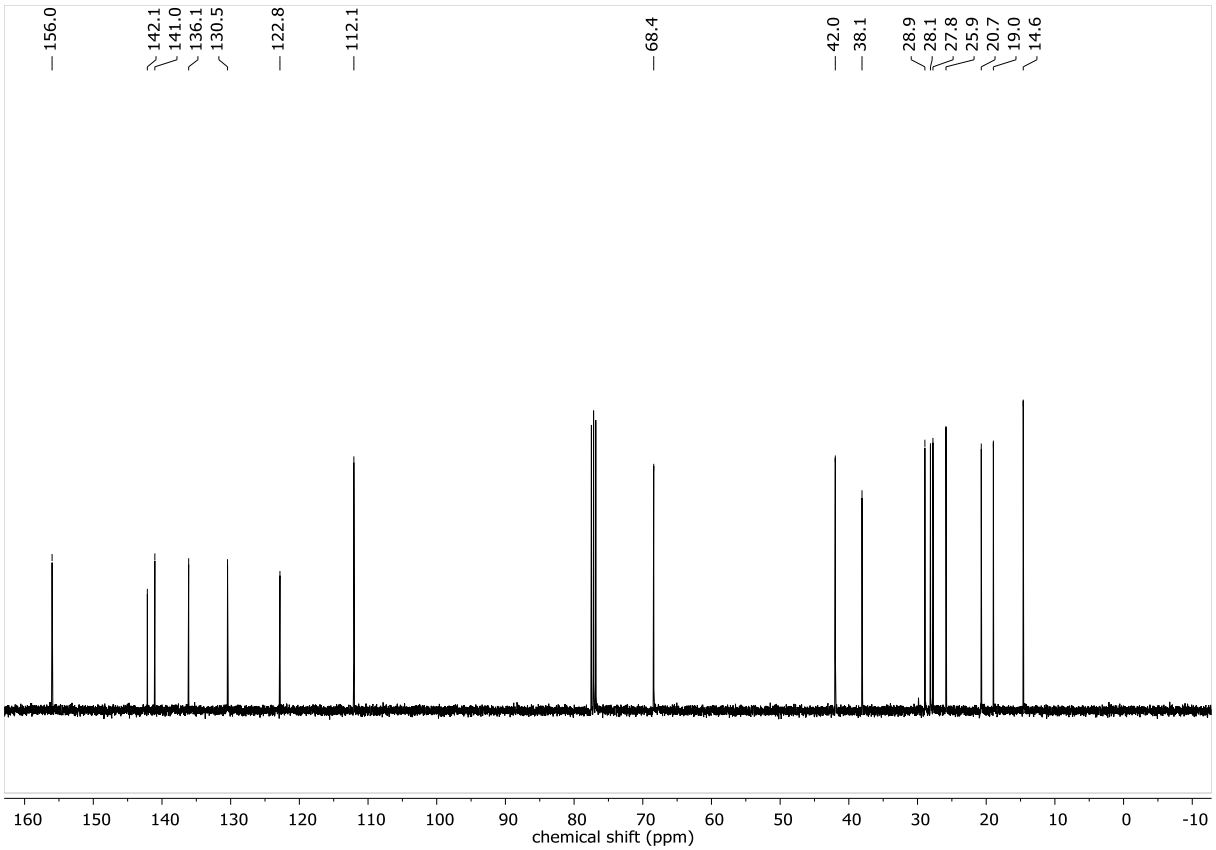
156.0
142.1 141.0 136.1 130.5
122.8
112.1
68.4
42.0
38.1
28.9 28.1 27.8 25.9 20.7 19.0 14.6
160 150 140 130 120 110 100 90 80 70 60 50 40 30 20 10 0 -10
chemical shift (ppm)

C12-*Zs*

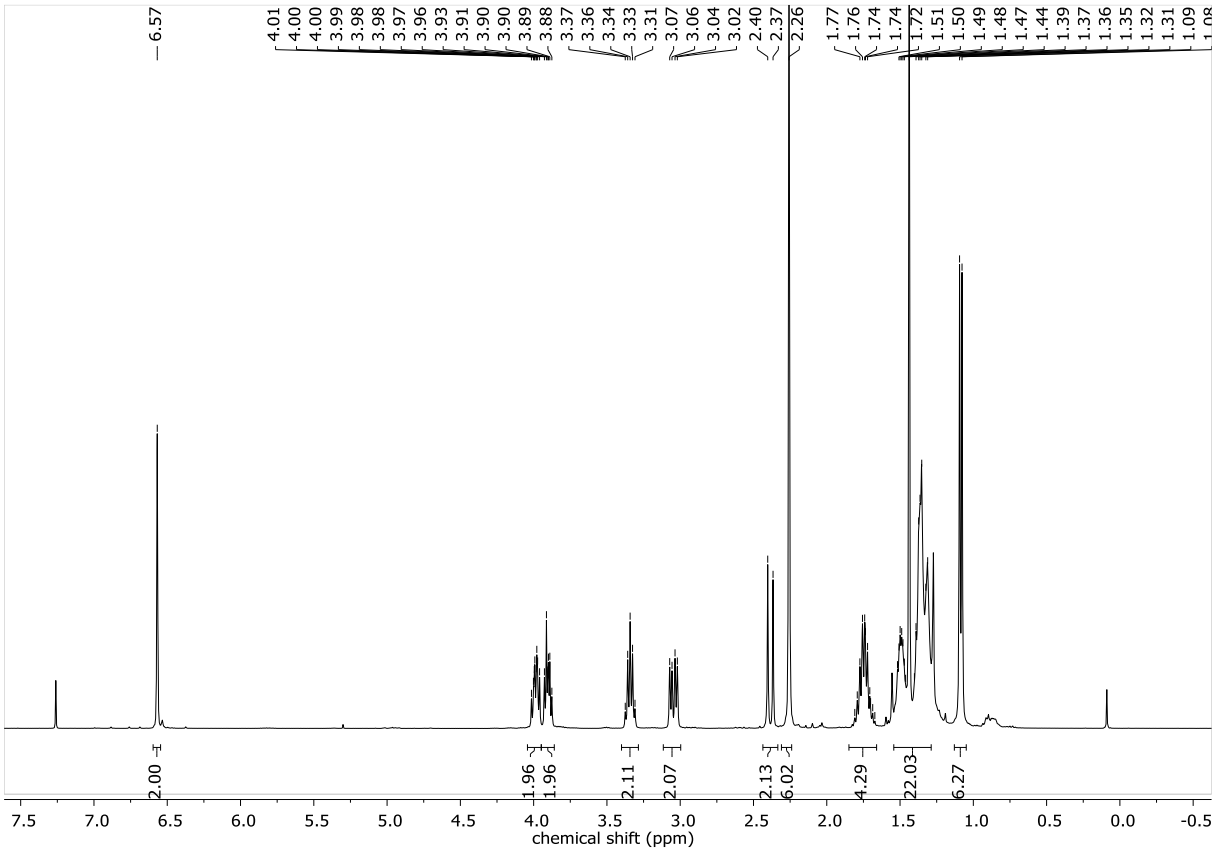
6.57
4.01
4.00
4.00
3.99
3.98
3.98
3.97
3.96
3.93
3.91
3.90
3.90
3.89
3.88
3.37
3.36
3.34
3.33
3.31
3.07
3.06
3.04
3.02
2.40
2.37
2.26
1.77
1.76
1.74
1.74
1.72
1.51
1.50
1.49
1.48
1.47
1.44
1.39
1.37
1.36
1.35
1.32
1.31
1.09
2.00
1.96
1.96
2.11
2.07
2.13
6.02
4.29
22.03
6.27
7.5 7.0 6.5 6.0 5.5 5.0 4.5 4.0 3.5 3.0 2.5 2.0 1.5 1.0 0.5 0.0 -0.5
chemical shift (ppm)

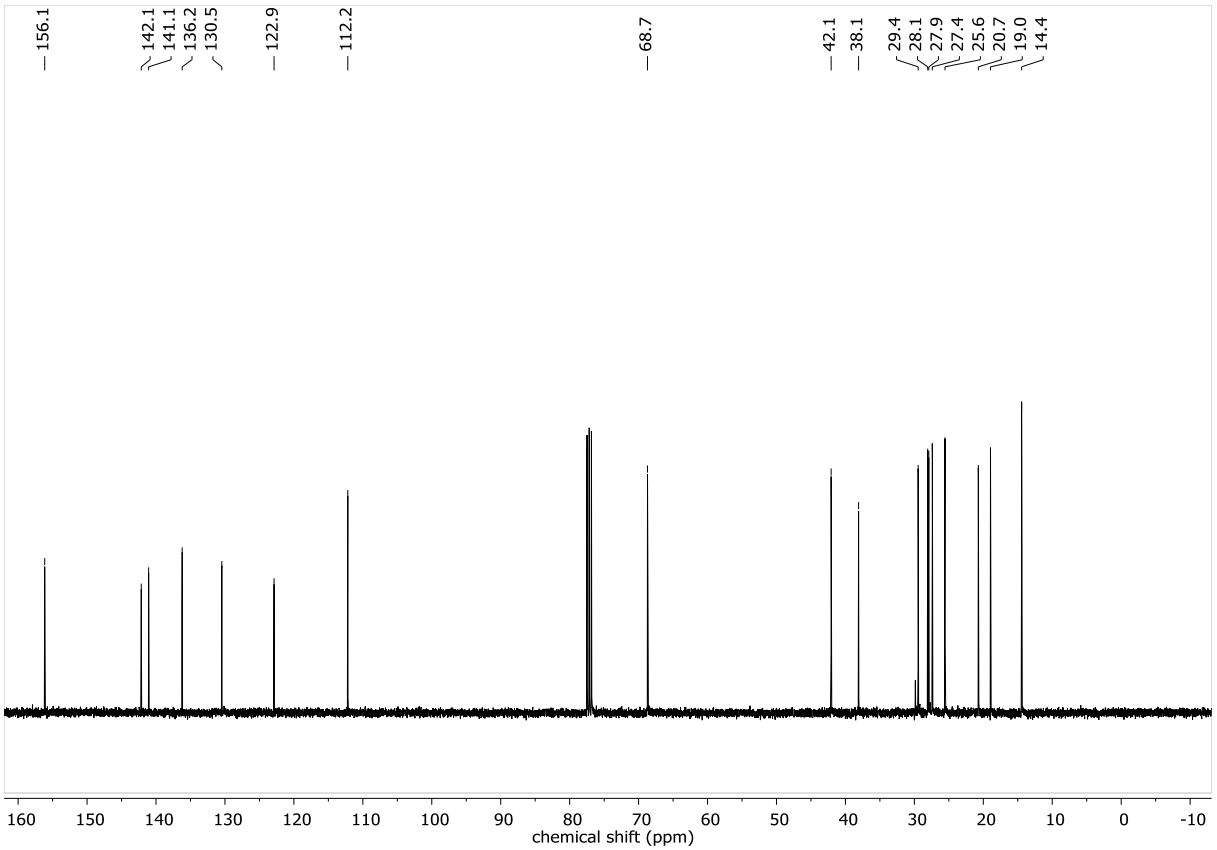
156.1
142.1
141.1
136.2
130.5
122.9
112.2
68.7
42.1
38.1
29.4
28.1
27.9
27.4
25.6
20.7
19.0
14.4
160 150 140 130 120 110 100 90 80 70 60 50 40 30 20 10 0 -10
chemical shift (ppm)

C14-*Zs*

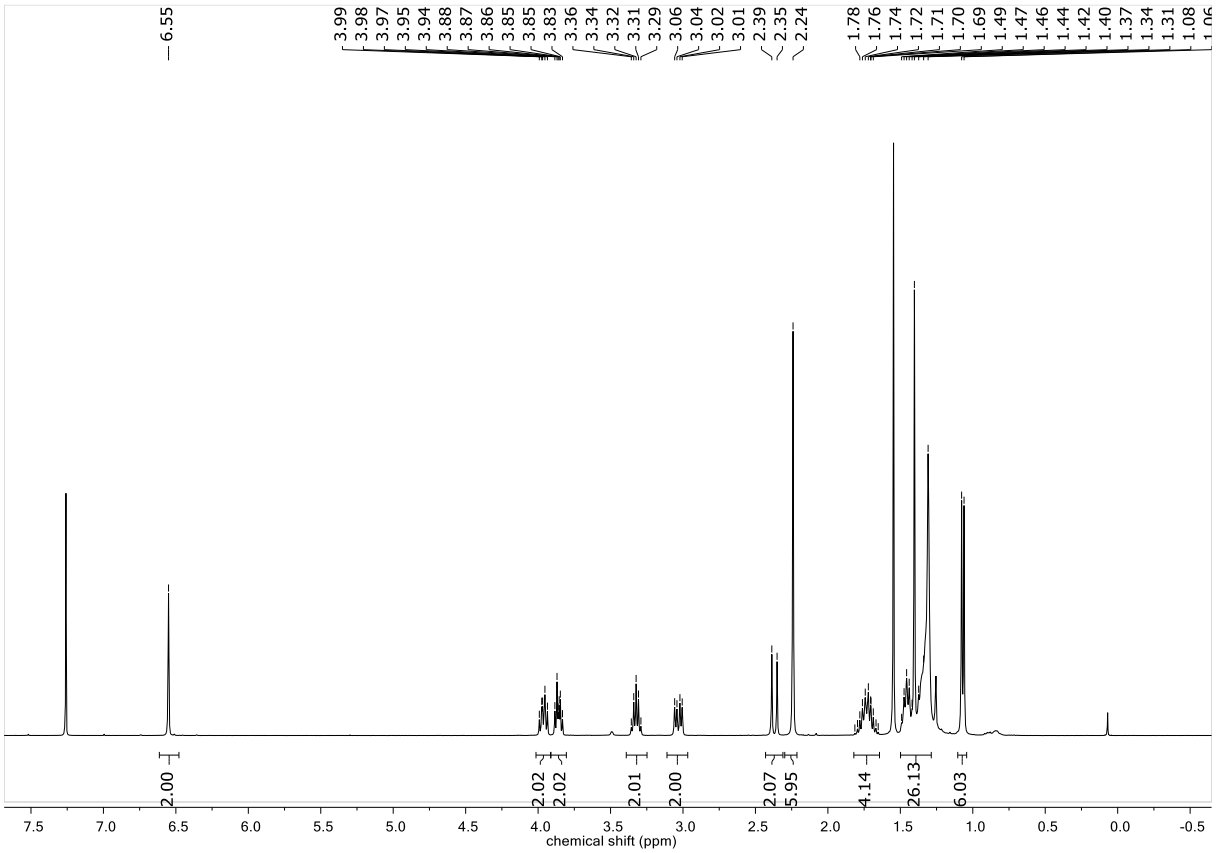
6.55
3.99
3.98
3.97
3.95
3.94
3.88
3.87
3.86
3.85
3.85
3.83
3.36
3.34
3.32
3.31
3.29
3.06
3.04
3.02
3.01
2.39
2.35
2.24
1.78
1.76
1.74
1.72
1.71
1.70
1.69
1.49
1.47
1.46
1.44
1.42
1.40
1.37
1.34
1.31
1.08
2.00
2.02
2.02
2.01
2.00
2.07
5.95
4.14
26.13
6.03
chemical shift (ppm)

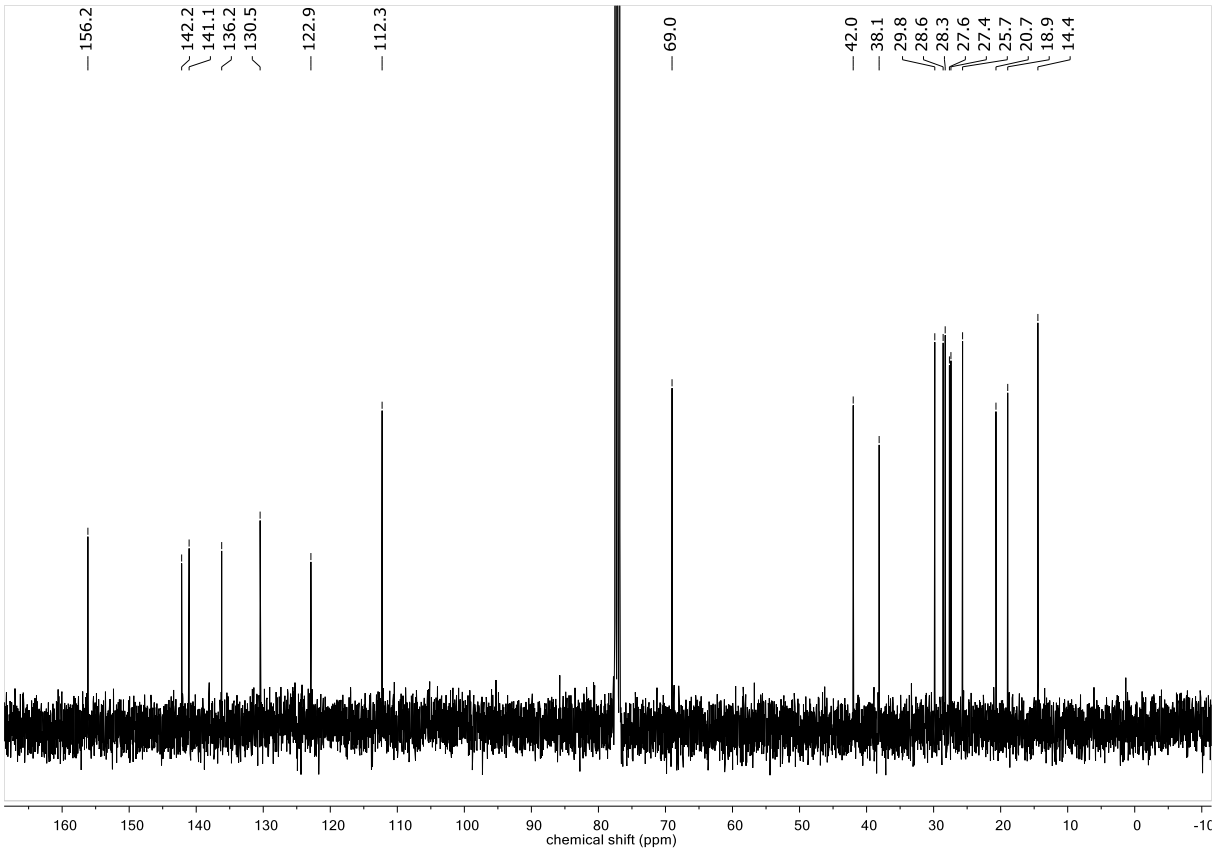
156.2
142.2
141.1
136.2
130.5
122.9
112.3
69.0
42.0
38.1
29.8
28.6
28.3
27.6
27.4
25.7
20.7
18.9
14.4
chemical shift (ppm)

C16-*Zs*

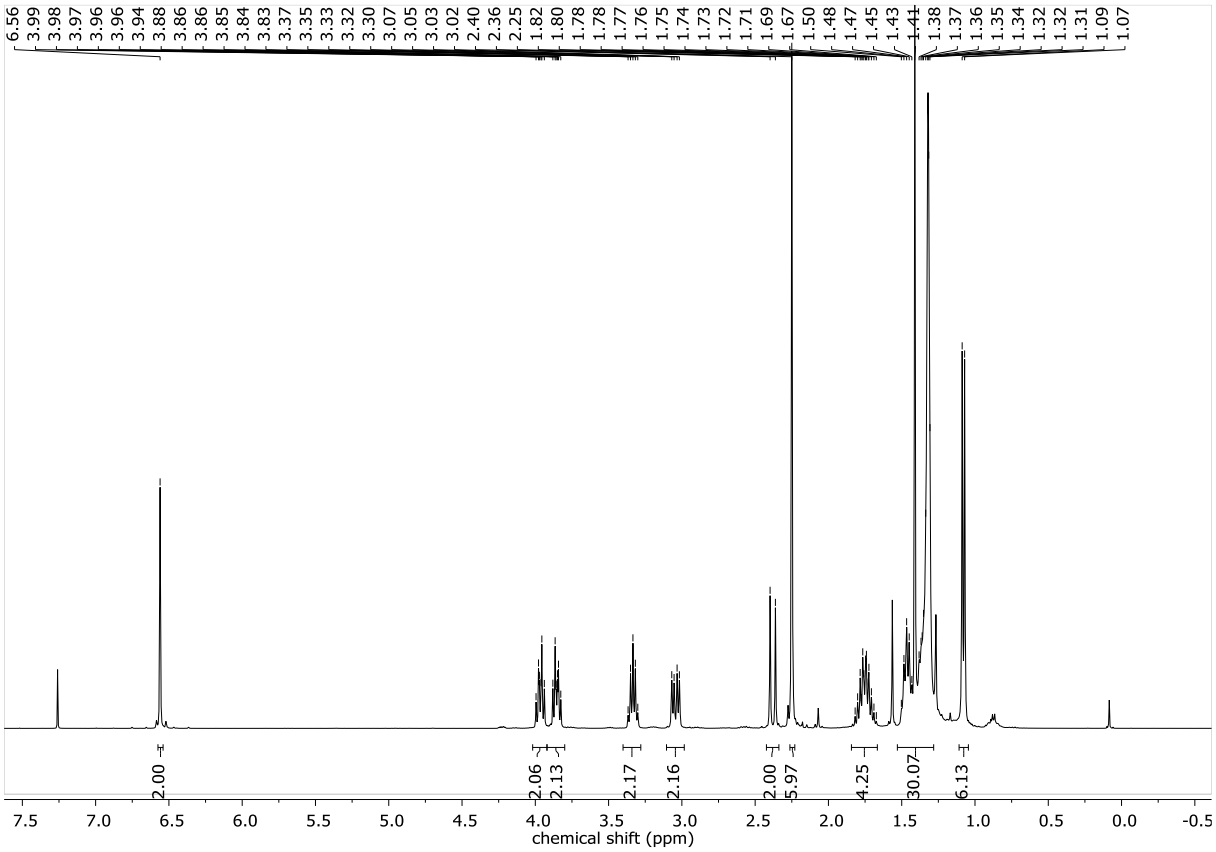
6.56 3.99 3.98 3.97 3.96 3.96 3.94 3.88 3.86 3.86 3.85 3.84 3.83 3.37 3.35 3.33 3.32 3.30 3.07 3.05 3.03 3.02 2.40 2.36 2.25 1.82 1.80 1.78 1.78 1.77 1.76 1.75 1.74 1.73 1.72 1.71 1.69 1.67 1.50 1.48 1.47 1.45 1.43 1.41 1.38 1.37 1.36 1.35 1.34 1.32 1.32 1.31 1.09 1.07
2.00 2.06 2.13 2.17 2.16 2.00 5.97 4.25 30.07 6.13
7.5 7.0 6.5 6.0 5.5 5.0 4.5 4.0 3.5 3.0 2.5 2.0 1.5 1.0 0.5 0.0 -0.5
chemical shift (ppm)

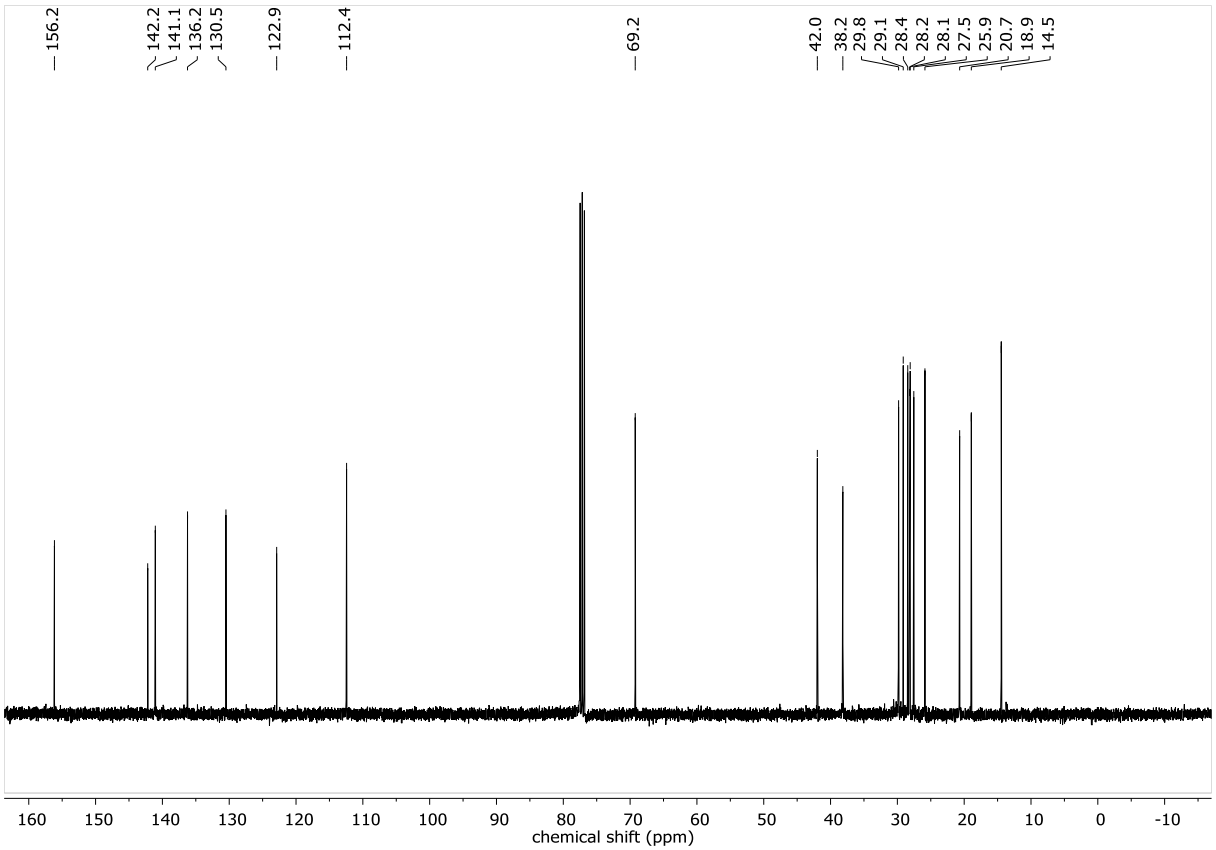
156.2 142.2 141.1 136.2 130.5 122.9 112.4 69.2 42.0 38.2 29.8 29.1 28.4 28.2 28.1 27.5 25.9 20.7 18.9 14.5
160 150 140 130 120 110 100 90 80 70 60 50 40 30 20 10 0 -10
chemical shift (ppm)

C18-*Zs*

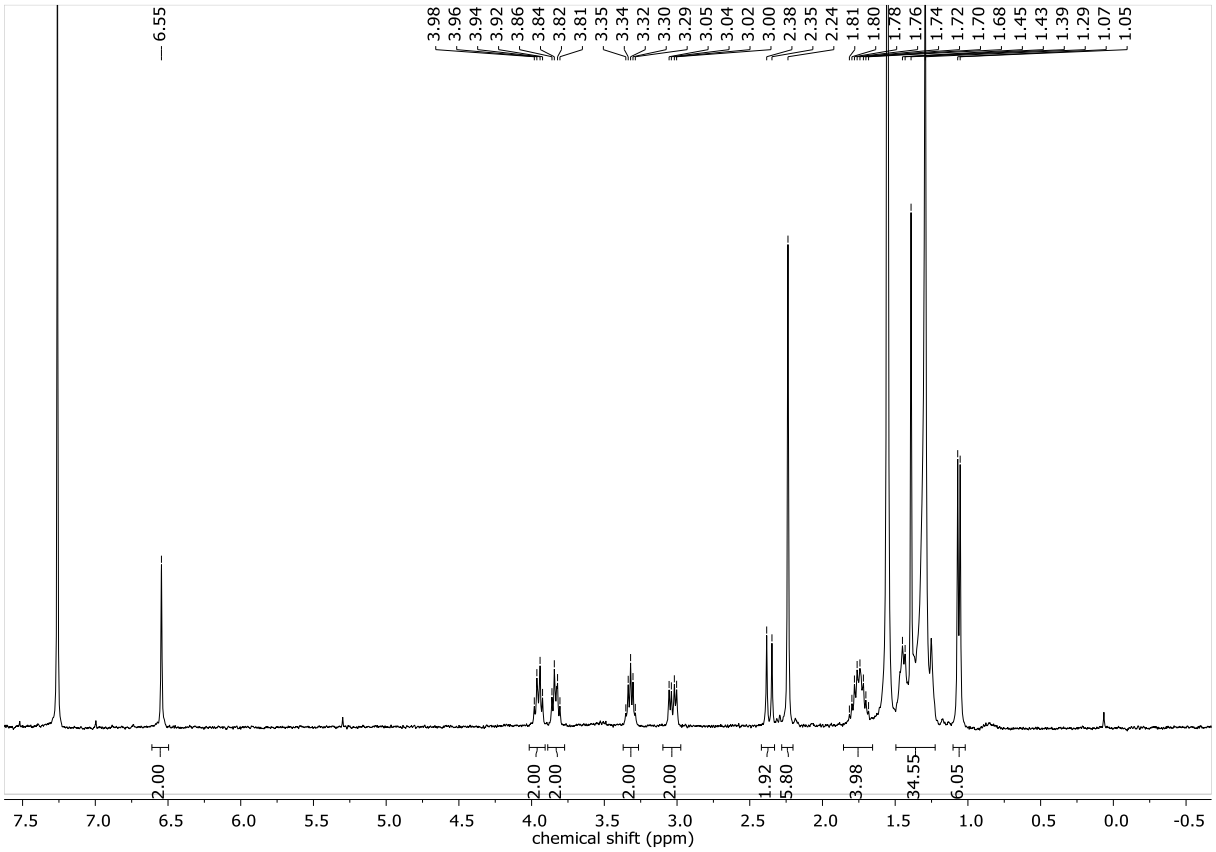
6.55
3.98
3.96
3.94
3.92
3.86
3.84
3.82
3.81
3.35
3.34
3.32
3.30
3.29
3.05
3.04
3.02
3.00
2.38
2.35
2.24
1.81
1.80
1.78
1.76
1.74
1.72
1.70
1.68
1.45
1.43
1.39
1.29
1.07
1.05
2.00
2.00
2.00
2.00
2.00
1.92
5.80
3.98
34.55
6.05
chemical shift (ppm)

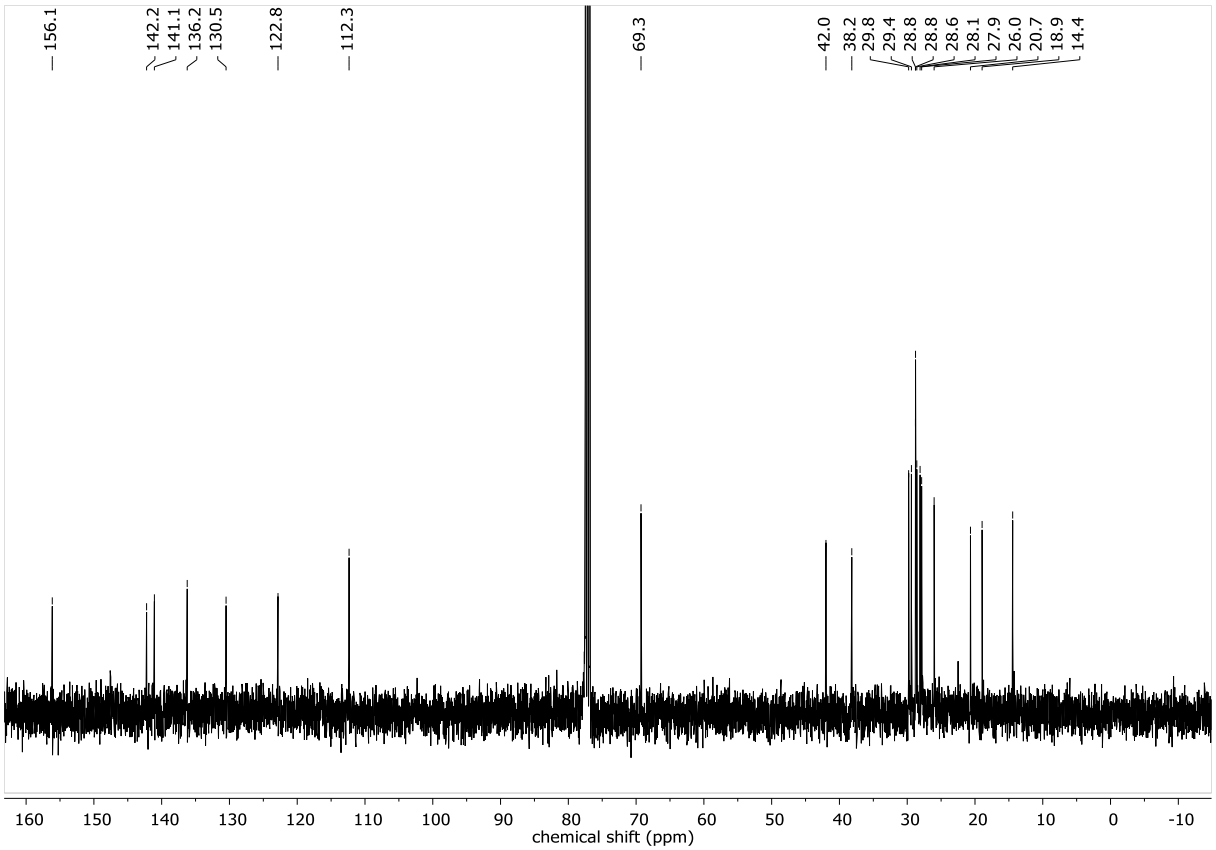
156.1
142.2
141.1
136.2
130.5
122.8
112.3
69.3
42.0
38.2
29.8
29.4
28.8
28.8
28.6
28.1
27.9
26.0
20.7
18.9
14.4
chemical shift (ppm)

C20-*Zs*

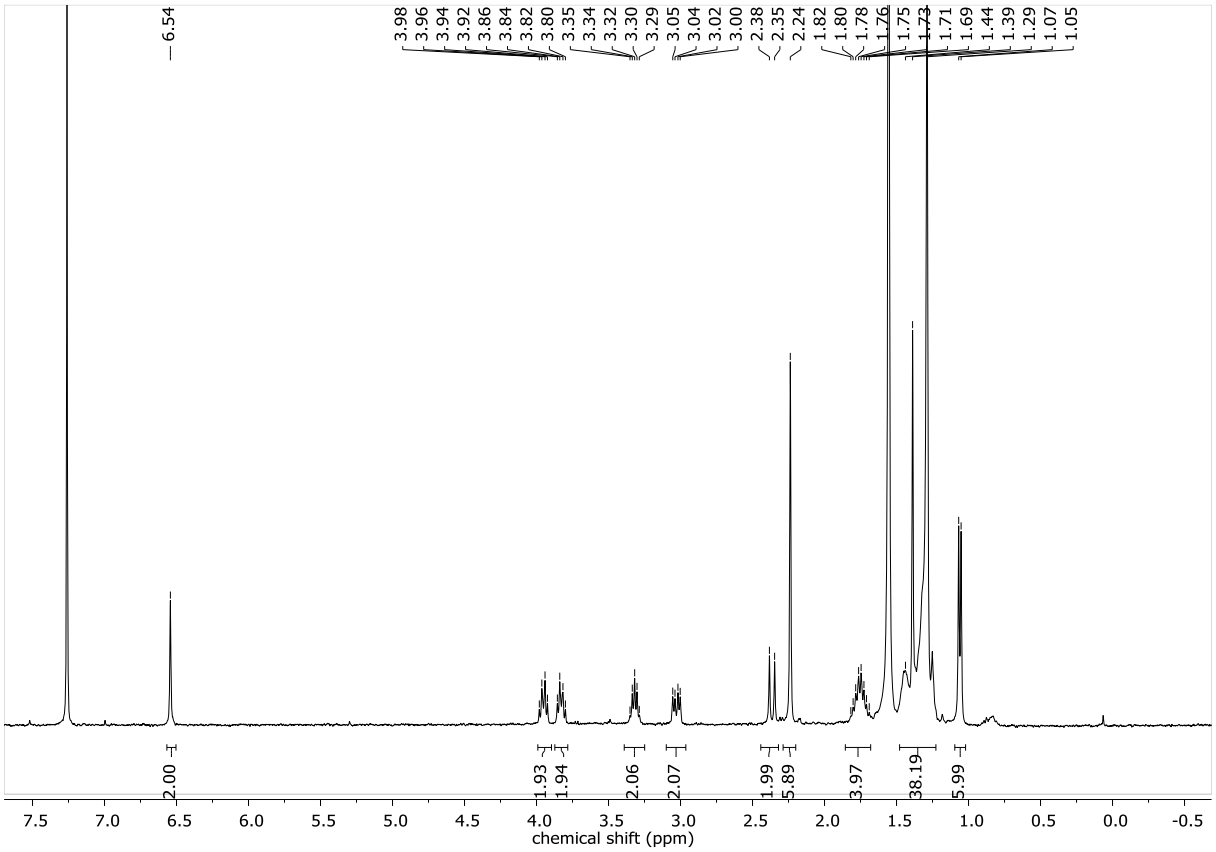
6.54
3.98
3.96
3.94
3.92
3.86
3.84
3.82
3.80
3.35
3.34
3.32
3.30
3.29
3.05
3.04
3.02
3.00
2.38
2.35
2.24
1.82
1.80
1.78
1.76
1.75
1.73
1.71
1.69
1.44
1.39
1.29
1.07
1.05
2.00
1.93
1.94
2.06
2.07
1.99
5.89
3.97
38.19
5.99
chemical shift (ppm)

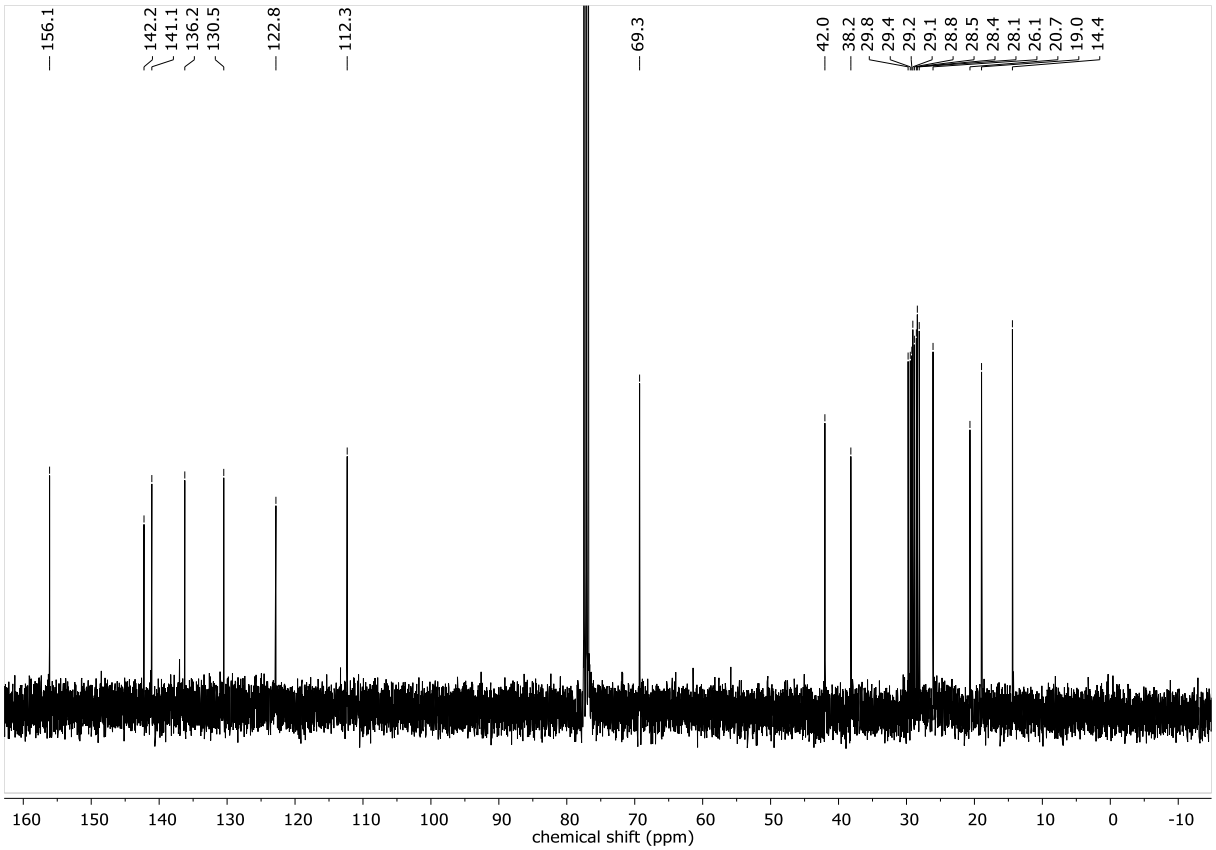
156.1
142.2
141.1
136.2
130.5
122.8
112.3
69.3
42.0
38.2
29.8
29.4
29.2
29.1
28.8
28.5
28.4
28.1
26.1
20.7
19.0
14.4
chemical shift (ppm)

C22-*Zs*

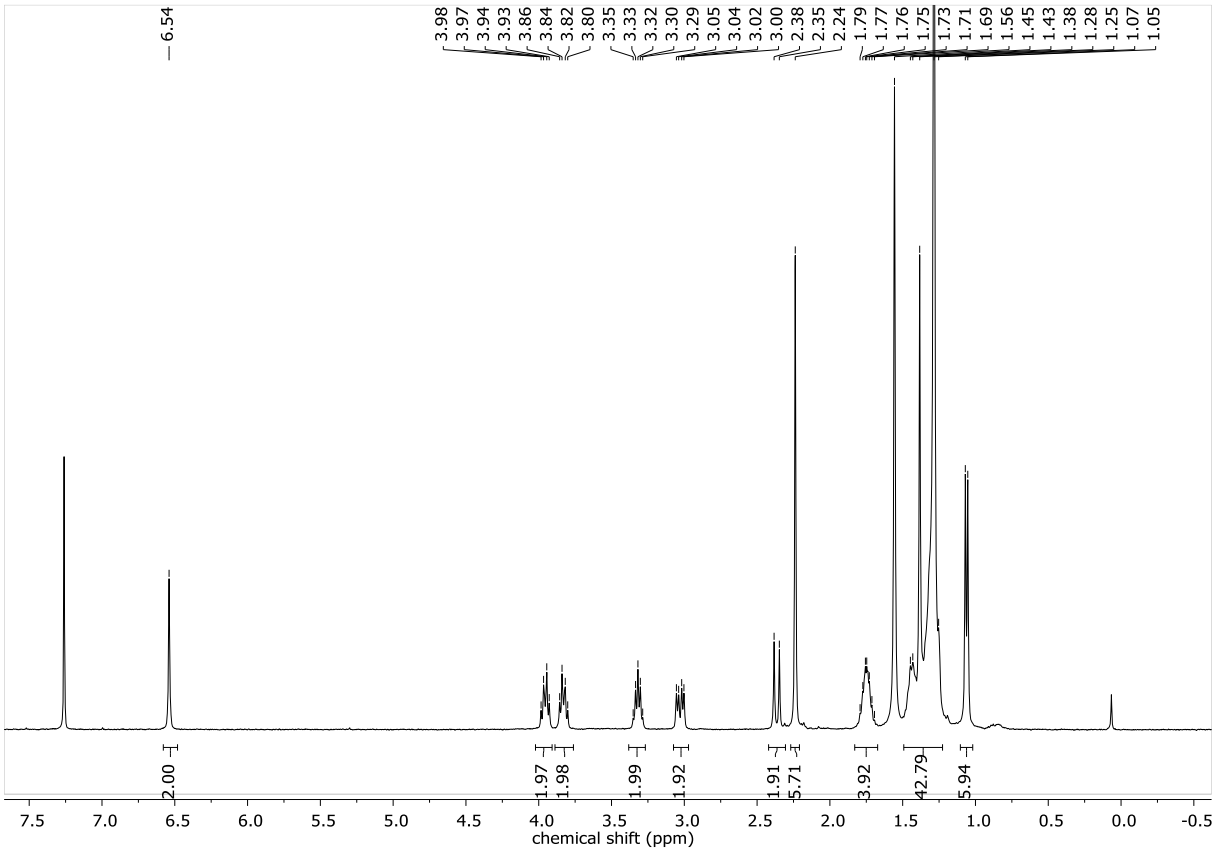
6.54
3.98
3.97
3.94
3.93
3.86
3.84
3.82
3.80
3.35
3.33
3.32
3.30
3.29
3.05
3.04
3.02
3.00
2.38
2.35
2.24
1.79
1.77
1.76
1.75
1.73
1.71
1.69
1.56
1.45
1.43
1.38
1.28
1.25
1.07
1.05
2.00
1.97
1.98
1.99
1.92
1.91
5.71
3.92
42.79
5.94
chemical shift (ppm)

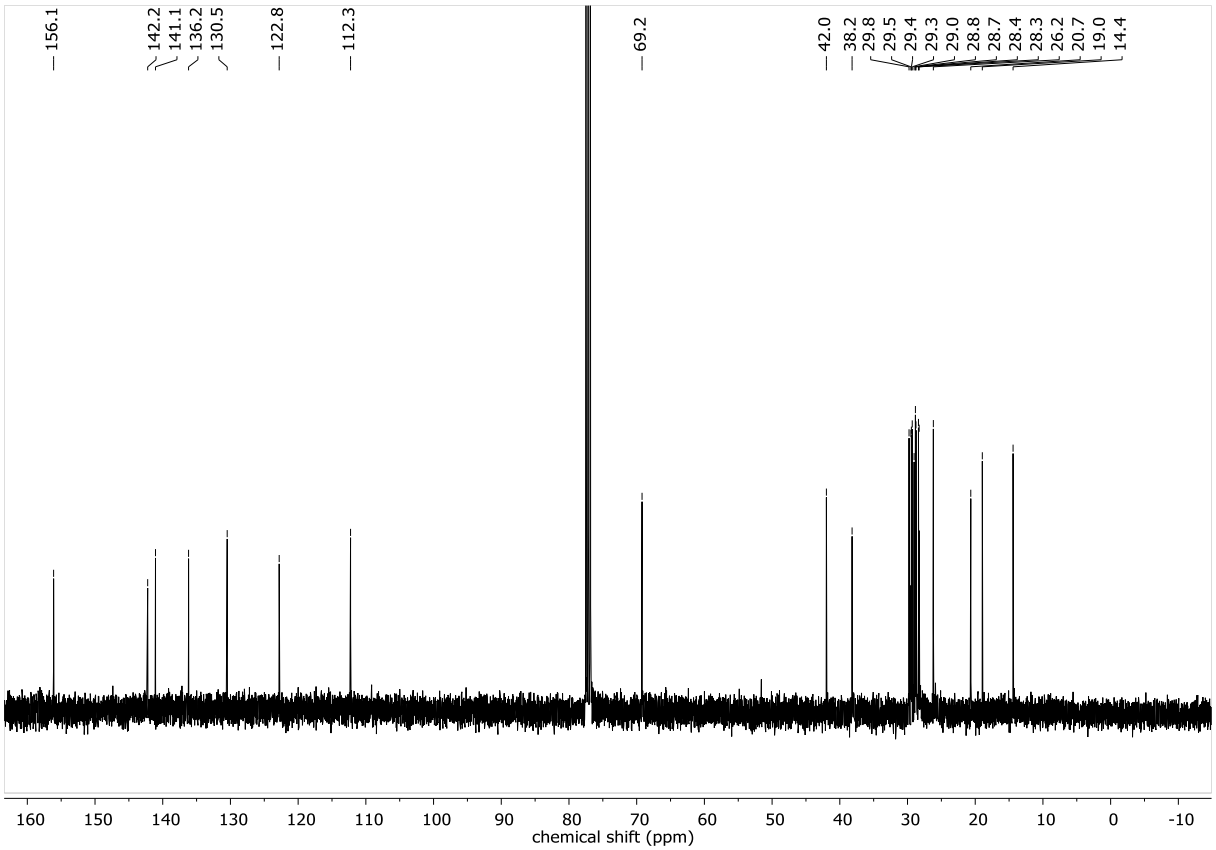
156.1
142.2
141.1
136.2
130.5
122.8
112.3
69.2
42.0
38.2
29.8
29.5
29.4
29.3
29.0
28.8
28.7
28.4
28.3
26.2
20.7
19.0
14.4
chemical shift (ppm)